

Vapour cloud formation

Experiments and modelling

Prepared by the **Health and Safety Laboratory**
for the Health and Safety Executive 2012

Vapour cloud formation

Experiments and modelling

Graham Atkinson & Simon Coldrick

Harpur Hill

Buxton

Derbyshire

SK17 9JN

Hazard analysis for overfilling of a tank with a volatile liquid is a complex and important problem but (prior to the Buncefield incident) had not been the subject of significant research effort. Since the incident [Reference 1] HSE has sponsored a programme of experimental and modelling research to investigate the technical issues involved and develop methods of analysis [References 2 and 3].

The objective is that HSE, and industries responsible for filling tanks, will be in a position agree on a reliable method to determine the character of the vapour cloud generated in the event of an overfill. This will allow appropriate consideration of the overfill scenario i.e fluid type, tank size, fill rate etc. to be taken into account in hazard assessments for land use planning and emergency planning purposes. HSE's Vapour Cloud Assessment method is detailed in Appendix 1. Some example cases are worked through in this Appendix.

This report and the work it describes were funded by the Health and Safety Executive (HSE). Its contents, including any opinions and/or conclusions expressed, are those of the authors alone and do not necessarily reflect HSE policy.

© Crown copyright 2012

First published 2012

You may reuse this information (not including logos) free of charge in any format or medium, under the terms of the Open Government Licence. To view the licence visit www.nationalarchives.gov.uk/doc/open-government-licence/, write to the Information Policy Team, The National Archives, Kew, London TW9 4DU, or email psi@nationalarchives.gsi.gov.uk.

Some images and illustrations may not be owned by the Crown so cannot be reproduced without permission of the copyright owner. Enquiries should be sent to copyright@hse.gsi.gov.uk.

ACKNOWLEDGEMENTS

The authors wish to acknowledge the major technical and conceptual contributions made by Simon Gant of the Health and Safety Executive throughout this research work.

They would also like to thank Rob Dakin and David Painter of the HSE (Chemical Industries Division) for their sustained support during the project.

KEY MESSAGES

Hazard analysis for overfilling of a tank with a volatile liquid is a complex and important problem but (prior to the Buncefield incident) had not been the subject of significant research effort. Since the incident [Reference 1] HSE has sponsored a programme of experimental and modelling research to investigate the technical issues involved and develop methods of analysis [References 2 and 3].

The objective is that HSE, and industries responsible for filling tanks, will be in a position agree on a reliable method to determine the character of the vapour cloud generated in the event of an overfill. This will allow appropriate consideration of the overfill scenario i.e fluid type, tank size, fill rate etc. to be taken into account in hazard assessments for land use planning and emergency planning purposes. HSE's Vapour Cloud Assessment method is detailed in Appendix 1. Some example cases are worked through in this Appendix.

The experimental and modelling work that underpins the method is described in the body of the report. The technical problem divides into a series of stages requiring very different types of analysis.

1. Initial liquid discharge
2. Liquid fragmentation
3. Developed cascade flow
4. Impact zone
5. Splash evaporation and/or fall out zone
6. Near field dispersion
7. Bund interactions
8. Long range dispersion

Each of these areas is covered in turn in this report. The last two issues require investigation on a larger scale than has been possible in the current experiments. This part of the problem can however be studied with CFD and important results relevant to the analysis of long-range dispersion are included in Sections 8 and 9.

A series of 14 well instrumented large scale cascade experiments have been undertaken using hexane as the test fluid. In addition to data on heat and mass transfer which can be used to validate CFD models, the experiments have yielded videos that graphically illustrate the overfill cascade as a mechanism of vapour cloud production.

The report presents the basic data and derives key summary findings - many of which are carried over into the Vapour Cloud Assessment method in Appendix 1. For example, measurements of liquid and vapour temperature in the outflow from the cascade impact zone show that the two phases are close to thermodynamic equilibrium. It is possible to calculate the rate of air entrainment, so the experimental observation that near equilibrium conditions are reached allows a relatively straightforward determination of source term flammable vapour concentration.

Other examples of important findings from the experimental and modelling work include:

- Fine liquid splash fragments generated in the splash zone contribute significantly to the overall rate of vaporisation
- Vapour recirculation and accumulation triggered by bunding is significant but the effect on vapour cloud formation is not particularly sensitive to bund design.

- Suppression of dilution by long term accumulation of a deep layer around the tank may be significant but fresh air is always drawn down into the vapour flow close to the tank, so there is always some dilution.

EXECUTIVE SUMMARY

Hazard analysis for overfilling of a tank with a volatile liquid is a complex and important problem but (prior to the Buncefield incident) had not been the subject of significant research effort. Since the incident [Reference 1] HSE has sponsored a programme of experimental and modelling research to investigate the technical issues involved and develop methods of analysis [References 2 and 3].

The objective is that HSE, and industries responsible for filling tanks, will be in a position agree on a reliable method to determine the character of the vapour cloud generated in the event of an overfill. This will allow appropriate consideration of the overfill scenario i.e. fluid type, tank size, fill rate etc. to be taken into account in hazard assessments for land use planning and emergency planning purposes. HSE's Vapour Cloud Assessment method is detailed in Appendix 1. Some example cases are worked through in this Appendix.

The experimental and modelling work that underpins the method is described in the body of the report. The technical problem divides into a series of stages requiring very different types of analysis.

1. Initial liquid discharge
2. Liquid fragmentation
3. Developed cascade flow
4. Impact zone
5. Splash evaporation and/or fall out zone
6. Near field dispersion
7. Bund interactions
8. Long range dispersion

Each of these areas is covered in turn in this report, which focuses mainly on the experimental programme. The last two issues require investigation on a larger scale than has been possible in the current experiments. This part of the problem can however be studied with CFD and important results relevant to the analysis of long-range dispersion are included in this report.

Conversely there are some elements of the problem – notably 1,2 and 4 – that are not currently amenable to modelling from first principles. Information about the size spectrum of droplet and the overall dimensions of the cascade has to be taken from experiments, to tune the modelling. Similarly the complex splashing process at the foot of the tank cannot be fully modelled and some information about the enhancement of heat and mass transfer and the production of fine splash fragments has to be taken from experiment.

A successful solution of this problem can only be achieved through close collaboration between experimentalists and CFD modellers.

A series of 14 large scale cascade experiments have been undertaken using hexane as the test fluid. In addition a large number of additional tests using cold water or decene have been carried out: cold water tests allow measurements of heat transfer (without rapid vaporisation) and decene tests allow liquid fragmentation processes to be observed with more freedom. Decene has a similar surface tension to lower molecular weight commodities like gasoline but the risk of a large explosion and fire is eliminated and this allows use of cameras and other equipment close to the cascade.

A large number of video records of the tests have been made including some in close up using a high speed camera. Some of these videos show tests in conditions where ambient temperature was close to the dew point. In these cases the cooling effect of vaporisation led to condensation of water which made the vapour cloud visible. These films graphically illustrate the overflow cascade as a mechanism of vapour cloud production.

On the other hand if the ambient temperature was well above the dew point the vapour cloud was only visible close to the source. Further out the cold vapour was too diluted for water vapour to condense. By repeating the same cascade experiments in different weather conditions the work has finally established beyond doubt that the mist observed at Buncefield and other similar events was water vapour and not finely divided or recondensed hydrocarbon droplets.

The main findings in all of the areas listed above are as follows

Initial liquid discharge: Previous work has been reviewed. The main features of liquid discharge from Buncefield type (fixed roof) tanks are relatively well defined [Reference 2]. A proportion of the overflowed liquid overtops the deflection plate and falls as a free cascade whilst the remainder falls down close to the wall and may hit a wind girder, if the tank has one. The balance between these two flows depends on the details of tank top layout.

The liquid discharge from a floating roof tank is generally a free cascade from the edge of the windgirder below the tank rim. The proportion of the tank perimeter covered by the liquid flow is an important variable and is a function of tank design, settlement etc. In principle detailed examination of a given tank (or a physical test) might allow the nature of the discharge to be determined but normally assumptions about this proportion of tank perimeter will have to be made and these are likely to dominate the uncertainty in the whole assessment method.

Liquid fragmentation: Photographs and high-speed videos of hexane and decene cascades under a range of conditions have shown that the bulk of the mass is concentrated in droplets with diameters of around 2mm but there are also a range of smaller sized droplets. Droplets of a few hundred microns tend to vaporise completely.

Developed liquid cascade: A simple theory is available to calculate the entrainment of air into the cascade. This allows the calculation of the final state if the released liquid reaches a state of thermodynamic equilibrium with the entrained air. Generally all of the test results showed that the hexane droplets in the cascade were fine enough that this equilibrium state gave a useful first indication of the extent of hexane vaporisation. At the base of the 10 m cascades (before the liquid entered the impact zone) the total amount of hexane vaporised was typically around 70% of the maximum that could have occurred (at equilibrium).

One significant and unexpected finding from both experiments and modelling was that the average liquid temperature at the base of the cascade was higher than the vapour. This is a consequence of the wide range of droplet sizes. When a large droplet fragments the small droplets formed cool very rapidly and the whole fragment may be turned into very cold vapour. Large droplets that do not fragment still hold the bulk of the mass and they cannot vaporise quickly enough during the drop to match the rate of vapour cooling.

Impact zone: Measurements of the temperatures of liquid and vapour entering and leaving impact zone show that the generation of fine splash fragments on impact and the high slip velocities between droplets and vapour lead to greatly enhanced rates of heat and mass transfer in the impact zone. No additional air is entrained but the liquid /vapour system is pushed much closer to equilibrium. The amount of hexane vaporised rises to at least 90% of the maximum possible (equilibrium level). A relatively large proportion of the liquid (~50%) forms finely divided droplets in the impact zone but most of these are immediately driven back into the

liquid flow on the ground – a few are snatched away from the surface by strong eddies and carried out of the impact zone by the vapour flow.

Splash evaporation zone: As vapour flows rapidly away from the impact point it entrains fresh air. In absence of droplets the temperature would rise rapidly, as warm air entered the vapour current. However, thermocouples outside the splash zone show the presence of droplets in the vapour flow for around 2000-2500mm from the impact point. The vaporisation of these droplets produces a cooling effect that offsets the inflow of warm air. Measurements of the vapour temperature just after the droplet disappear suggests that total amount of extra vaporisation associated with these fine splash products was about 15-20% of the total. Overall the rate of vaporisation was around 100-110% of that which would have been predicted on the basis of the entrainment into the cascade (only) and attainment of full equilibrium.

Near field dispersion: Some surprisingly well characterised results have been obtained for the rate of dilution of the vapour current out to a distance of around 16 m from the tank wall. These data provide a useful test for modelling efforts. Over this range the reciprocal of temperature drop (and concentration) varies linearly with distance from the impact point. This is the normal behaviour for a momentum driven impinging 3D wall jet.

Bund interactions: This work was done using CFD and is described in this report and Reference 3. Generally a bund intercepts the vapour flow and allows back flow of vapour towards the tank foot. Where this occurs near field entrainment is less effective in diluting the vapour current (because the air entrained is a contaminated backflow from the bund). Concentrations in the bund progressively increase. The final state does not appear to be particularly sensitive to the bund location or profile.

Long range dispersion: Again this work was done in the modelling part of the project. If an overflow continues for many tens of minutes, the depth of the vapour cloud around the tank bund progressively increases. The rate at which this occurs is dependent on the level of obstructions to vapour flow around the site and in particular any changes in ground level. Accumulation of deep layers around the tank (similar to that which occurred at Buncefield) was studied by surrounding the modelled tank by a barrier at some distance from the tank. One interesting and highly significant observation was that even if there was a deep vapour layer around and within the bund there was still always entrainment of fresh air close to the cascade impact point. The entrainment is so vigorous in this early flow that vapour from the layer in the bund could not run back into the centre fast enough to prevent the drawing in of fresh air from above. This means that the early dilution of the vapour current is never entirely prevented by the accumulation of a deep cloud.

Vapour Cloud Assessment method – Appendix 1

The method involves a sequence of calculations that could be readily implemented as a spreadsheet, if a number of cases are to be assessed. Alternatively, analysis of a single case could be easily carried out using a calculator and noting the results at various stages. This has been done for two example cases.

This is a basic method suitable for general use. Inevitably there are issues where appropriate general assumptions have to be made. The most important examples of this are: the specification of the liquid release distribution from a floating roof tank and the effects of site topography on cloud shape. If site-specific data is available, improvements on the general treatment will be possible. If the case is critical such improvements may be necessary.

CONTENTS PAGE

KEY MESSAGES	3
EXECUTIVE SUMMARY	5
CONTENTS PAGE	8
1. INITIAL LIQUID DISCHARGE	10
1.1 Appropriate liquid discharge assumptions	14
2. LIQUID FRAGMENTATION AND AIR ENTRAINMENT	15
2.1 Air entrainment	16
3. DEVELOPED FREE CASCADES	18
3.1 Instrumentation	19
3.1.1 Vapour temperatures outside the cascade.....	19
3.1.2 Liquid temperatures.....	19
3.1.3 Vapour temperatures	23
3.2 Free cascade results	27
3.3 Measured vaporisation efficiency in the cascade	29
3.4 Analysis of Heat and mass transfer in the cascade	29
4. IMPACT ZONE	34
5. VAPOUR CURRENT	38
5.1 Vapour current dilution beyond the zone affected by liquid spray	38
5.2 Enhancement of hexane vaporisation by splashing	48
5.3 Time scale of splash spray evaporation	51
5.4 Pool evaporation	52
5.5 Vapour back flow towards the wall	52
6. SUMMARY OF RESULTS FOR A FREE CASACDE	54
7. BIFURCATED CASCADES (BUNCEFIELD TYPE TANKS) ...	60
7.1 Test 13 – A bifurcated cascade in very stable conditions	62
8. CFD MODELLING	71
8.1 The CFD model	71
8.2 Sensitivity analysis on the CFD model	73
8.3 Model validation	75
8.4 Identification of important parameters	79
8.5 Effect of splashing droplets	81
8.6 Simulations with gasoline	83
8.7 Discussion of results	84

9.	MODELLING OF VAPOUR ACCUMULATION	86
9.1	Effect of accumulation on cascade properties	87
9.2	Results	89
9.3	Effect of accumulating vapour layer	93
9.4	Summary	97
10.	REFERENCES	99
11.	APPENDIX 1: VAPOUR CLOUD ANALYSIS METHOD ...	100
11.1	Mass entrainment	100
11.1.1	Effects of surface tension	100
11.1.2	Effects of liquid mass flow	101
11.1.3	Effects of cross-sectional area of the cascade	102
11.1.4	Effects of height of free fall	106
11.1.5	Formulation adopted in the VCA method	107
11.2	Concentration of fuel at the tank foot	108
11.2.1	Gasoline composition.....	108
11.2.2	Formulation of thermodynamic input to the VCA method	109
11.2.3	Vaporisation of fuel in the cascade	109
11.3	Additional vaporisation of fine splash products	109
11.3.1	Splash fraction selection	109
11.4	Near field entrainment	110
11.4.1	Dilution factors adopted.....	111
11.4.2	Total mass flow in the cloud	111
11.5	Cloud volume and concentration	111
11.6	Hazard ranges	112
11.6.1	Range to which cloud may prevent escape	113
11.6.2	Range to which a low level ignitable cloud may extend.....	113
11.6.3	Source Term/Dispersion for Windy Conditions.....	114
11.7	Example Calculations	115
11.7.1	Example 1: A gasoline tank similar to that at Buncefield.....	115
11.7.2	Example 2: A ship filled methanol tank.....	116
11.8	References for the VCA method	118
12.	APPENDIX 2 – CALCULATION OF MASS ENTRAINMENT	119

1. INITIAL LIQUID DISCHARGE

The results of this and previous studies of the overflow problem suggest that the form of the initial liquid discharge affects the process of vapour cloud formation only inasmuch as it determines the overall dimensions and trajectory of the cascade. The cascade dimensions (length measured along the tank rim and width on a section perpendicular to the tank wall) are crucial in determining the efficiency of vapour cloud formation but the character of the liquid discharge is generally a strong (and sometimes) complex function of tank top design and consequently not readily investigated in a general way.

What is important (in the analysis of liquid flow) is to determine the total mass of discharge and the distance along the tank perimeter over which the liquid is discharged (or the distances if liquid falls from several parts of the tank roof). The speed of discharge is generally low and although this affects throw of the cascade (the distance of the impact point from the foot of the tank wall) there is a relatively minor effect on the vapour cloud.

One rather well defined liquid discharge pattern is that exhibited by the Buncefield Tank 912. This tank had a floating internal deck and there were substantial ventilation holes close to the edge of the fixed tank roof with a separation of 10m (Figure 1).

Liquid flowing out of these vents spread out and ran down the sloping roof to the tank rim where it impacted a firewater deflection plate. A portion of the liquid ran down the wall striking a wind girder part way down whilst the remainder of the liquid flowed directly over the deflection plate to form a **free cascade** that was projected away from the tank wall (Figures 2 and 3). The overall length (along the tank rim) of the cascade from each vent was around 2.5 m.

This type of overflow liquid discharge will be common to a significant proportion of gasoline tanks in the UK, although there are some design variations: for example the ventilation holes may be in the vertical plane at the top of the tank wall.

The liquid flow from an overflowed floating roof tank may be much more variable. As the liquid level rises beyond the design limit it will eventually reach the lowest part of the top of the tank wall – perhaps flowing up past the floating deck if this jams. By this stage parts of the tank rim may have been damaged – particularly if there is a hinged ladder providing access to the tank top.

If the tank is perfectly level and the top of the wall has not been damaged, liquid may be discharged from all or a large proportion of the tank perimeter. On the other hand, a height difference of an inch or two between different parts of the tank wall will have the effect of concentrating the release in parts of the tank rim.

Normally floating roof tanks have a substantial windgirder just below the top of the wall (which may serve as a walkway). Liquid would flow over this girder and the majority would be discharged as a free cascade at the edge of the walkway (Figures 4 and 5).



Figure 1: Typical (Buncefield type) petrol tank – shrouded vents around the tank perimeter

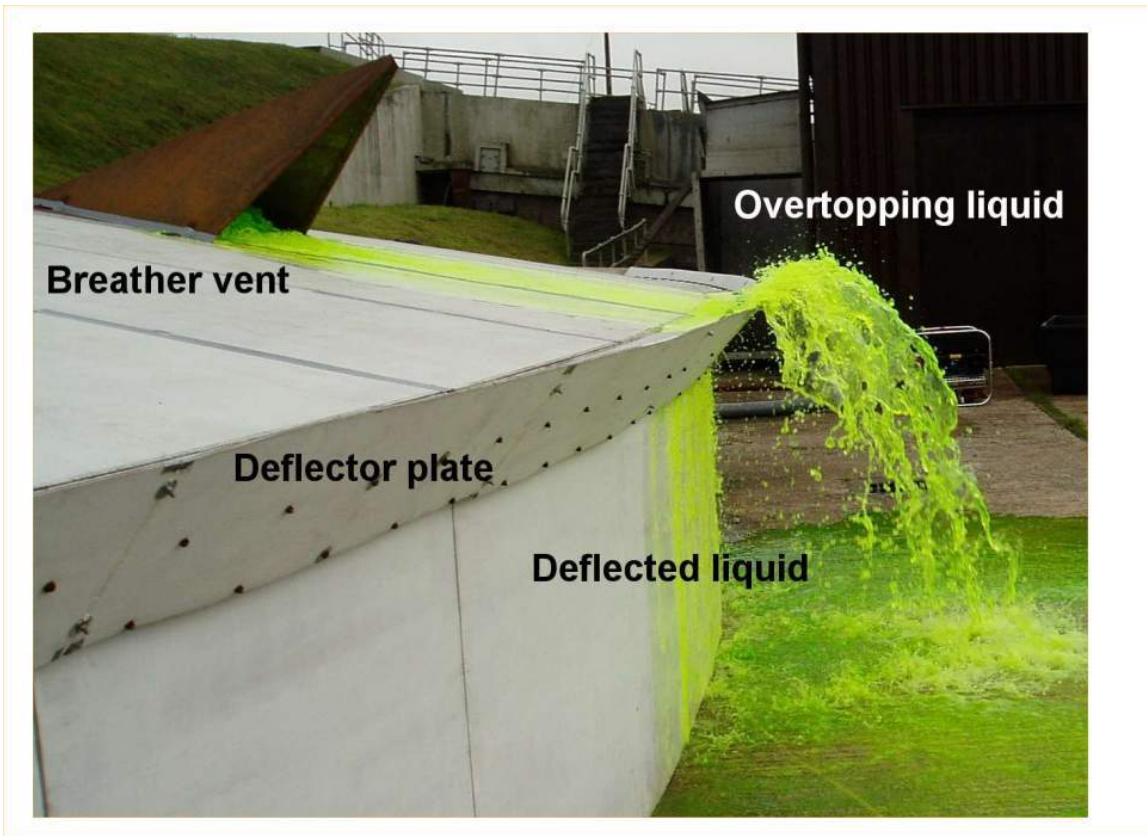


Figure 2: Liquid flow from the vent of a Buncefield type tank.

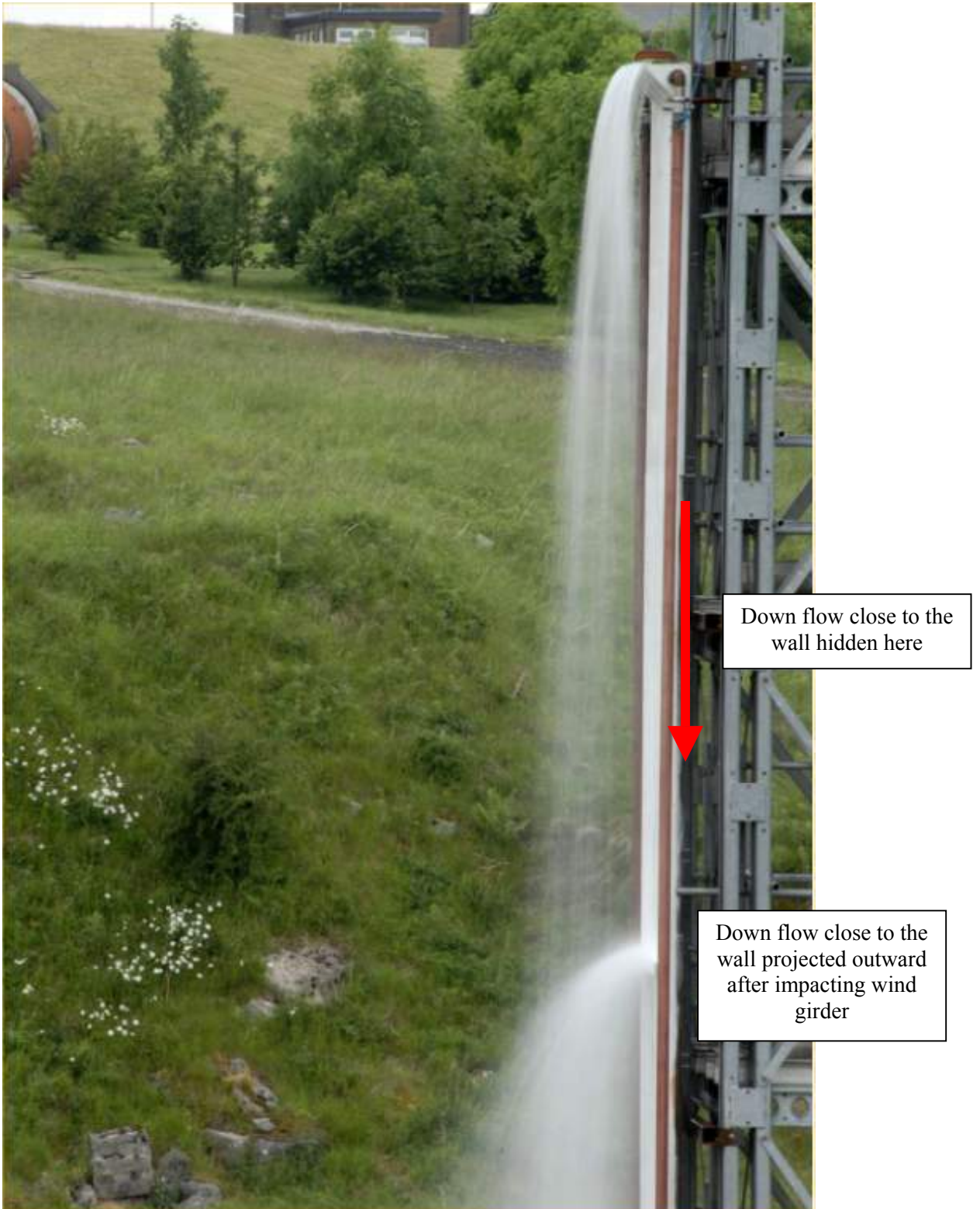


Figure 3: Impact of flow close to the wall on a model wind girder. The resulting spray is projected horizontally out from the tank, intersecting the free cascade caused by flow over the deflector plate.



Figure 4: Windgirder/walkway at the top of a typical floating roof tank. The arrows indicate liquid path in the event of overflow.



Figure 5: Wide view of windgirder/walkway at the top of a typical floating roof tank. The arrows indicate liquid path in the event of overflow.

1.1 APPROPRIATE LIQUID DISCHARGE ASSUMPTIONS

Direct application of the results in this report to the calculation of a vapour cloud source term requires detailed understanding of dimensions of the liquid discharge(s). Careful surveying of tanks and some structural analysis would be required and this is may well be practical but it is not considered further here.

If such an analysis is not undertaken and assumptions have to be made about the dimensions of the liquid cascade then these assumptions are likely to be the main source of uncertainty in the whole of the source term analysis.

If the pattern of liquid discharge is uncertain then a reasonably conservative worst case may be appropriate. The specification of the worst case (for flammable risks) depends on the liquid volatility. For very volatile materials (such as gasoline) the vapour cloud emerging from the bund is typically in the flammable range – however large the proportion of the tank over which the release is spread. If the release extends to a high proportion of the tank top the vapour volume production rate increases whilst remaining within the flammable range. The flammable cloud therefore grows more rapidly and this is a worst case.

If, on the other hand, the liquid has a low volatility or a small mole fraction of light hydrocarbons (for example a light crude oil) dilution of the flow close to the tank and as it flows over the bund may reduce the concentration below the LFL. In this case a flammable cloud may only be produced if the release is concentrated in a small proportion of the tank perimeter. In this case the rate of growth of the flammable cloud is slower but a localised release is still the worst case.

Somewhat similar considerations apply to toxic releases. Again spreading the liquid release over a larger proportion of the tank perimeter reduces the maximum concentration of a volatile contaminant but increases the rate at which the contaminated cloud grows.

Specific recommendations on appropriate liquid discharge assumptions for practical assessments are given in the description of the Vapour Cloud Assessment method (Appendix 1)

2. LIQUID FRAGMENTATION AND AIR ENTRAINMENT

As any liquid stream accelerates downwards under gravity it thins and eventually becomes susceptible to the Rayleigh instability. If highly turbulent at the discharge point this stage may be short circuited. In any case, chains of relatively large droplets are formed which continue to accelerate. The surface stresses associated with aerodynamic drag increase and the droplets become flattened. This increases the drag and a catastrophic break-up process into a large number of much smaller fragments occurs. This is illustrated in Figure 6. This flattening and fragmentation of large droplets is so violent that product droplets are flung outwards in all directions. This produces a rapid expansion in the cascade width and is a main driver of broadening of the cascade throughout its fall.

A review of aerodynamic breakup is given in Reference 4. The process is characterised by the ratio of aerodynamic to surface tension forces i.e. a Weber number. Broadly speaking a critical Weber Number defines the relative speed at which a droplet of a given size and surface tension will fragment. The surface tension of most hydrocarbons is roughly similar and in all cases is much less than that of water. This means that the fragmentation of a hydrocarbon liquid stream to form a spray takes place at smaller relative velocities and consequently smaller distances below the release point - compared with water.

Photographs and high-speed videos of hexane and decene cascades under a range of conditions have shown that the bulk of mass is concentrated in droplets with diameters of around 2mm but there is also a range of smaller sizes. The high optical density and large physical size of a full-scale spray makes it a difficult subject for detailed droplet sizing – especially in the lower size ranges. Fortunately considerable progress can be made in source term calculation without detailed knowledge of the precise size spectrum. A detailed demonstration of how this can be done is one of the main subjects of this report.

In fact useful information about the partitioning of the total droplet mass between 2mm and smaller droplets can be derived from separate measurements of vapour and liquid temperature. This is covered in Section 3 (Developed Cascade).

The basic reason that the overall source term (for dense hydrocarbon cascades) is relatively insensitive to the details of droplet size is that even the largest droplets are fine enough that the flow tends towards heat and mass transfer equilibrium. The rate of vaporisation is then controlled by the rate of air entrainment into the cascade.

At the foot of the tank there is an impact zone where the cascade hits the ground (Section 4 – Impact zone). This is an area where larger droplets impact the wetted solid surface, producing fine splash products initially moving counter to the bulk vapour flow. It is consequently an area of high heat and mass transfer. Generally this study has found that the extent of vaporisation immediately before (above) the impact zone is around 70% of that to be expected in conditions of full equilibrium. Within the impact zone the phases move rapidly closer to equilibrium and the flow out of the impact zone has realised at least 90% of the maximum potential vaporisation rate corresponding to full equilibrium.

This is the basic reason why the source term problem can be tackled successfully without complete knowledge of the droplet size spectrum: the spray structure can vary relatively widely and the flow still ends up close to the equilibrium state.

This is an important finding for practical assessment; if the dimensions of the cascade are known the liquid mass flux density and entrainment rate can be calculated. The equilibrium

state for the released liquid and entrained air can be determined and this gives a reasonable prediction for the degree of vaporisation at the foot of the tank.

In fact the experiments have shown that some very fine droplets are carried out of the impact zone in the vapour flow. More fresh air is rapidly entrained into the ground level vapour current and vaporisation of the fine spray from the impact zone adds a small but significant amount of additional hexane vapour to the final source term.

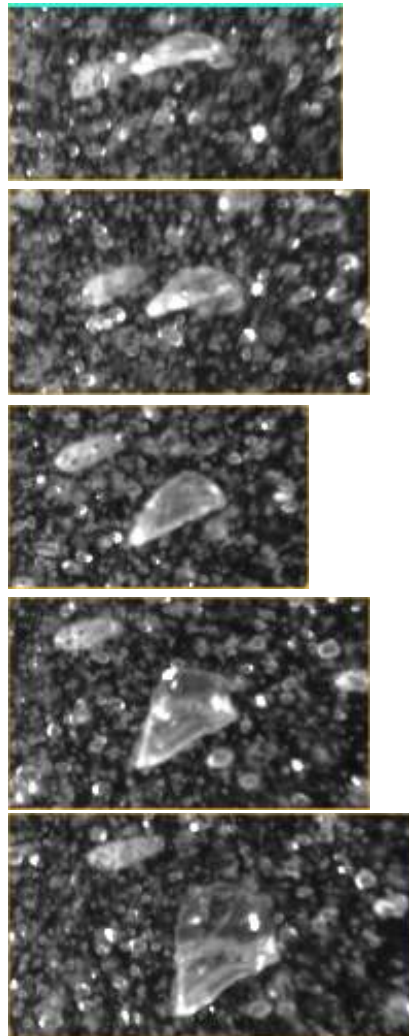


Figure 6: Sequence of images showing the flattening and then bag breakup of a water droplet.

2.1 AIR ENTRAINMENT

The basic analysis of mass entrainment into a dense cascade of droplets a few millimetres in diameter and is described in Appendix 2 and Reference 2. This analysis is significantly different to that of Ghosh and Hunt for much finer sprays from high pressure nozzles (Ref 16). In the cascade flow the larger droplets are not significantly deflected by the induced vapour phase entrainment. Vapour entrainment occurs without the generation of large scale engulfing vortices that develop across the whole cross-section of the flow and which characterise most plumes and

jets. The boundary layer between moving air in the cascade and stationary air in the surroundings does not grow and become unstable leading to large vortices but instead the fluid of intermediate speed is continually drawn away in a steady manner by the suction effect of droplet drag in the cascade.

Spread of liquid droplets is largely determined by the fragment velocities developed in early phases of liquid breakup and thereafter the cascade broadens very slowly (Figure 15).

This view of the flow structure is supported by IR images of the edge of developing cascade obtained as part of the Buncefield Phase II JIP. For legal reasons this data cannot be published until 2013.

The consequence is that air and liquid flows in the cascade remain very compact and closely correlated. The fundamental assumption in Appendix 2 that liquid and vapour flows are coincident produces remarkably accurate estimates of mass entrainment without any allowance for shear driven entrainment at the cascade edge. The mass entrainment is simply a function of the mass flux density of the liquid spray. This is determined by the mass of the release and the cross section of the cascade (which changes very slowly).

In developing the results used for entrainment in the VCA method a base case overfill of 115 kg/s from a tank similar to that at Buncefield has been used. The effect of changes in liquid fill rate F , tank height H , diameter D and top design on the mass density in the cascade have been determined together with the consequent changes in overall mass entrainment. The results of these analyses are combined in the following equation for cascade mass entrainment.

$$M_{air} = 90kg/s \left(\frac{D}{25m} \right)^{0.75} \left(\frac{H}{10m} \right)^{0.45} \left(\frac{F}{115kg/s} \right)^{0.25}$$

Detailed justification for this equation is given in Appendix 1. It is worth noting that the assumed mass entrainment is not sensitive to the tank top design in particular whether the liquid discharge leads to a free cascade or the kind of bifurcated cascade that occurred at Buncefield. The reasons for this are discussed in Appendix 1.

A parameterised entrainment model of this sort has been adopted to simplify application of the VCA method and avoid the need for the direct solutions of the equations given in Appendix 2.

3. DEVELOPED FREE CASCADES

Flow rates between 7 and 21 kg/s have been studied. In all cases the length of the discharge (along the tank rim) was 1500 mm and the height of the discharge was 10m above the concrete floor. The maximum width of the cascades (measured perpendicular to the wall) did not vary greatly with flow rate and in stable conditions and amounted to 350 – 400mm. This width can be judged from photographs and videos of the flow or - more satisfactorily – from profiles of liquid or vapour temperature in very stable conditions.

Commercial hexane was used for most experiments. A typical composition is shown below:

Table 1: Typical composition of commercial hexane used in the experiments

<i>Name</i>	<i>Content</i>	<i>Boiling point (°C)</i>	<i>Temperature for 40mmHg vapour pressure (°C)</i>
n-Hexane	53%	69	-2.3
2-methylpentane	17%	60.3	-9
3-methylpentane	15%	63.3	-7
Methylcyclopentane	13%	71	-0.6
Cyclohexane	2%	80	+6

The quantity of liquid discharged in Tests 1 to 11 was between 700 and 800 litres. It became clear that longer releases would provide much more reliable information on many of the key variables and a larger discharge chamber was constructed to allow releases of 2000-2200 litres for Tests 12 to 14. Improvements were also made to the design of the discharge chamber that removed a tendency to discharge instability at low flow rates.

In parallel with these increases in the scale of the experiments, additional instrumentation was progressively installed as the test programme developed and understanding of the detailed technical issues to be addressed was refined.

The quality of the data obtained primarily depended on the stability of the atmosphere. The production of a very large vapour cloud similar to that at Buncefield depends on an extremely low windspeed and the idealised problem of a cascade in zero ambient flow is of most interest. Successful tests have been carried out in both highly stable conditions (i.e. a strong morning inversion layer) and on calm overcast days with low thermal gradients.

Both types of condition are suitable for the study of the development of the cascade. The larger scale dispersion of the ground vapour current is somewhat problematic if there are very stable thermal gradients – especially if the test only lasts a few minutes. This is because after a few tens of metres the rapidly diluting vapour current cannot displace the cold ambient air layer close to the ground.

If there is strong solar radiation it is not possible to study either cascades or long range dispersion. This is because stray thermals destabilise the cascade. On clear, calm summer days experiments can only be done satisfactorily at first light.

3.1 INSTRUMENTATION

Five types of temperature measurement were made:

1. Bare 1.5mm diameter stainless steel sheathed thermocouples to monitor the development of the vapour current outside the cascade.
2. Bare 0.5mm diameter stainless steel sheathed thermocouples to monitor the development of the vapour current (and assess time response of larger thermocouples)
3. Liquid temperature thermocouples in pots
4. Aspirated vapour temperature thermocouples
5. Bare thermocouples immersed in the liquid flow across the impact surface.

Other measurements made included ambient temperature at various elevations, liquid discharge temperature (on the discharge chute), relative humidity and commercial hexane composition.

Figures 7 and 8 shows an annotated photograph of instrumentation used in Test 14.

3.1.1 VAPOUR TEMPERATURES OUTSIDE THE CASCADE

Comparison of temperature records from co-located 1.5mm and 0.5mm thermocouples suggested that the typical response time in conditions of use (even for the larger size) was around 5 seconds. The success of the experiment depended on establishing and maintaining stable flows for much longer than this so both types of thermocouple were suitable for use.

3.1.2 LIQUID TEMPERATURES

The thermocouples designed to measure liquid temperature were located in small upward facing Perspex pots to maintain liquid cover on the thermocouple near the base (Figure 8). This was done to prevent the rapid evaporative cooling observed in wetted thermocouples exposed to unsaturated air. This design proved successful at least in the most important areas within the cascade where the liquid flow density was large. The time response of the arrangement is governed by the liquid exchange time of the pot. The typical liquid flux density in the test was 25 kg/m²/s or 38 mm linear fill per second. The pots in the cascade were consequently refilled every few seconds. Again the success of the experiment depended on establishing and maintaining stable flows for much longer than this so the time response was certainly adequate. Predictably it proved difficult to measure liquid temperatures where there was little or no liquid flow.

The technique proved so successful and informative that the number of liquid pots was progressively increased during the campaign: from 1 to 4 then finally 16. In all cases profiles of final liquid temperature in the cascade were obtained at an elevation of 400mm.

Figure 9 shows liquid temperature profiles in a typical test of a free cascade in fairly stable conditions.

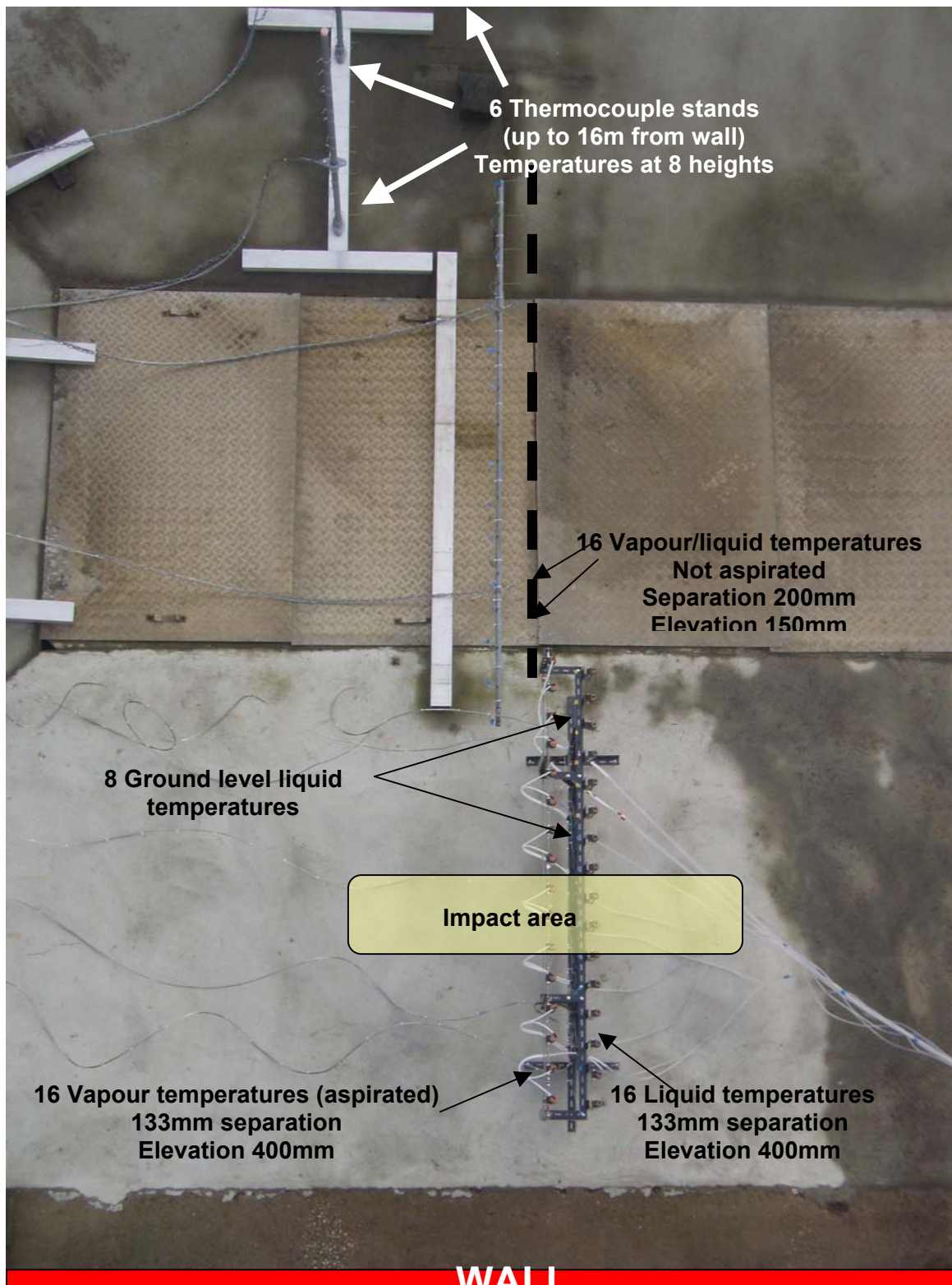


Figure 7: Instrumentation used in the final test (Test 14). Instrument arrays are supported on rods to clear the ground level liquid flow. Previous tests did not have the 150mm elevation array or ground level array. They did however have thermocouple trees at 3200mm and 4200mm from the wall. These were removed to minimise possible disturbance of the vapour and liquid ground flows.

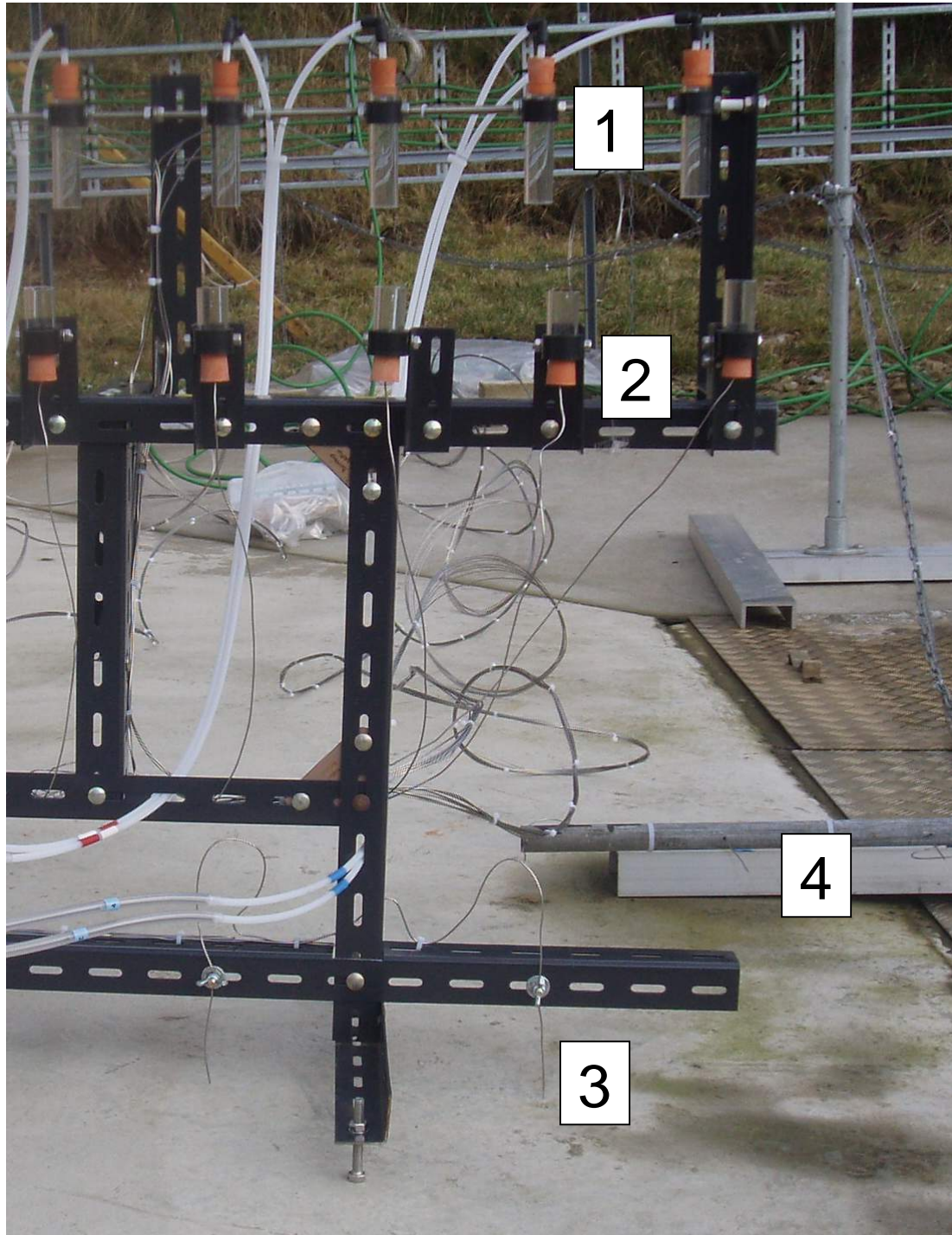


Figure 8: Close up showing instrumentation used in Test 14. The camera angle makes liquid and vapour temperature tube inlets appear at different heights. Perspex sample tubes are OD 22mm and ID 16mm.

Vapour temperature aspirated tubes [1] are 100mm long with a central thermocouple. Aspirating flow is an average of 1 m/s across the sample tube section.

Liquid pots [2] are 50mm deep, with a thermocouple 10mm from the centre of the base.

Ground level liquid thermocouples [3] and vapour current (150mm elevation) thermocouples [4] are 1.5mm stainless sheathed.

Liquid temperature profiles

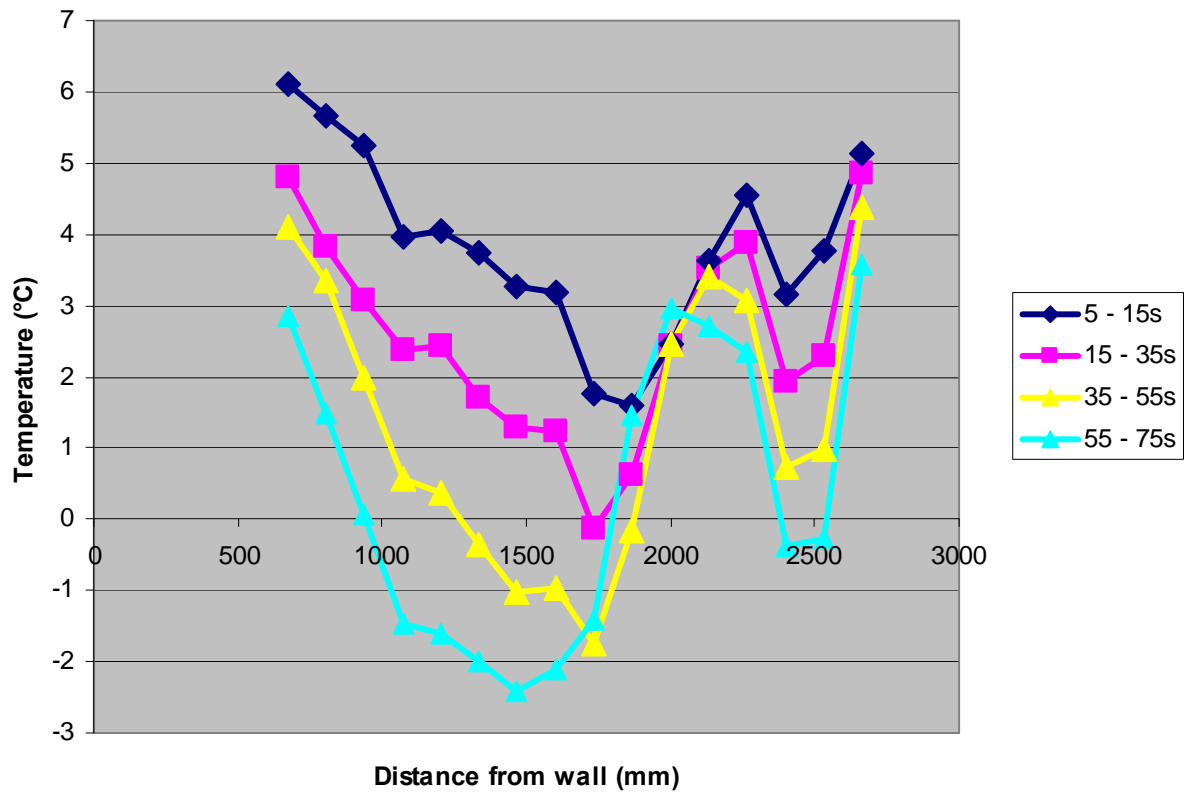


Figure 9: Average liquid temperatures at different times after the start of Hexane Test 12 (15 kg/s Hexane 12.6°C, Ambient 10°C Neutral stratification conditions). Liquid flow is almost exclusively confined to the region between 2000 and 2400mm from the wall. Below - snap shot of the flow at around 30 seconds.

There is an initial period of around 10 seconds when the heat capacity of the collection pot depresses the observed temperature drop. After that the maximum liquid temperature drop (in the core of the cascade) and the width of the cascade flow remain fairly stable until near the end (55-75 seconds). At this stage video records show some deterioration in cascade stability which causes a broadening of the peak in temperature and an increase in the apparent maximum temperature drop.

It is important to note that the temperatures recorded by thermocouples within collection pots provide a mass weighted average temperature. If the mass flux and temperature both vary in a correlated way (which is very much the case at the edge of the cascade) the output is biased towards the temperature during periods of high mass flow. This actually makes the output more directly useful for comparison with thermodynamic analysis.

To illustrate this point Figure 10 shows a comparison between the measured liquid temperature drop and that to be expected in equilibrium conditions. These results are significant, and are considered in more depth later, but what is interesting is that useful liquid temperature measurements were obtained in all cases – even in some early tests when the discharge was relatively unstable because of leakage through the tank plenum. Even if the cascade moved around, the liquid pot retained and measured material characteristic of the core (where the mass flux was very large).

3.1.3 VAPOUR TEMPERATURES

Measuring the vapour temperature (separately from liquid temperatures) is a challenge in such a dense liquid cascade. Aspirated thermocouples in downward facing perspex tubes were used with an aspiration flow low enough (1 m/s average across the tube cross-section) to prevent the drawing of fine droplets upwards and into contact with the thermocouple. The technique was successful although recirculation of gas and heat transfer to the inner face of the tube led to a relatively long time constant for response (several tens of seconds). In favourable circumstances stable conditions were maintained over a longer period than this and satisfactory measurements were obtained.

In all cases profiles of vapour temperature in the cascade were obtained 400mm above the ground .

Figure 11 shows vapour temperatures in Test 12 that correspond to the liquid temperatures shown in Figure 9. It takes at least 30 seconds for the output temperature to approach its final value. It is apparent from Figure 12 that the vapour temperature drops further than that of the liquid. This is surprising at first sight but is a consequence of the wide range of droplet sizes in the cascade. Small droplets transfer mass to, and remove heat from, the vapour very efficiently. They drive the relatively large drop in vapour temperature. Larger drops simply do not have time to lose as much heat because of their low surface area to volume ratio and since larger droplets dominate the liquid mass flow the overall temperature drop of the liquid collected in pots is less. A quantitative analysis of heat and mass transfer in both the cascade and splash zone is given in later.

Cacade area 0.6 m2, Drop 10m

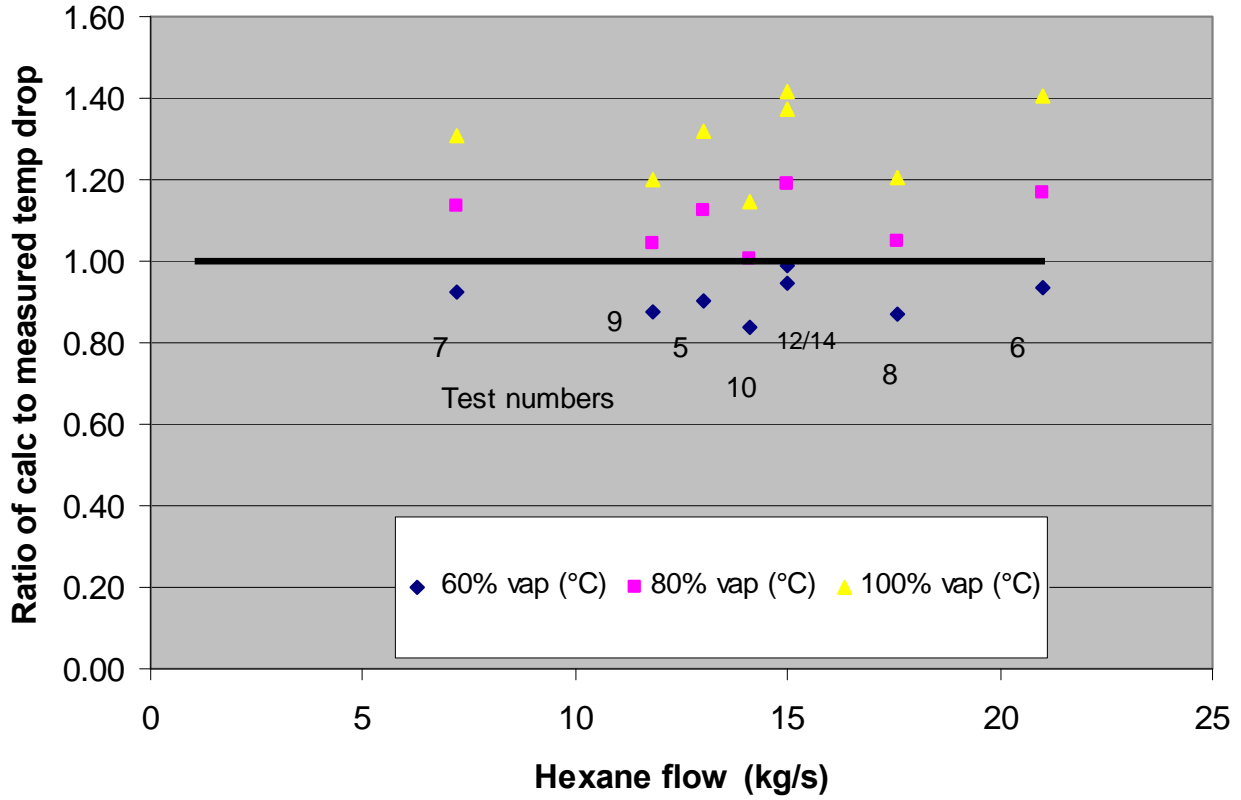


Figure 10: Representative measurements of liquid temperatures could be made even for relatively unstable cascades with the collection pots being filled from the core of the cascade where mass fluxes are very high.

Vapour temperature profiles

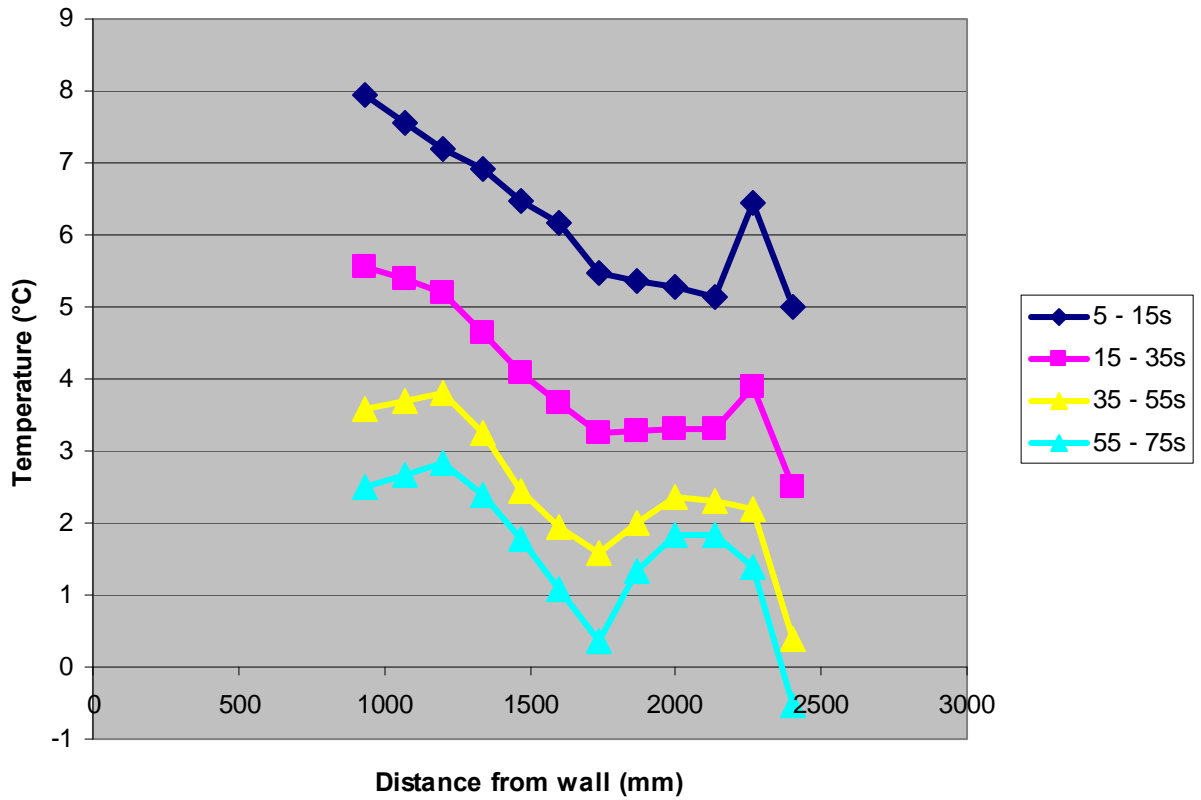


Figure 11: Average vapour temperatures at different times after the start of Hexane Test 12 (15 kg/s Hexane 12.6°C, Ambient 10°C Neutral stratification conditions). Liquid flow is almost exclusively confined to the region between 2000 and 2400mm from the wall.

Liquid and vapour temperature profiles

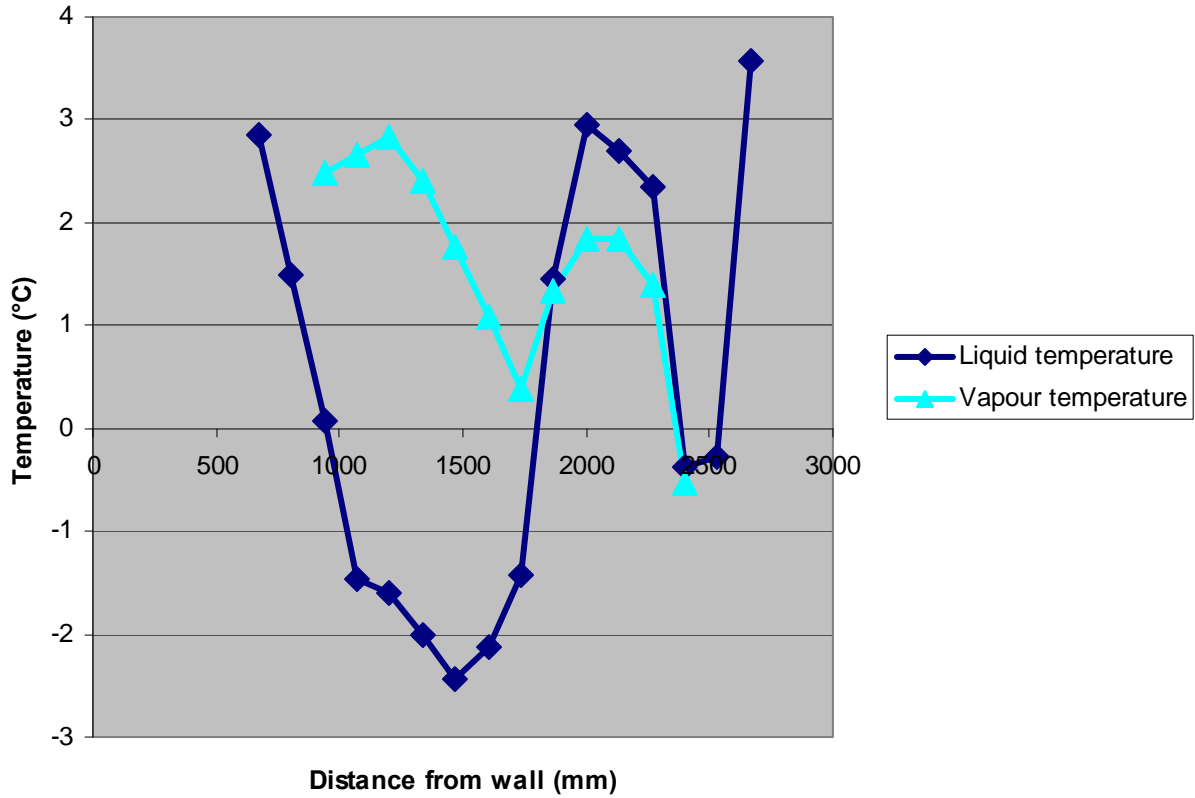


Figure 12: Comparison of final liquid and vapour temperatures in Hexane Test 12 (15 kg/s Hexane 12.6°C, Ambient 10°C Neutral stratification conditions). Liquid flow is almost exclusively confined to the region between 2000 and 2400mm from the wall. In the core of the cascade the drop in temperature of the vapour is larger than the liquid – a consequence of the spread in droplet sizes.

3.2 FREE CASCADE RESULTS

Table 2 gives a summary of the results obtained for all of the free cascade experiments undertaken.

Table 2: Data summary for free cascade experiments

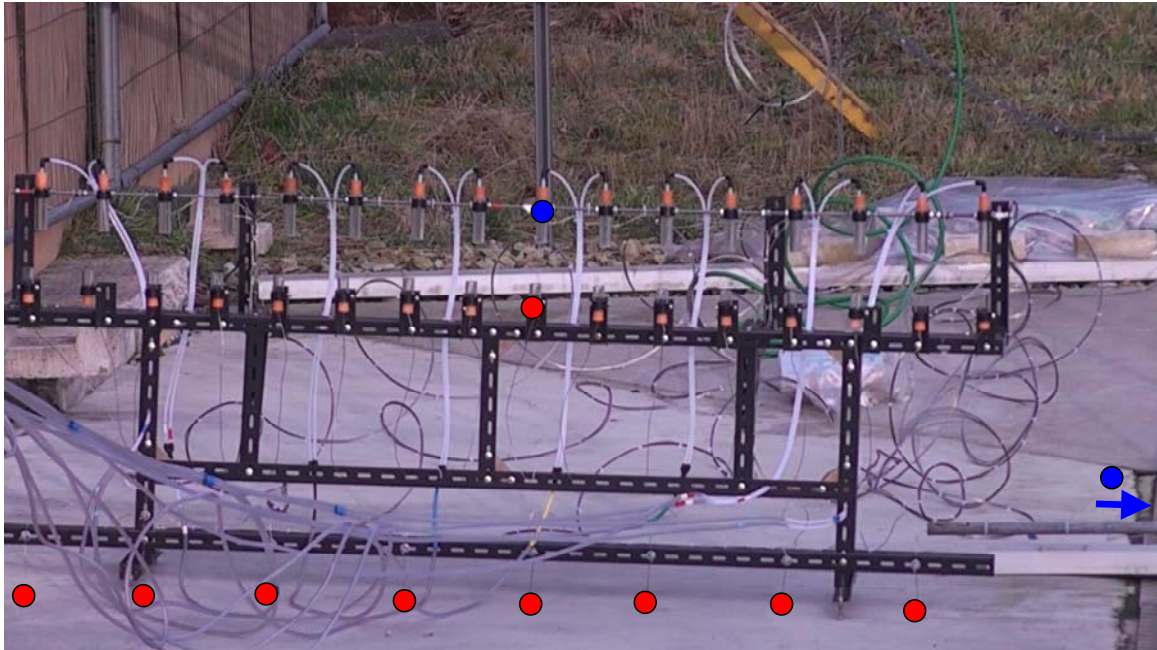
Test	Hexane supply rate (kg/s)	Entrained air (calc) (kg/s)	Hexane supply temperature (°C)	Ambient air temperature (°C)	Measured final liquid temperature (°C)	Measured drop in liquid temperature (°C)
5	13	6.39	0.8	2.3	-5.5	6.3
6	21	7.1	1.4	4.9	-3.3	4.7
7	7.2	5.5	2.4	4.4	-5.7	8.1
8	17.6	6.84	6.4	5	-1.4	7.8
9	11.8	6.24	6.4	6	-2.6	9
10	14.1	6.51	10.3	8.5	0.25	10.1
12	15	6.6	12.6	10	4	8.6
14	15	6.6	3.3	3	-2.5	5.7

The final equilibrium thermodynamic state of the hexane/air mixture was calculated and is compared with the observations in Figure 10. The effect of condensation of atmospheric moisture is relatively small at these low temperatures but it has been included. The method of calculation of air entrainment is described in Reference 2. The essentials of the method are reproduced in Appendix 2.

It is clear that the cascade of hexane droplets does not reach equilibrium with the co-flowing air. Figure 10 also shows two additional sets of thermodynamic results obtained by assuming the final state is one in which the temperature is common to the phases but the partial pressure of the solvent is a fixed proportion (80% and 60%) of its saturation value. The results suggest that the extent of vaporisation is roughly 70% of that which could occur if the system fully reached equilibrium.

These are approximate figures that take no account of the vapour temperature profile in the developed cascade (which is typically different to the liquid profile). This approximation is not as crude as it might appear, because the heat capacity of the system is dominated by the liquid and the drop in liquid temperature gives quite a clear indication of the degree of vaporisation. For later tests in which more data were obtained it is possible to make more accurate estimates.

Figure 13 shows selected liquid and vapour temperature measurements made in Test 14 that can be used in such an analysis.



Highlighted liquid temperature measurement (Red) / Vapour temperature (Blue)

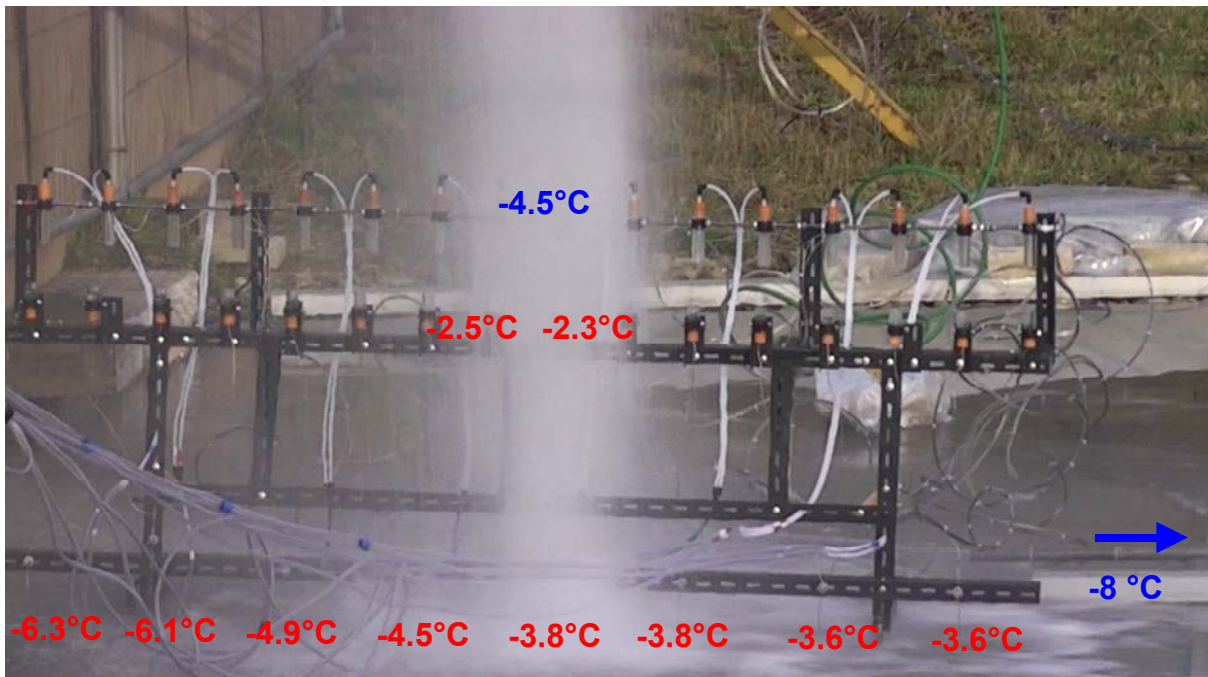


Figure 13: Selected average temperature measurements in Test 14. Liquid temperatures shown are at an elevation of 400mm or in the ground level liquid flow. The temperature (-8°C) indicated by the blue arrow is a (spray wetted) thermocouple 750mm from the impact zone.

3.3 MEASURED VAPORISATION EFFICIENCY IN THE CASCADE

Equilibrium calculation (Test 14) :

15 kg/s* Hexane	3.3 °C	drops to - 5.0 °C	Enthalpy change 286 kW	Hexane vaporisation 854 g/s
6.6 kg/s Air	3 °C	drops to - 5.0 °C	Enthalpy change 53 kW	Hexane vaporisation 157 g/s

Total rate of hexane vaporisation 1011 g/s

Measurements in cascade at a height of 400mm above floor

15 kg/s* Hexane	3.3 °C	drops to - 2.5 °C	Enthalpy change 194 kW	Hexane vaporisation 579 g/s
6.6 kg/s Air	3 °C	drops to - 4.5 °C	Enthalpy change 49 kW	Hexane vaporisation 147 g/s

Total rate of hexane vaporisation 726 g/s

*a small amount of hexane ends up as vapour – with a slightly different heat capacity

At this stage the rate of vaporisation is $726/1011 = 72\%$ of the predicted on the basis of an equilibrium assumption. The hexane vapour concentration is 0.036% v/v.

3.4 ANALYSIS OF HEAT AND MASS TRANSFER IN THE CASCADE

It is useful to examine the basic mass and heat transfer processes in the cascade. This helps to explain the closeness of approach to equilibrium, the role of smaller droplets and allows a proper appreciation of how variations in input conditions are likely to affect outcomes.

The mass loss rate of a droplet of diameter d is

$$\frac{dm}{dt} = \pi \cdot d \cdot (\rho_{gas} D) \cdot Sh \cdot \frac{W_c}{W_G} (X^* - X_g) \quad \text{Equation 1 [Reference 4]}$$

ρ_{gas} is the density of the vapour/air mix

D is the diffusion coefficient (of hexane through air in this case)

Sh is the Sherwood number $Sh = 2 + 0.6 \cdot Re^{1/2} \cdot Sc^{1/3}$

Sc is the Schmidt number i.e. the analogue of the Prandtl number for mass transfer processes.
 $Sc^{1/3} \sim 1$

W_c is the molecular weight of the contaminant (hexane)

W_g is the molecular weight of air

X^* is the saturated mole fraction at the gas temperature

X_g is the mole fraction of hexane in the gas through which the particle is moving

This can be rearranged to give an expression for the time taken for a particle to lose a fraction f of its mass (f should be fairly small compared to 1).

$$\Delta t = \frac{f}{6} \cdot \frac{\rho_{liq}}{\rho_{gas} D_{gas}} \cdot \frac{1}{Sh} \cdot \frac{W_G}{W_c} \cdot \frac{1}{(X^* - X_g)} \cdot d^2$$

The time taken for evaporation is extremely sensitive to droplet size.

To reach an equilibrium state droplets in a typical cascade (e.g. Test 14) have to lose about 7% of their mass. Equation 2 allows us to determine how long this would take if they were falling through gas at different levels of saturation.

Case 1: Clean Air – 2 mm diameter drops

Substituting as follows:

$$f=0.07, \quad D_{gas} = 7 \times 10^{-6} \text{ m}^2/\text{s}, \text{ [Reference 5]} \quad \rho_{gas} = 1.3 \text{ kg/m}^3, \quad \rho_{liq} = 650 \text{ kg/m}^3,$$

$$Sh = 17 \text{ (Re} = 642), \quad Wc = 86, \quad Wg = 29, \quad X^* = 0.05 \text{ (at the eqm temperature),}$$

$$Xg = 0 \text{ (Clean air), } d = 0.002 \text{ (m)}$$

$$\text{Time for 7\% evaporation} \quad \Delta t = 1.5 \text{ seconds}$$

Case 2: Air 75 % saturated - 2mm diameter drops

Substituting as above and:

$$Xg = 0.75 X^* \text{ (75\% saturated), } d = 0.002 \text{ (m)}$$

$$\text{Time for 7\% evaporation} \quad \Delta t = 6.4 \text{ seconds}$$

$$\text{Time for } 0.75 \times 7\% \text{ (5.25\% evaporation) } = 4.8 \text{ seconds}$$

The time taken for 2mm droplets to fall 10m within the cascade can be calculated straightforwardly (Appendix). The result is 1.53 seconds for a mass flux density of 25 kg/m²/s. The mass density in the cascades is quite high, so the time of drop is not much in excess of the in free fall value, which is 1.4 seconds.

These results show that droplets of 2mm alone would not be expected to vaporise sufficiently to reach the observed saturation level of around 75% during the drop. Heat and mass transfer are strongly affected by the much smaller droplets that are produced in droplet break up events. It is

not possible to develop this analysis further without detailed information about the mass of these smaller droplets.

The spectrum of droplet sizes generated in droplet breakup and splashing processes is discussed in Reference 6. It is useful to compare these rates of mass transfer from large drops with those from the typical small droplets generated in breakup and splashing processes – which are around 100 microns in diameter.

Case 3: Clean Air – 100 micron diameter drops

Substituting as follows:

$$f=0.07, \quad D_{\text{gas}} = 7 \times 10^{-6} \text{ m}^2/\text{s}, \quad \rho_{\text{gas}} = 1.3 \text{ kg/m}^3, \quad \rho_{\text{liq}} = 650 \text{ kg/m}^3, \quad Sh \sim 3$$

$$Wc = 86, \quad Wg = 29, \quad X^* = 0.05 \text{ (at the eqm temperature)}, \quad Xg = 0 \text{ (Clean air)}, \quad d = 0.0001 \text{ (m)}$$

$$\text{Time for 7\% evaporation} \quad \Delta t = 0.023 \text{ seconds}$$

Case 4: 75% saturated air– 100 micron diameter drops

Substituting as follows:

$$f=0.07, \quad D_{\text{gas}} = 7 \times 10^{-6} \text{ m}^2/\text{s}, \quad \rho_{\text{gas}} = 1.3 \text{ kg/m}^3, \quad \rho_{\text{liq}} = 650 \text{ kg/m}^3, \quad Sh \sim 3$$

$$Wc = 86, \quad Wg = 29, \quad X^* = 0.05 \text{ (at the eqm temperature)}, \quad Xg = 0.75 X^*, \quad d = 0.0001 \text{ (m)}$$

$$\text{Time for 7\% evaporation} \quad \Delta t = 0.092 \text{ seconds}$$

These results show that 100um drops generated in break-up and collision events in the cascade will start to vaporise very much more rapidly than larger droplets – and that this will occur even if the saturation level rises.

In this case it is reasonable to assume the Sherwood number does not change much with size and in this case the droplet mass loss equation can be integrated in closed form.

$$t = \frac{1}{2k} (d_0^2 - d^2) \quad \text{Equation 3}$$

$$\text{where} \quad \frac{1}{2k} = \frac{1}{4} \cdot \frac{\rho_{\text{liq}}}{\rho_{\text{gas}} D_{\text{gas}}} \cdot \frac{1}{Sh} \cdot \frac{W_G}{W_c} \cdot \frac{1}{(X^* - X_g)}$$

This gives an estimate for the time taken for complete evaporation

$$t_{\text{complete.evaporation}} = \frac{1}{2k} d_0^2$$

In clean air (Case 3 $X_g = 0$) complete vaporisation of 100um drops takes around 0.39 seconds. In a 75% saturated atmosphere (Case 4 $X_g = 0.75 X^*$) complete vaporisation takes around 1.5s.

Small droplets generated in the cascade will tend to evaporate completely. This agrees with the photographic observations of the cascade; the droplet distribution is concentrated around the 1-2mm size (Figure 14). Observations of droplet breakup processes do show the generation of much smaller fragments but these apparently vaporise rapidly and consequently do not accumulate in large numbers.

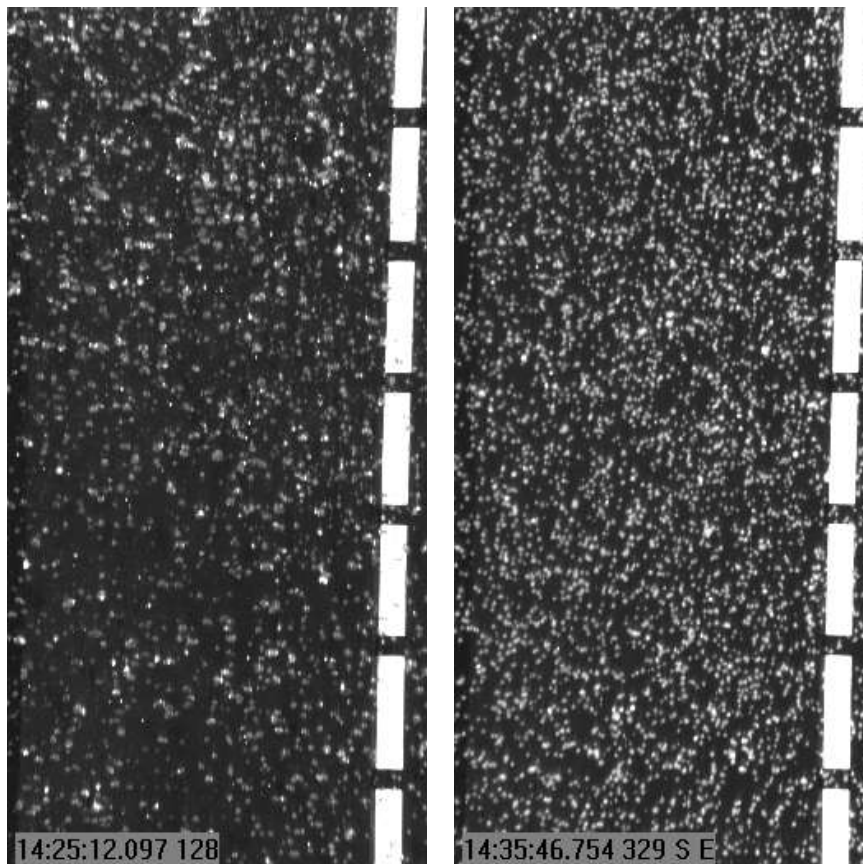


Figure 14a: Droplets are smaller and more uniform in a petrol spray (right) than for water (left) in similar conditions.

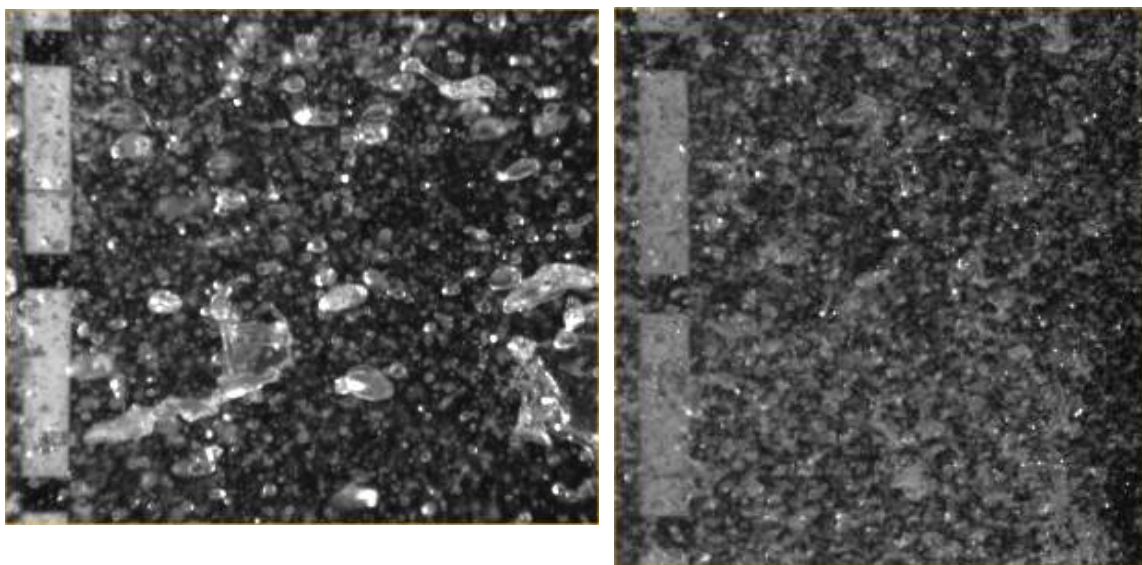


Figure 14b: Comparison between cascade droplet structure in water (left) and decene (right) in similar conditions

4. IMPACT ZONE

Figure 13 shows the impact zone at the base of the cascade and some results of measurements around this area. Vapour temperatures are extremely difficult to measure because of the three-dimensional, unsteady character of the flow and the dense fine splash spray. Liquid temperatures on the floor can however be easily and reliably recorded.

A precise calibration of thermocouples above the impact zone and on the floor is clearly of great importance as the difference between two sets of devices must be taken to determine the rate of liquid cooling within the impact zone. A specially detailed check of relative calibration was made between liquid thermocouples just above the impact zone and those in the floor flow. This was done by simultaneously immersing thermocouples in well-stirred pots of water at a range of temperatures.

This exercise confirmed the results shown in Fig 13. The average liquid temperature falls rapidly as the liquid moves into the impact zone and hits the ground.

Initial (discharge) liquid temperature	= 3.3 °C
Equilibrium temperature	= -5°C
Liquid temperature 400mm above impact	= -2.5 °C
Liquid temperature at floor level	= -3.8 °C

The equilibrium temperature for this cascade (including the small amount of enthalpy released by water vapour condensation) is -5°C .

Unfortunately there are no measurements of liquid or vapour immediately leaving the impact zone. The nearest (wetted) thermocouple (750mm from impact) registered about -8°C . By this stage substantial amounts of additional air would have been entering the vapour current lowering the saturation level and allowing evaporative cooling of a wetted thermocouple (and liquid droplets) below the temperature of the vapour.

Notwithstanding the lack of direct measurements there is enough information from other measurements to put quite close limits on the vapour temperature leaving the impact zone. Some relevant arguments are given below:

1. Measurements outside the spray area show that the amount of spray is relatively small (~1% total mass flow). This means the heat capacity of the outflow is dominated by vapour.
2. Given the rapid approach to equilibrium and high saturation level, the liquid and vapour must be close to thermal equilibrium. Because the amount of liquid is small anyway, minor deviations from the vapour temperature makes very little difference to the heat balance. For the purposes of calculating vapour temperature any deviation in liquid temperature can be ignored.
3. The vapour temperature can only marginally exceed the equilibrium temperature – otherwise the saturation level would rise above 100%.

This last point can be illustrated with a heat balance calculation

14 kg/s	Hexane	3.3 °C	drops to -3.8 °C	Enthalpy change 228 kW	or Hexane vaporisation	680 g/s
1kg/s	Hexane	3.3 °C	drops to -4.5 °C	Enthalpy change 18 kW*	or Hexane vaporisation	53 g/s
6.6 kg/s	Air	3 °C	drops to -4.5 °C	Enthalpy change 49 kW	or Hexane vaporisation	147 g/s

Total rate of hexane vaporisation (minimum) 880 g/s

Vapour pressure of hexane = $29/86 \cdot 880/(6600+880 \cdot 29/86) = 4.4\% \text{ v/v}$ (33 mmHg)

Saturated vapour pressure of hexane at -4.5 °C is 35 mmHg

The saturation level is still just under 100%.

If the vapour temperature were as low as -8°C (the reading from the nearest wetted thermocouple)

14 kg/s	Hexane	3.3 °C	drops to -3.8 °C	Enthalpy change 228 kW	or Hexane vaporisation	680 g/s
1kg/s	Hexane	3.3 °C	drops to -8 °C	Enthalpy change 20 kW*	or Hexane vaporisation	59 g/s
6.6 kg/s	Air	3 °C	drops to -8 °C	Enthalpy change 72 kW	or Hexane vaporisation	216 g/s

*a small amount of hexane ends up as vapour – with a slightly different heat capacity

Total rate of hexane vaporisation (maximum) 955 g/s

Vapour pressure of hexane = $29/86 \cdot 955/(6600+955 \cdot 29/86) = 4.7\% \text{ v/v}$ (36 mmHg)

Saturated vapour pressure of hexane at -8 °C is 29 mmHg

The saturation level is now well over 100%. Such a low vapour temperature is not possible.

These simple heat balance calculations do not take into account water condensation but even if this is done the vapour temperature must be close to equilibrium temperature, which is -5°C. The extent of vaporisation must be around 900 g/s - which is 90% of the level possible in full equilibrium.

Comparing this figure with the degree of vaporisation in the flow entering the impact zone (72%) shows that liquid fragmentation and high gas/droplet slip velocities in the impact zone have driven the flow much closer to equilibrium.

A relatively large proportion of the liquid must be finely divided by break up in the sharply decelerating flow close to the ground or in droplet impact. This is clear from the difference between the liquid temperature on approach and in the ground level drainage.

Assume a proportion M_{splash} of the liquid splashes and is cooled to -5°C and rejoins the liquid and a proportion M_{stick} simply joins the liquid without splash. The measured final liquid temperature is -3.8 °C which means that:

$$-5^{\circ}\text{C} \times M_{\text{splash}} + -2.5^{\circ}\text{C} \times M_{\text{stick}} = -3.8^{\circ}\text{C} , \quad (M_{\text{stick}} + M_{\text{splash}}) = 1$$

Fraction splashing = M_{splash} = 52%

This is not unreasonable – splash fragment mass fractions in the relevant regime typically vary between 20 and 110% depending in the depth of the impacted liquid layer.

These fine fragments are generated very close to the liquid surface and almost all will be immediately driven back into the liquid very close to the impact point. A small proportion of the finest droplets are picked up by the flow and transported away from the surface by turbulence. These fine fragments appear in the vapour current leaving the impact zone – measurements in the next section suggests that they make up roughly 1-2% of the total liquid release.

As a footnote to this discussion on the impact zone it is worth noting that there is a flow of liquid backwards (towards the wall) out of the impact zone. The concrete floor is inclined down - away from the wall - and towards a sump so this liquid flow rapidly thins and slows. These free cascades have a diffuse inner boundary – all the way down liquid becomes detached from the main cascade and falls as a diffuse, distributed spray between the main cascade and the wall (Figure 15). The liquid in this diffuse spray becomes colder than liquid in the main cascade and impact and splashing of this material produces a marked cooling effect on the low mass flux parts of the back flow (Figure 13).



Figure 15: Development of a free cascade (21 kg/s). A diffuse spray separates from the inner edge of the cascade and falls between the main flow and the tank wall.

5. VAPOUR CURRENT

What emerges from the impact zone is a two phase flow comprising cold vapour and fine splash products. This section seeks to characterise the splash products carried out of the impact zone by addressing the following questions:

1. How much additional mass is carried out of the impact zone as a fine spray
2. How much of this mass of fine droplets then vaporises?
3. How close to equilibrium are the two phases as they exit the impact zone?
4. How does this change as additional air is entrained into the flow?

The objective is to determine how important splashing is in the overall source term and develop appropriate methods to include its effects.

The liquid mass density is much too high to have any chance of measuring spatially resolved vapour temperatures in the actual impact region but just outside there is much less liquid and the records of bare thermocouples are useful - although for the first few metres they are intensively impacted by fine droplets of liquid and have to be interpreted with care.

An array of 16 bare thermocouples were used in Test 14 to measure the vapour current temperature (at an elevation of 150mm) between about 750 and 3750 mm from the impact point (2750 to 5750mm from the wall).

Figure 16 shows typical results. The chute thermocouple is immersed in the outflow liquid and then exposed to air when the release stops. This gives a clear indication of the outflow temperature and the release end point but it also shows the typical variation of recorded temperature after the release. The thermocouple is exposed to air and undergoes rapid evaporative cooling. Eventually it dries and the temperature recorded climbs to the air temperature. A similar pattern is exhibited by the wetted thermocouple close to the impact zone.

On the other hand the reading from the thermocouples that are unwetted at the end recover to close to the air temperature immediately. Figure 17 shows results from all of the thermocouples in this array. The closest thermocouple (407) is approximately 750mm from the impact point. Others follow at intervals of 200mm moving away from the cascade impact.

The impact point is around 2000mm from the wall. Devices closer than about 2000mm (407 to 401) are always wetted. Others further than 4700mm from the impact zone (505 to 500) are never wetted. In the range 4000 - 4700mm (400, 506 and 507) thermocouples are intermittently wetted. Some temperature profiles are shown in Figure 18.

It is clear that the vapour current divides into two zones. For the first 2500mm or so the entraining gas flow carries a fine spray of liquid with which it interacts strongly. After this the flow is simply vapour and dilutes in a straightforward way as additional air is mixed in.

5.1 VAPOUR CURRENT DILUTION BEYOND THE ZONE AFFECTED BY LIQUID SPRAY

The sequence of this report, following from liquid release through the cascade to impact zone and so on, is interrupted here. The data from unwetted thermocouples in the later (liquid free) section of the vapour current is somewhat easier to interpret and analyse.

Longer range vapour current dispersion data are shown in Figure 19. These records and the measurements 505 to 500 in Figure 17 show the difficulties associated with analysis of the development of the vapour current – the recorded temperatures vary significantly with time over the duration of the release.

The main source of this variation is weak currents of air. The magnitude of these currents is small compared with the velocities induced by the release. Videos of the release show no sign of stirring in long blades of grass or loose strips of plastic prior to the discharge. Whereas, there is violent agitation of loose objects to a range of at least 10m whilst the release is in progress and this stops at the end.

The magnitude of the draughts is small so they probably have little effect on the shear at the top surface of the vapour current and rate of entrainment in the vapour current close to the cascade. Nevertheless, the incremental effect on the cascade over the fall means that the point of impact moves. Because the free cascades are much wider (1500mm) than they are thick (350-400mm) the vapour current is initially highly directional, shooting out forwards in a relatively narrow jet. Any sideways deflection consequently has a dramatic effect on the recorded temperature.

One solution to the problem of extracting meaningful data on the ideal (steady) case is to look at relatively short periods when the temperature is stable and the temperature drop is close to its maximum – at these time the centre of the vapour current is being sampled. An analogy for this strategy would be the measurement of decay in intensity of light in a scanning lighthouse beam. In this case the intensity measurements around the periods of maximum intensity should be selected.

This type of data analysis reveals a remarkably consistent picture of vapour current dilution over the area covered by thermocouple trees (up to about 16 m from the wall) see Figure 21. The form of variation of temperature at distances greater than 4700mm from the wall (approximately 2700mm from the impact centre) is typical for dilution of an axisymmetric momentum jet – the reciprocal of temperature drop varies linearly with distance. This is equivalent to a linear increase in total mass flux with distance from a virtual origin.

Tests 12 and 14 show similar patterns of dilution – with the temperature drop being systematically greater for Test 12. This difference is simply a result of the higher release temperature in Test 12 (Table 2) which leads to a higher level of vaporisation. If the (well defined) drop in liquid temperature in the cascade is used as a temperature scale the pattern of dilution in the two experiments is very similar (Figure 22).

Between the edge of the zone affected by splashing and a distance of 10m from the wall the flow is diluted by a factor of approximately five. These results for dilution should be regarded as preliminary. Further testing in extremely stable conditions is required.

Results from additional tests in the Buncefield Phase II project will be reported in 2013. These test were done in very stable conditions and the cascades were surrounded by a bund at various distances from the tank. High stability gave much clearer results but the conclusions drawn from the data reported here were substantially unaltered.

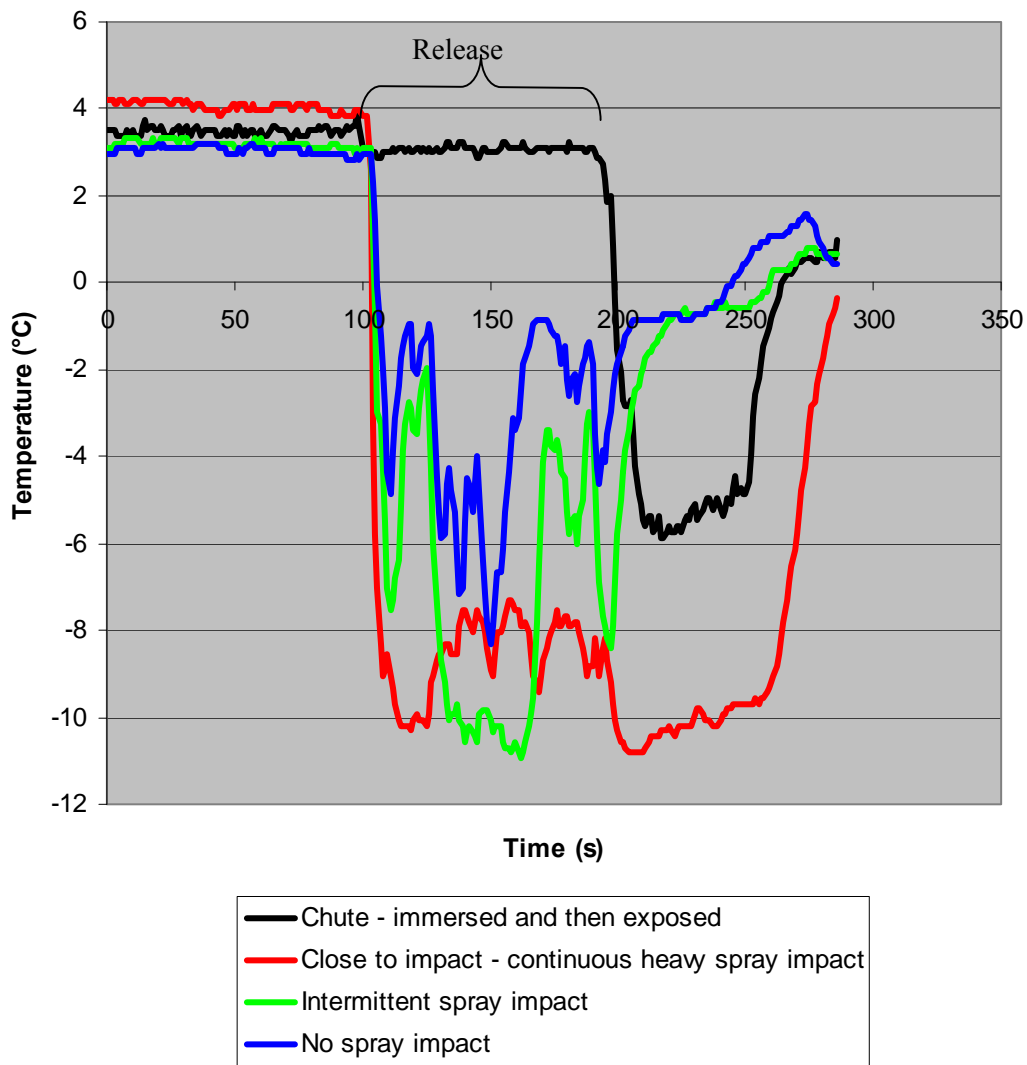


Figure 16: Chute and bare thermocouples 150mm above the ground.

The wetted TC (red) is ~950mm from the impact point. The unwetted thermocouple (blue) is beyond the range of the liquid spray. The intermittent thermocouple (green) is wetted by the spray at around 120s but then dries and measures vapour temperatures again. The chute thermocouple is immersed in the outflow liquid and then exposed to air when the release stops.

Results from additional tests in the Buncefield Phase II project will be reported in 2013. These test were done in very stable conditions and the cascades were surrounded by a bund at various distances from the tank. High stability gave much clearer results but the conclusions drawn from the data reported here were substantially unaltered.

Horizontal array at 150mm elevation All thermocouples

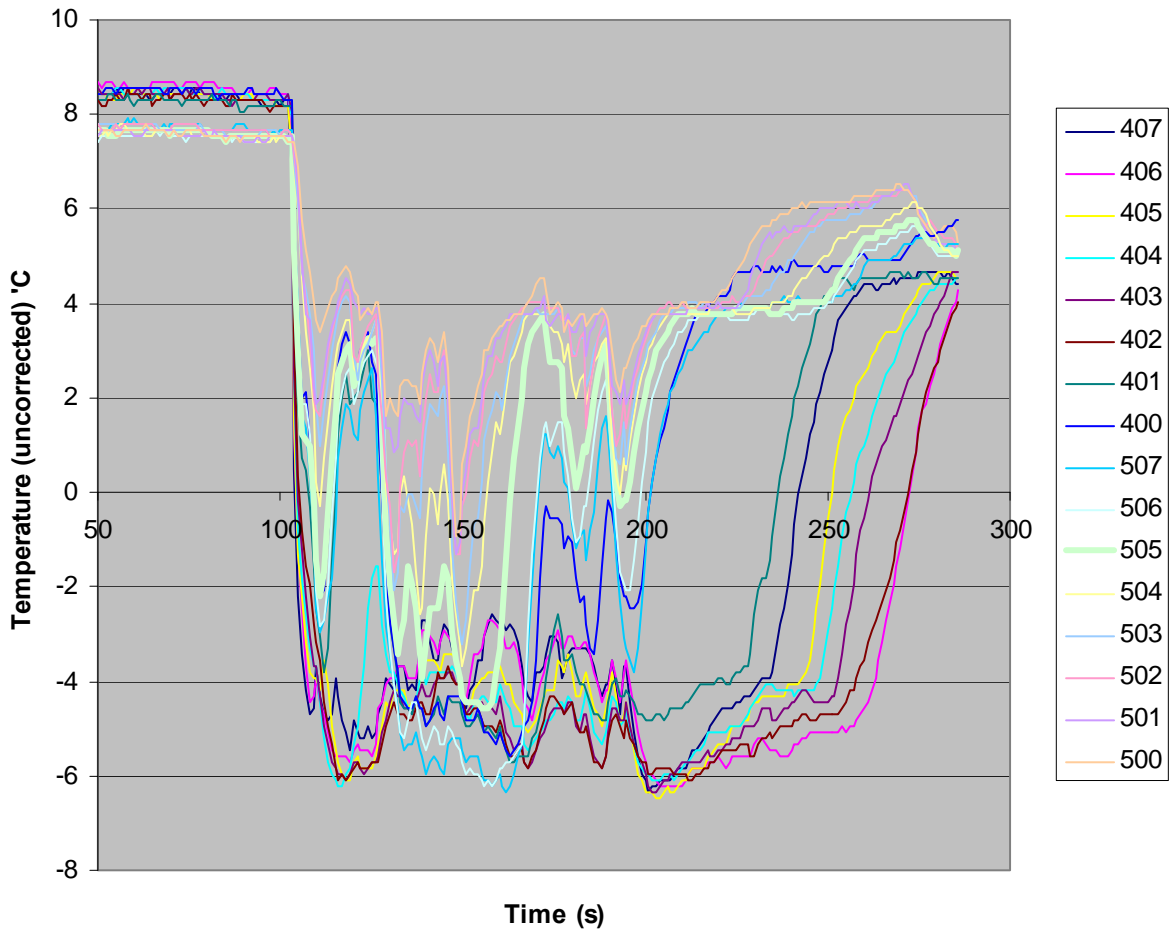


Figure 17: Bare thermocouples 150mm above the ground. The closest thermocouple (407) is approximately 750mm from the impact point. Other follow at intervals of 200mm moving away from the impact zone. Devices closer than about 2000mm (407 to 401) are always wetted. Others further than 4700mm from the impact zone (505 to 500) are never wetted. In the range 4000-4700mm (400, 506 and 507) thermocouples are intermittently wetted

The impact point is around 2000mm from the wall.

Note the “uncorrected” indication on temperature axis. Offsets have not been removed here as it is the form of the curves that is significant.

Results from additional tests in the Buncefield Phase II project will be reported in 2013. These test were done in very stable conditions and the cascades were surrounded by a bund at various distances from the tank. High stability gave much clearer results but the conclusions drawn from the data reported here were substantially unaltered.

**Temperature profiles close to the impact point in
various circumstances
(Ambient temperature 3 °C)**

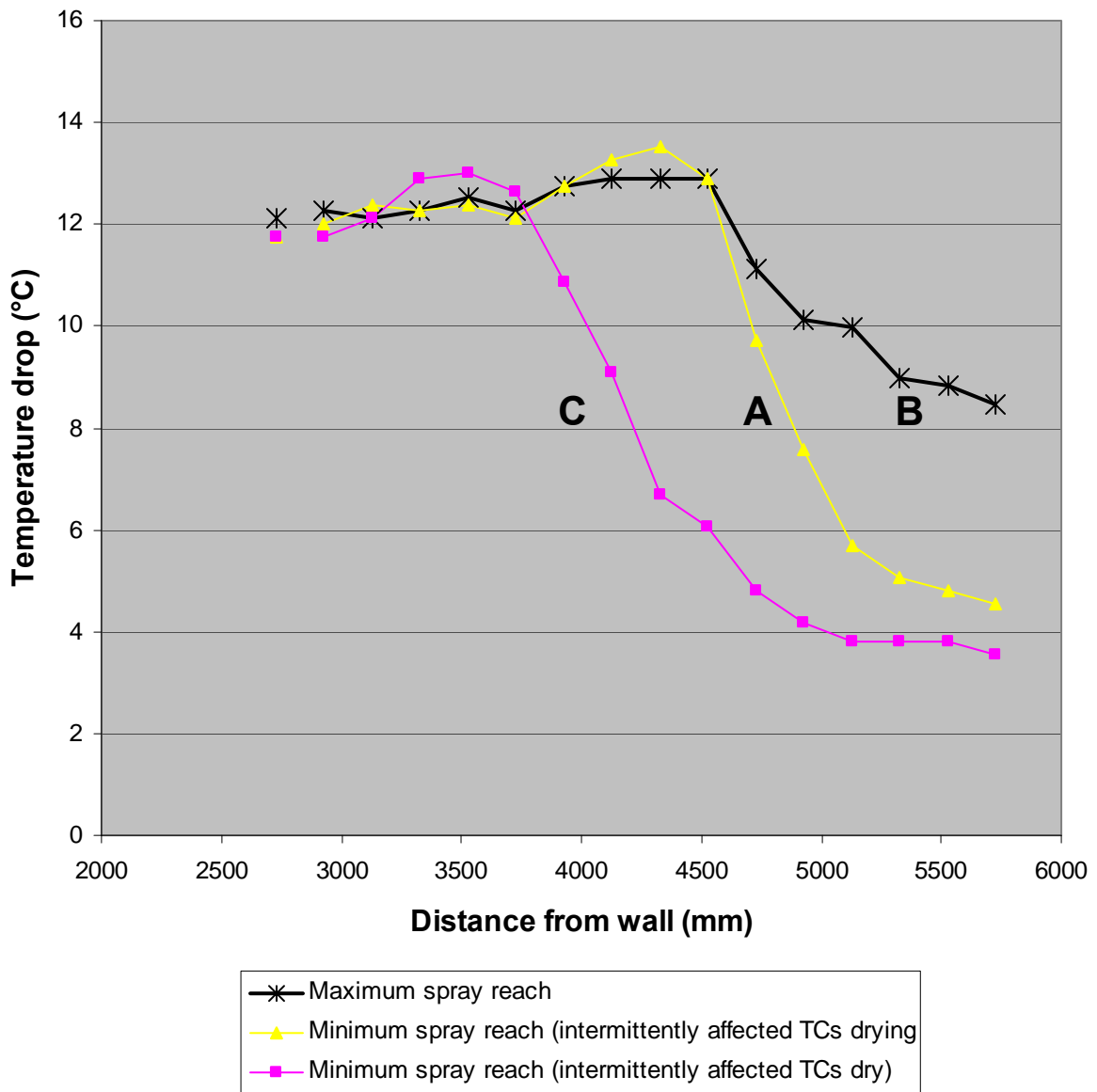


Figure 18a: Temperature profiles close to impact point recorded by bare thermocouples.

The reach of the spray varies by about 750mm. The readings of thermocouples in the intermittent region strongly depend not only on the instantaneous reach of the spray but on whether they have dried completely from previous exposures to spray.

The times A, B and C at which these profiles were obtained are detailed in the following graph (Figure 18b).

Horizontal array
All thermocouples - times for sample profiles shown

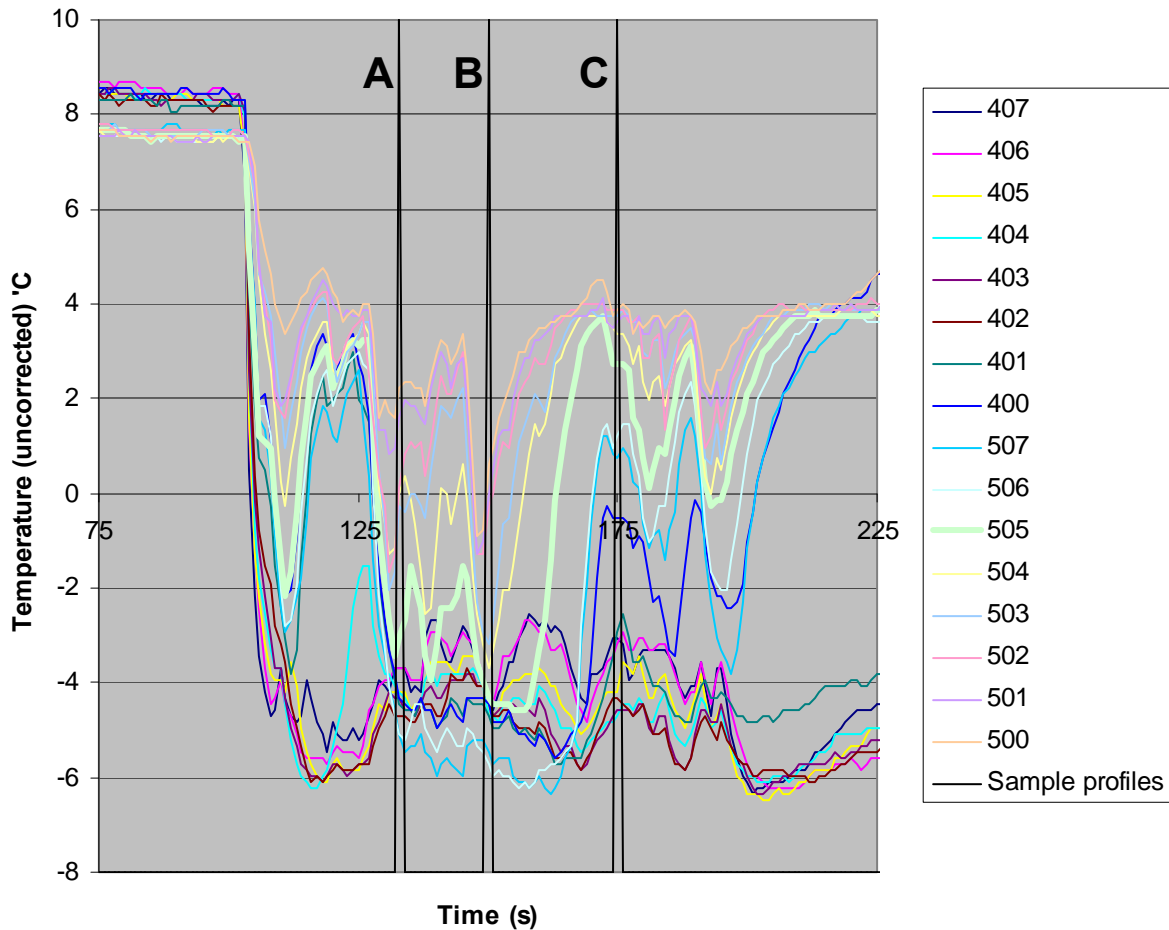


Figure 18b: This figure shows the times at which the temperature profiles in Figure 18a were measured.

A – A time of low spray reach. Thermocouples in the intermittent region have been previously wetted and are still drying (and consequently are showing the effects of evaporative cooling).

B – A time of high spray reach. Thermocouples in the intermittent region are being rewetted).

C – A time of low spray reach. Thermocouples in the intermittent region have dried out and are showing vapour temperatures.

Hexane 14 long range dispersion

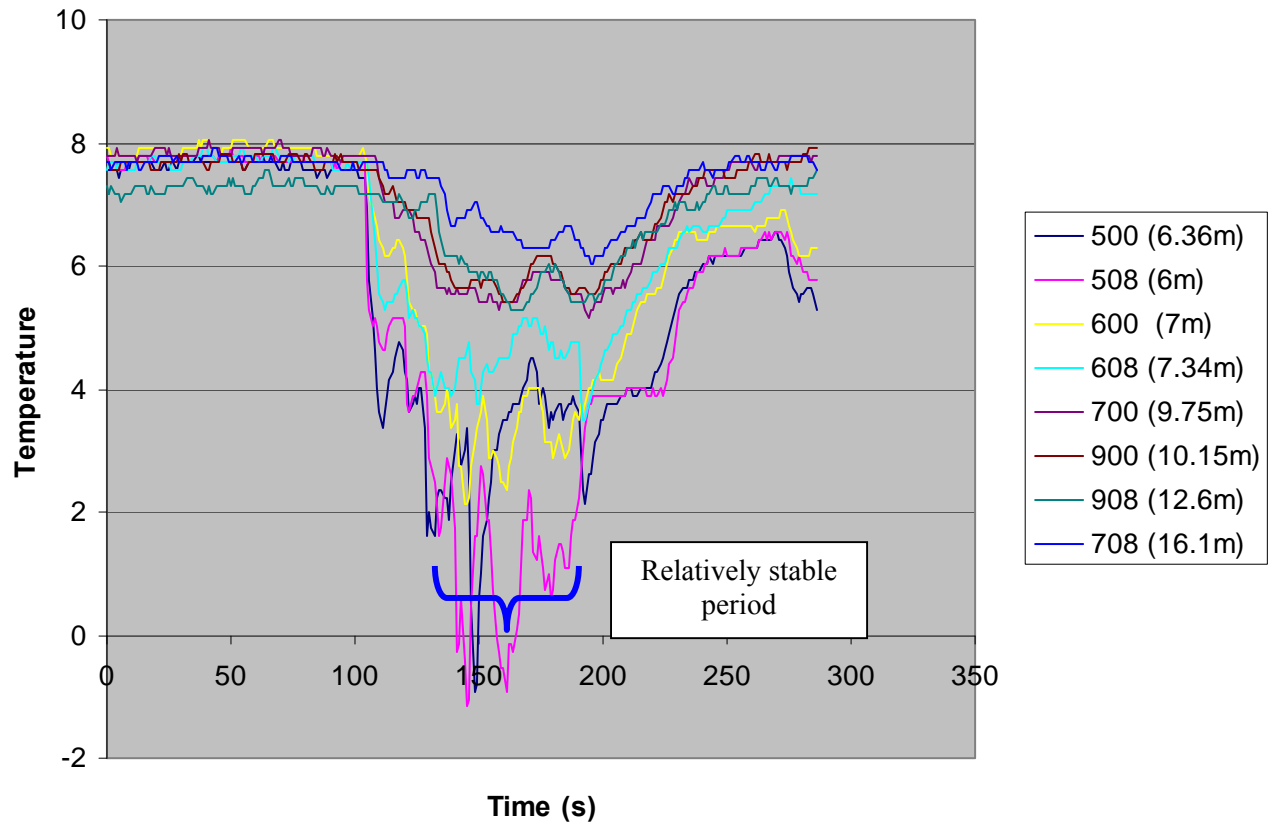


Figure 19: Typical longer range vapour current dispersion data - thermocouples at 250mm elevation. All data have a temperature offset of +4.6 degrees throughout.

The cascade is somewhat affected by a cross draft for about 30 seconds after the start. During this time the apparent width increases and the throw varies – see Figure 20. After this there is a period of around 60 seconds when the cascade appears stable and compact – this period yields the most useful data.

Results from additional tests in the Buncefield Phase II project will be reported in 2013. These test were done in very stable conditions and the cascades were surrounded by a bund at various distances from the tank. High stability gave much clearer results but the conclusions drawn from the data reported here were substantially unaltered.

Correlation between cascade throw (red) and temperature recorded (4.7 metres from wall, 150mm elevation)

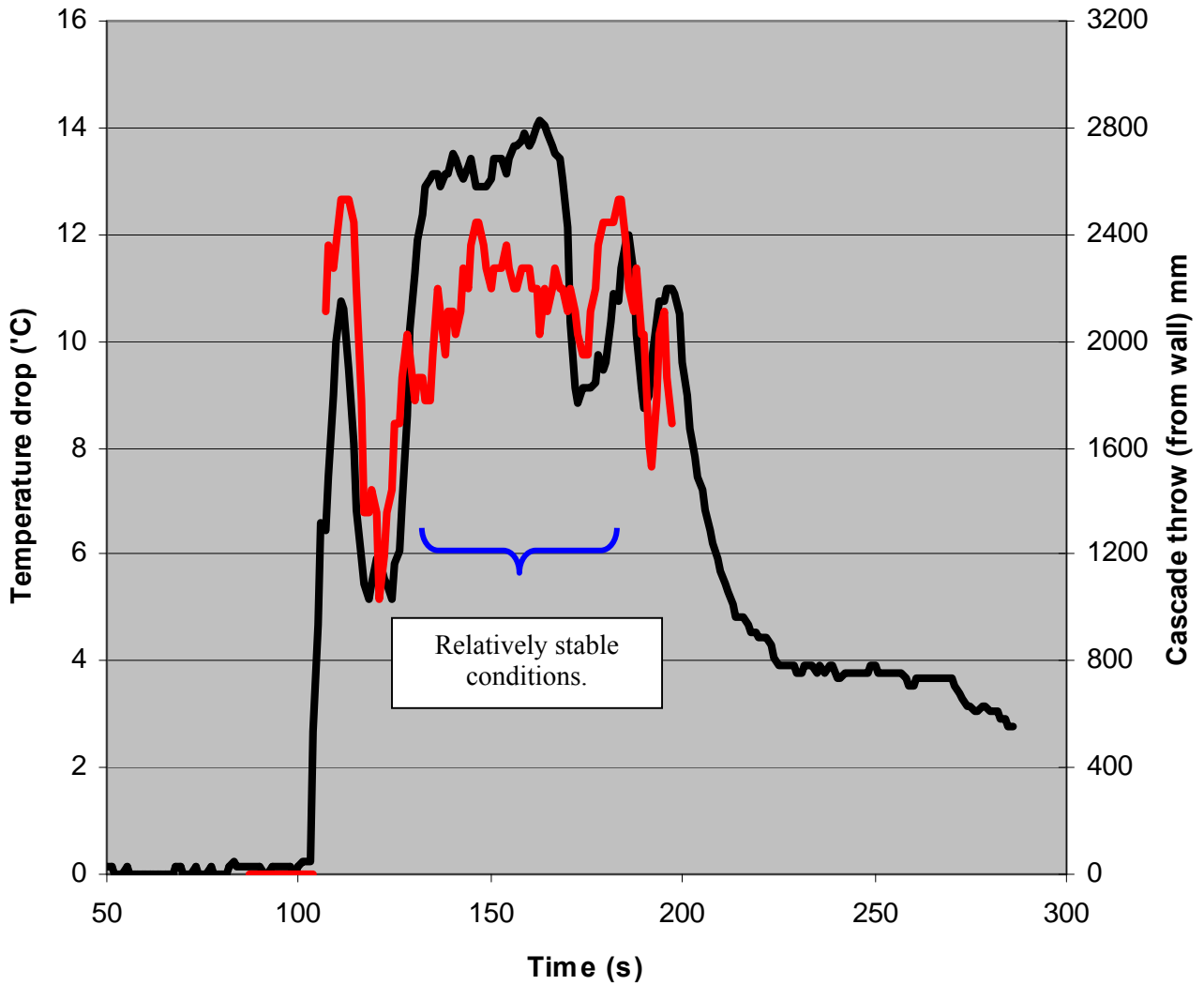


Figure 20: Relationship between cascade throw (from wall) and measured temperature (black). The cascade is somewhat affected by a cross draft for about 30 seconds after the start. During this time the apparent width increases and the throw varies. After this there is a period of around 60 seconds when the cascade appears stable and compact – this period yields the most useful data.

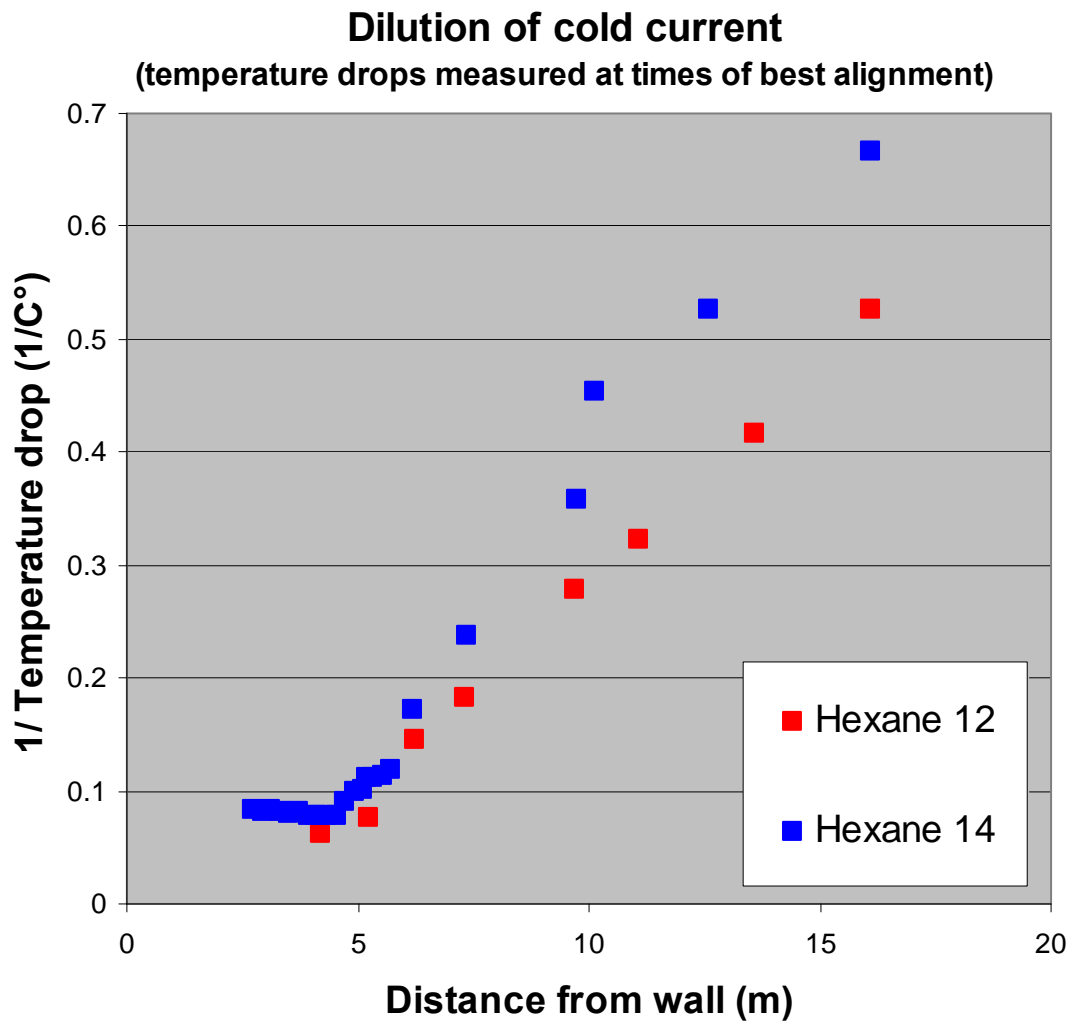


Figure 21: Dilution of the vapour current in two free cascade experiments. Measurements for distances smaller than about 4700mm are affected by splashing and are not a reliable indication of vapour temperature.

Dilution of cold current

Reduced temperature drop = $T_{\text{drop}}(\text{air measured}) / T_{\text{drop}}(\text{liquid measured})$

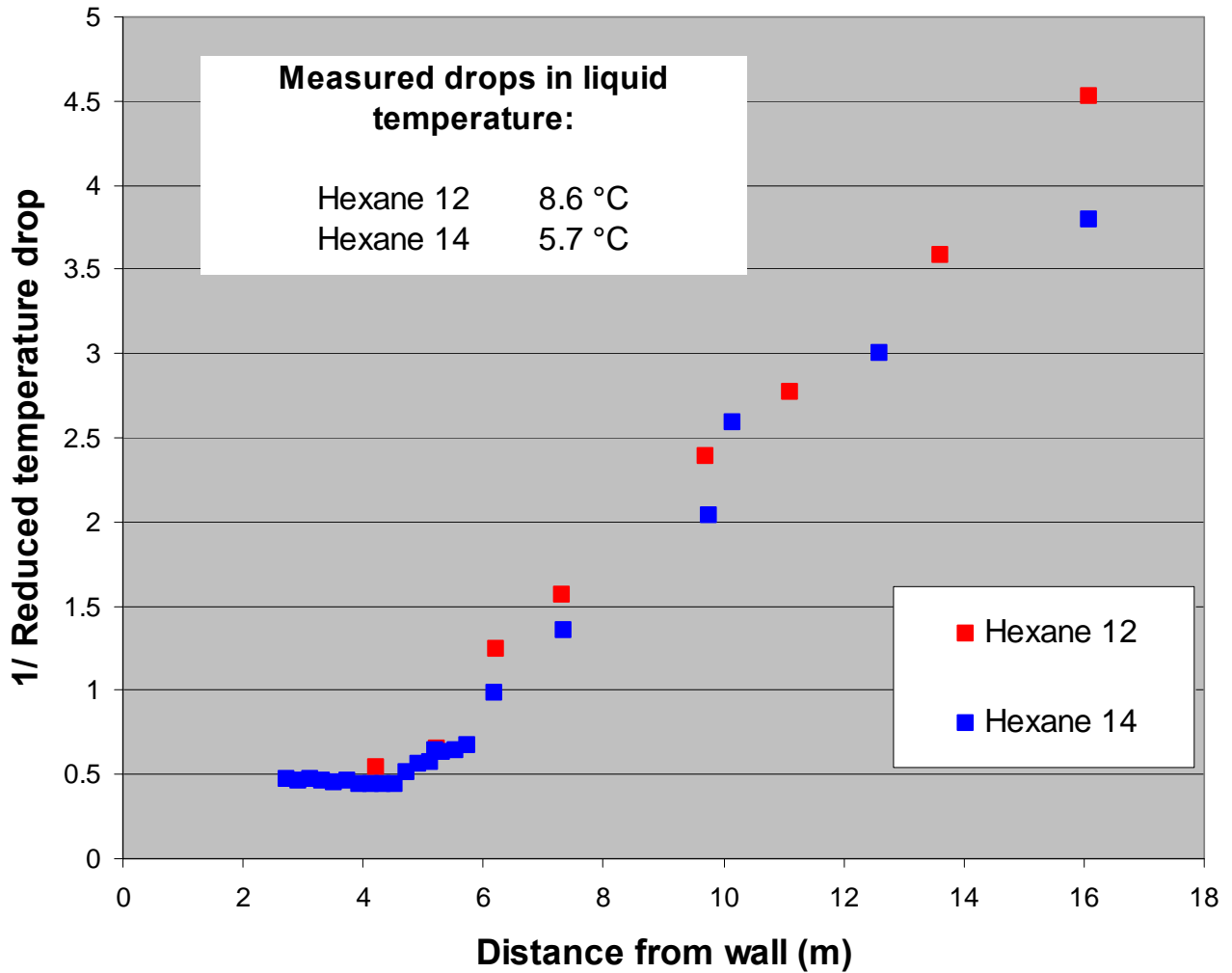


Figure 22: Vapour current dilution with temperatures reduced by division by the liquid temperature drop (which is a particularly well-defined variable measured in both tests)

5.2 ENHANCEMENT OF HEXANE VAPORISATION BY SPLASHING

A mass balance at the point where all the hexane has evaporated is of interest

Evaporation (or liquid dropout) is complete at about 2700 mm from the impact zone. Calculations by Simon Coldrick have shown that the mass flow at this distance has roughly doubled because of entrainment (Figure 23). This mass flow against distance curve is insensitive to the amount and fineness of splash products.

The temperature of the (pure vapour) flow when thermocouples are just clear of the effects of splashing is around -5°C and the calculation of hexane vaporisation becomes:

14 kg/s Hexane	3.3°C drops to -3.8°C	Enthalpy change 228 kW	or Hexane vaporisation	680 g/s
1kg/s Hexane	3.3°C drops to -5°C	Enthalpy change 19 kW*	or Hexane vaporisation	58 g/s
13.2 kg/s Air	3°C drops to -5°C	Enthalpy change 106 kW	or Hexane vaporisation	316 g/s
Total rate of hexane vaporisation				1054 g/s

*Includes phase change at standard temperature (liquid and vapour heat capacities are not the same)

The experimental estimate of the actual vaporisation rate within the cascade and impact zone was around 900g/s. In this case splashing and vaporisation of splash fragments has increased the overall rate of vaporisation by ~ 150 g/s. The additional vaporisation is possible because liquid spray is carried into parts of the floor vapour current where there is vigorous entrainment of additional air.

It appears that vaporisation of splash product outside the impact zone makes a moderate but significant difference to the overall source term.

It is interesting to compare the hexane concentration rate derived above with the saturated vapour pressure at the measured temperature

$$\text{Vapour pressure of hexane} = 29/86 \cdot 1054/13,600 = 2.6 \% \text{ v/v (19.8 mmHg)}$$

$$\text{Saturated vapour pressure of hexane at } -5^{\circ}\text{C is } 35 \text{ mmHg}$$

It appears that at the point where the splash products have evaporated the concentration is well below saturated (roughly 50-60% saturation) – even near the ground. Another completely different method to estimate the degree of saturation at the edge of the spray is illustrated in Figure 24 – the result (61% saturation) is fairly similar. A saturation level just above 50% at the edge of the spray is not a surprise: compared with the saturated outflow from the impact zone the mass flow is doubled and there is proportionally little extra vaporisation or change in vapour temperature – hence a halving of the relative saturation.

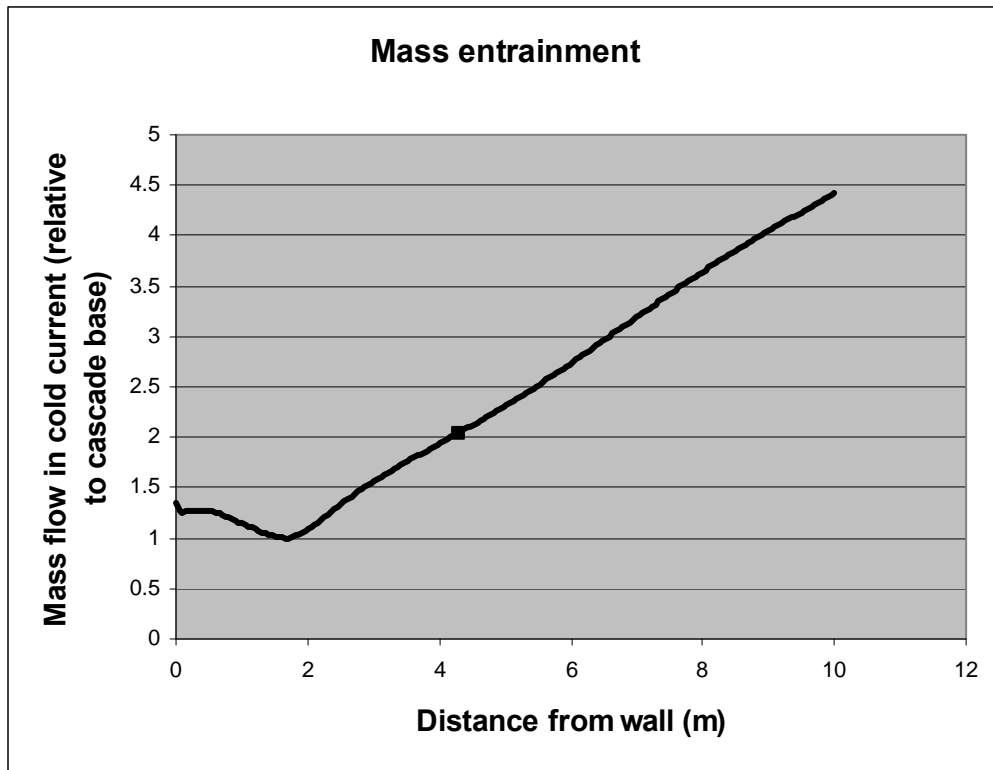


Figure 23: Estimates of mass entrainment based on CFD calculations by S. Coldrick

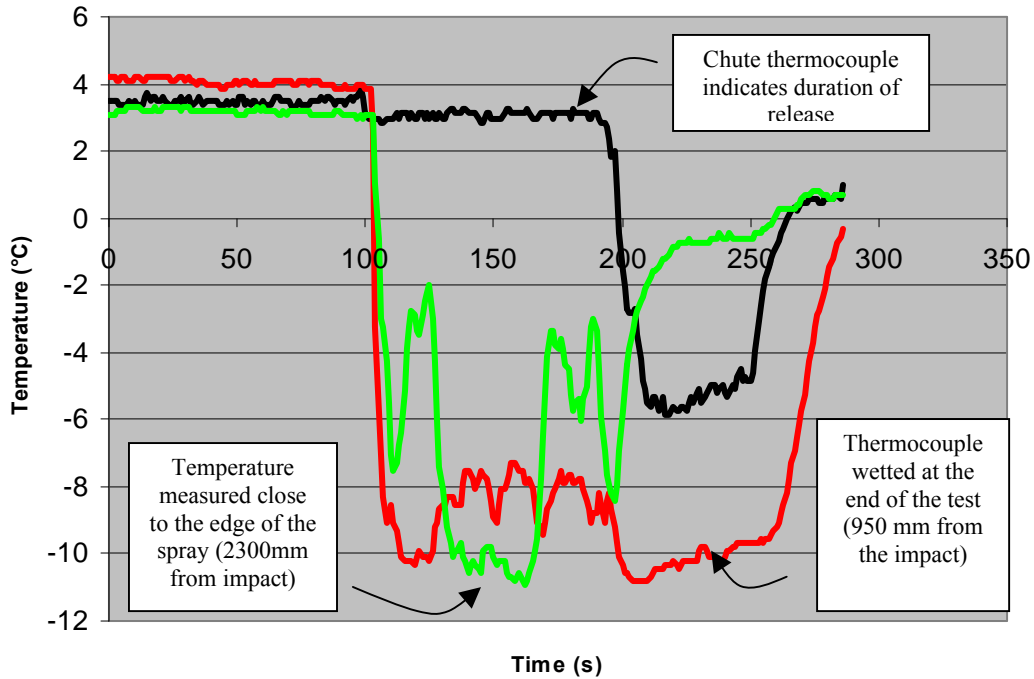


Figure 24: Alternative estimate for vapour saturation fraction at the edge of the vapour spray. The thermocouple at the edge of the spray (green) is wetted at around 120 s and then is evaporatively cooled. The thermocouple closer in is continuously impacted by liquid and only dries at the end.

If a solvent wetted surface is maintained at a temperature below ambient by evaporative cooling the degree of cooling is related to the partial pressure of solvent in the ambient atmosphere as

$$\Delta T = \frac{\rho_g D_g}{\lambda} \frac{Sh}{Nu} \frac{W_c}{W_g} \Delta H_{vap} (X^* - X_g)$$

This is particularly useful as the ratio of Sherwood and Nusselt numbers (mass and heat transfer) is fairly insensitive to flow conditions.

Substituting appropriate values gives approximately $\Delta T = 469(X_{film}^* - X_g)$ Equation 2

For a thermocouple (green trace above) near the edge of spray the ambient temperature is around -5°C and the film temperature is around -8°C ($X_{film}^* = 0.038$). In this case the level of evaporative cooling is around -5.5°C . Equation 2 suggests that $(X_{film}^* - X_g) = 0.012$ and hence $X_g = 0.038 - 0.012 = 0.026$

Saturation at the bulk gas flow temperature would be $X_{bulk}^* = 0.046$. So the relative degree of saturation relative to the main gas flow $X_g/X_{bulk}^* = 0.026/0.046 = 56\%$

The uncertainty in both methods of calculating the concentration is quite high (at least $\pm 10\%$) but this result based on measurements of evaporative cooling is reasonably consistent with figure derived from mass balance analysis (54%).

5.3 TIME SCALE OF SPLASH SPRAY EVAPORATION

The mass concentration in the flow out of the impact zone appears to be close to saturated. This makes sense- the impact zone contains very high densities of fine liquid droplets with high slip velocities.

The flow also carries a fine spray of hexane droplets generated in the splash process. As additional air is entrained further from the impact zone the level of saturation falls. There is some additional vaporisation from the droplet spray but this is relatively sparse and cannot keep pace with the additional air input and the degree of saturation continues to fall.

Eventually the droplets are gone and the saturation level has dropped towards 50%.

It is worth revisiting the analysis of droplet evaporation times.

$$t_{complete\ evaporation} = \frac{1}{2k} d_0^2$$

where
$$\frac{1}{2k} = \frac{1}{4} \cdot \frac{\rho_{liq}}{\rho_{gas} D_{gas}} \cdot \frac{1}{Sh} \cdot \frac{W_G}{W_c} \cdot \frac{1}{(X^* - X_g)}$$

In clean air complete vaporisation of 100um drops takes around 0.39 seconds. In a 50% saturated mixture complete vaporisation takes around 0.78s.

CFD calculations of the flow field (Figure 25) suggest that the average velocity of droplets carried out of the impact zone is around 4 m/s close to the ground - somewhat less towards the upper and lower edges of the vapour current. This means that the travel time from the edge of the impact zone to the limit of droplet travel is of order $2.7/4 = 0.65$ seconds.

There is at least a rough correspondence between the calculated lifetime of droplets (at the relevant level of saturation) and the observation that they always disappear beyond 2700mm from the impact point.

However, given that the saturation level starts close to 100% at the edge of the impact zone and vaporisation can only get going in earnest as more air is entrained it seems somewhat surprising that complete vaporisation occurs so quickly.

It is possible that this points to some fundamental limitations in the mass transfer theory (Equation 1). The Sherwood number is a function of the slip velocity Reynolds number. The theory uses the particle settling velocity as this slip velocity. For 100um droplets this settling velocity is around 0.12 m/s. The Reynolds number and consequently mass transfer rates are relatively low.

In reality the relative velocity between droplet and gas may be substantially greater - in this flow. This is because the whole flow will be violently disturbed by the growth of vortices in the shear layer near the top and bottom of the vapour current. The characteristic velocity of these vortices will be similar to the flow speed (4 m/s) and their size will be similar to the depth of the flow (0.2 m). Droplets caught in these eddies will experience maximum centripetal accelerations of order $4 \times 4 / 0.2 = 80 \text{ m/s}^2$. This acceleration is much larger than the acceleration due to

gravity (9.8 m/s^2) and the associated relative velocities will be greater than the settling velocity. Such slippage driven by large-scale structures in the flow does not happen continuously but nevertheless there is likely to be a significant enhancement of mass (and heat) transfer.

Another consequence of the strong eddies and rapid mixing in the vapour flow is that droplets are mixed through the depth much more rapidly than they can settle. The sharp cut off in droplet impact must indicate complete vaporisation rather than droplet deposition.

5.4 POOL EVAPORATION

The liquid temperatures in the ground level (liquid) flow away from the impact point show no sign of significant cooling even in the area close to the impact where vapour /liquid slip speed is greatest. This suggests that vaporisation of liquid in the pool makes a very small contribution to the overall rate of vaporisation.

This conclusion is supported by CFD analysis which showed little difference in flow, temperature or hexane concentration between cases where heat transfer to the wall and floor were included and those where adiabatic conditions were enforced. Similar conclusions are likely to apply to mass transfer from liquid in a pool.

These experiments have focussed on heat and mass transfer between air and finely divided liquid droplets; the flow of waste liquid was trapped in a sump within a few meters of the tank. Some additional vaporisation could be expected if liquid accumulated over a very large area in a bund. This issue deserves additional investigation.

5.5 VAPOUR BACK FLOW TOWARDS THE WALL

Video records of the free cascade tests show that there is a strong backflow of vapour from the impact zone towards and then up the wall. This reaches to a height of around 5m before the cold vapour slump down sideways. No detailed measurements have been in this flow but heavy icing of the lower 400mm of the wall is observed corresponding in the place where the backwards jet of cold vapour impinges.

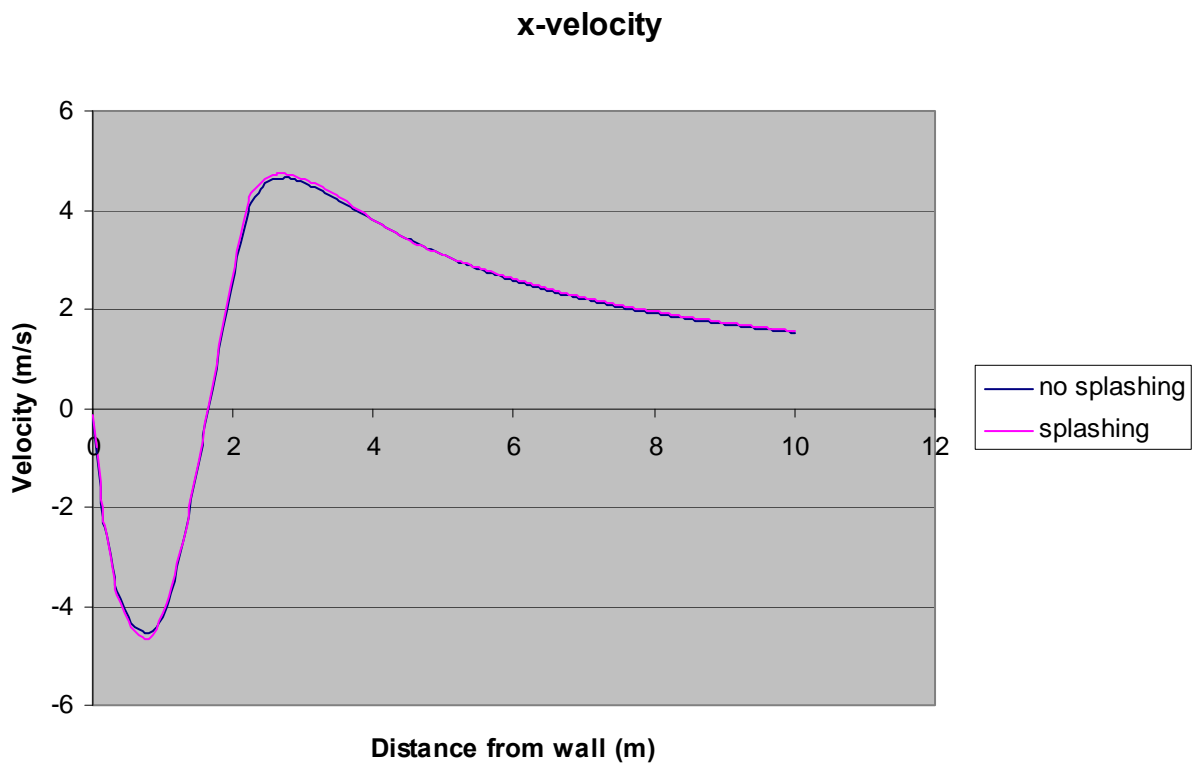


Figure 25: CFD calculations of flow field by S. Coldrick. In the splashing case 10% of the total mass release is reinjected into the flow as 100 μm droplets. There is hardly any change to the flow field. The velocity is evaluated at a height of 150mm.

6. SUMMARY OF RESULTS FOR A FREE CASACDE

The most completely instrumented test was Test 14. The discharge rate was 15 kg/s. Images in the following pages summarise the results of in the following areas (Figures 26 to 30):

Liquid temperature (Figure 26)

Vapour temperature (Figure 27)

Vapour saturation level (Figure 28)

Hexane vapour flow rate (Figure 29)

Hexane concentration (Figure 30)

These are some of the data that have been used in the modelling part of the project to tune the representation of the polydisperse spray in the cascade and the treatment of splashing.

They would be a suitable basis for testing any other CFD treatment of the cascade problem. Such numerical methods can then be used to address problems that are outside the range of practical investigation e.g. very long timescale accumulation of vapour clouds in more or less confined conditions.

CFD modelling work of this sort by Simon Coldrick and Simon Gant is described in Sections 8 and 9 of this report.

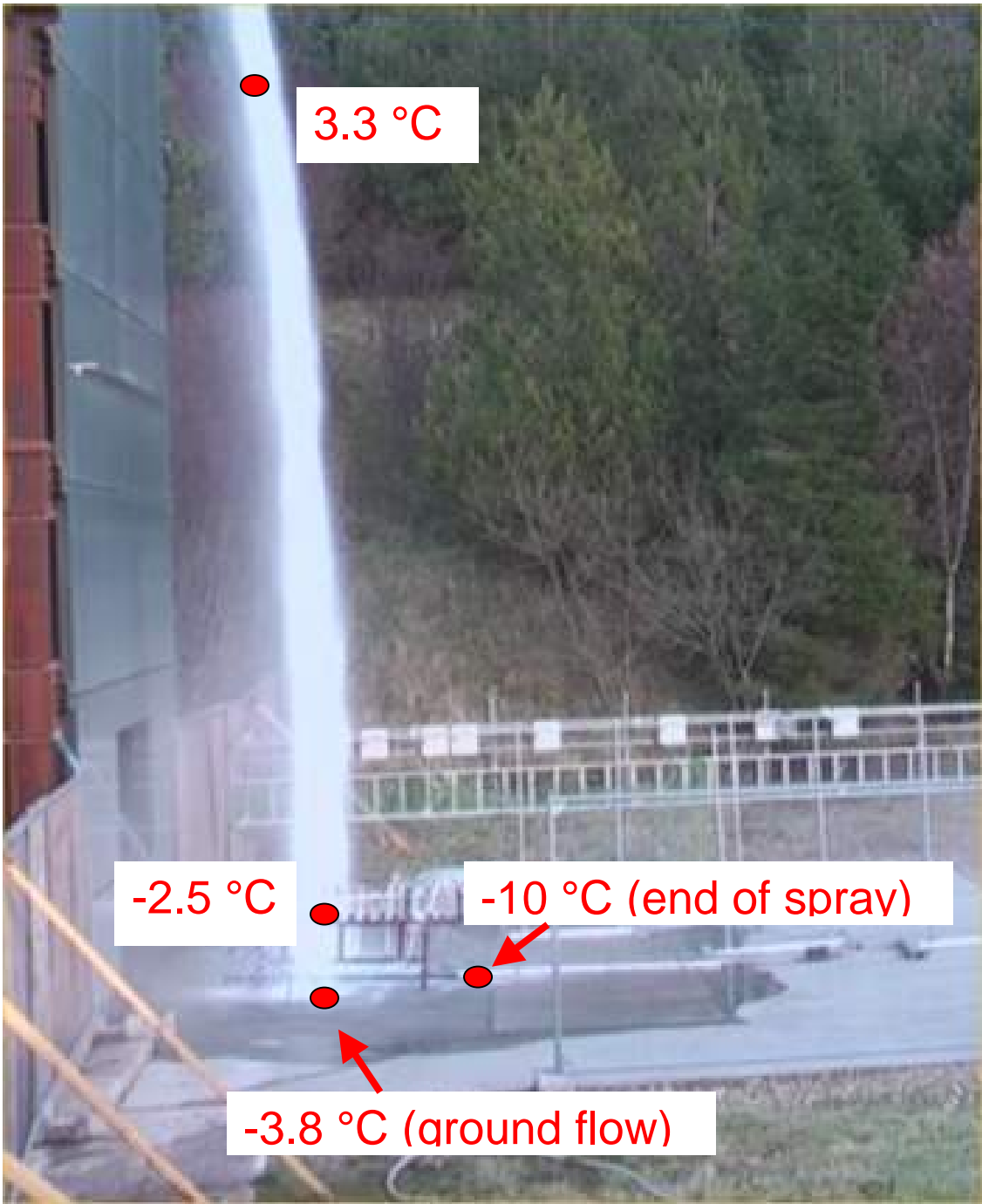


Figure 26: Liquid temperatures

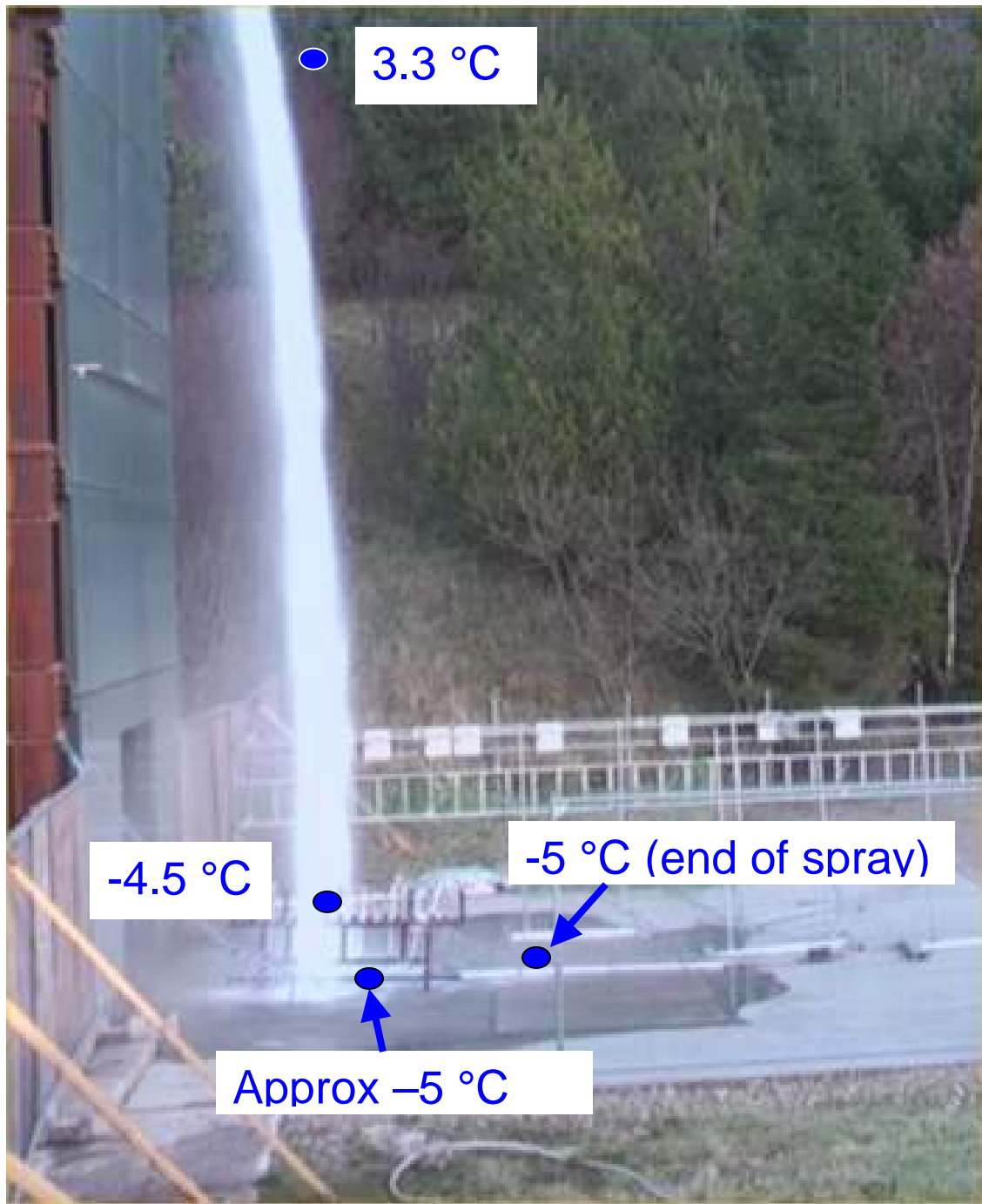


Figure 27: Vapour temperatures



Figure 28: Saturation level

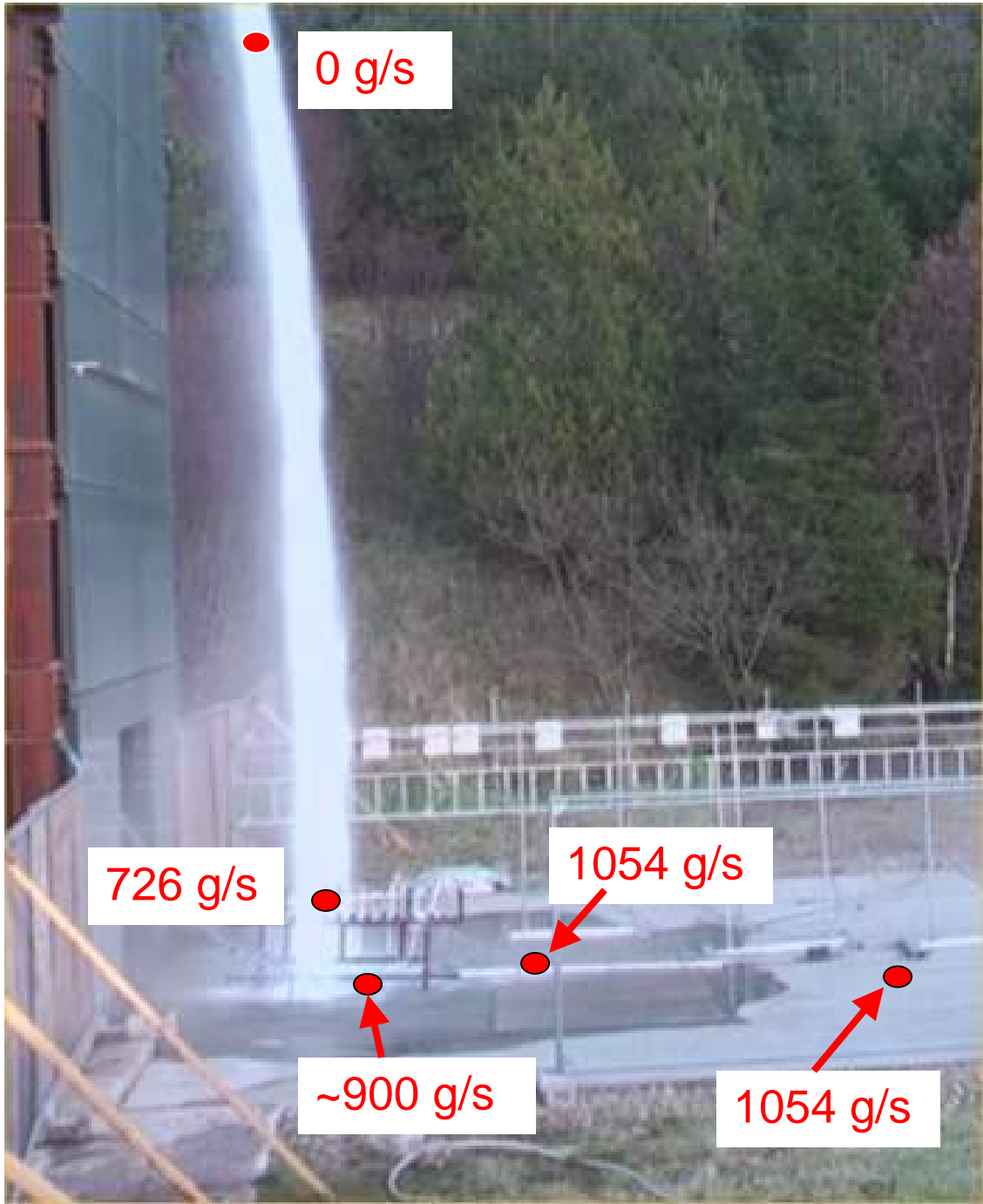


Figure 29: Total Hexane vapour flow

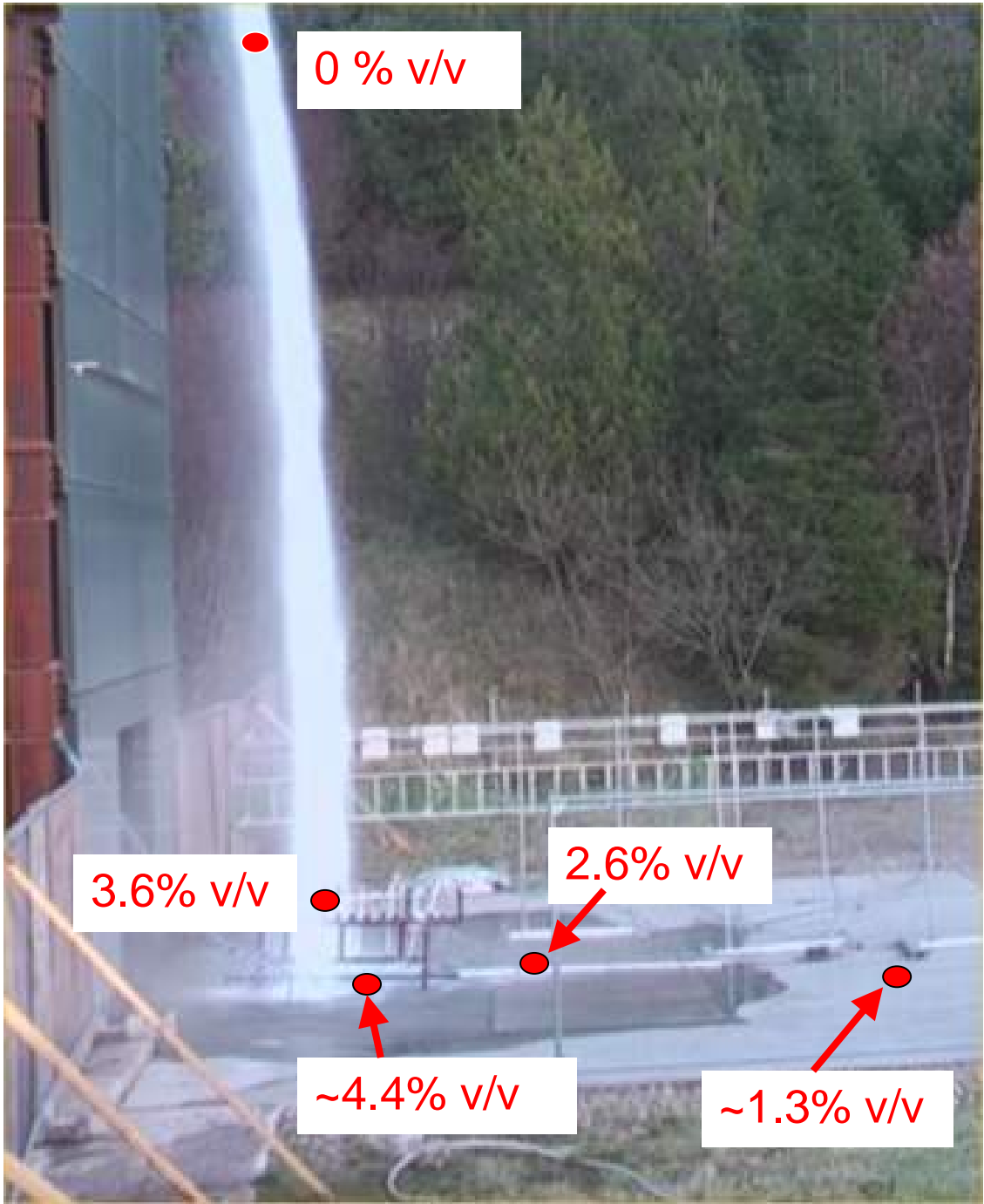


Figure 30: Hexane concentration (the lower flammable limit for hexane is 1.2% v/v)

7. BIFURCATED CASCADES (BUNCEFIELD TYPE TANKS)

The basic features of overflow discharge from the top of a Buncefield type tank were described in Section 1. The proportion of liquid forming a free cascade by flowing over the rim of the deflector plate rises with the total flow rate. The distance that this free cascade is thrown from the tank base also increases with total flow rate (Figures 31 and 32).

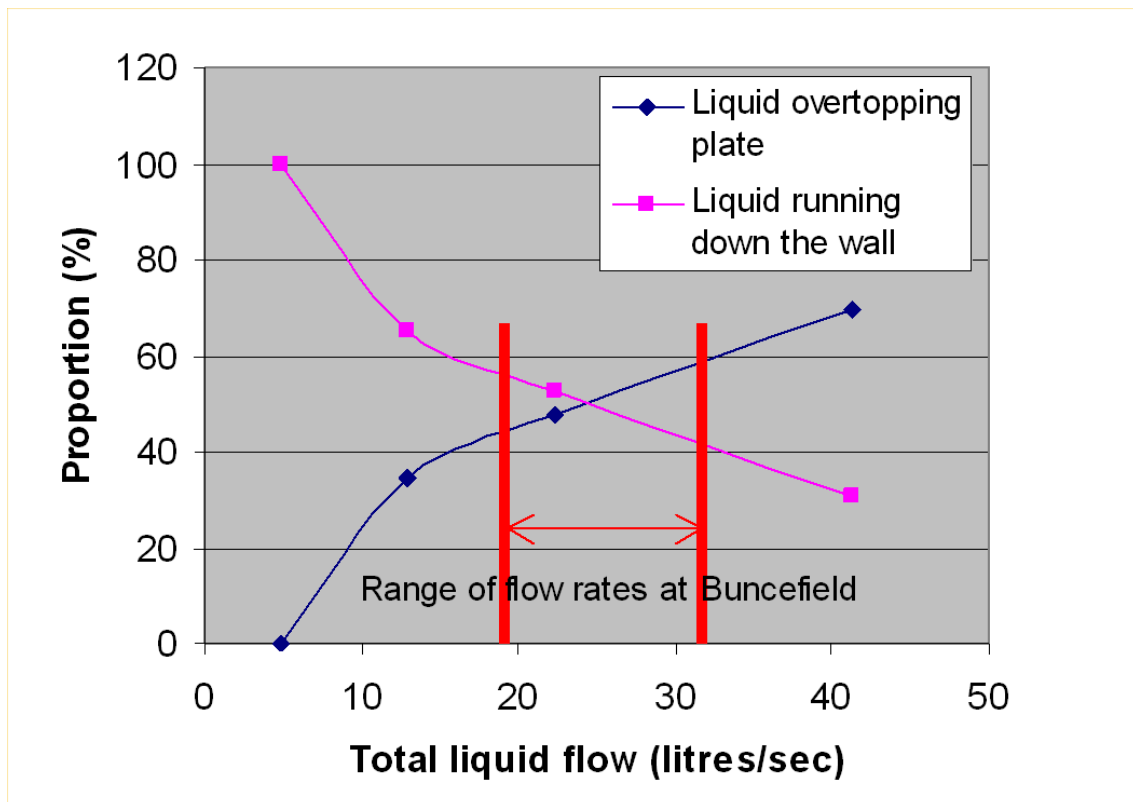


Figure 31: Data on partitioning of liquid discharge between wall flow and free cascade

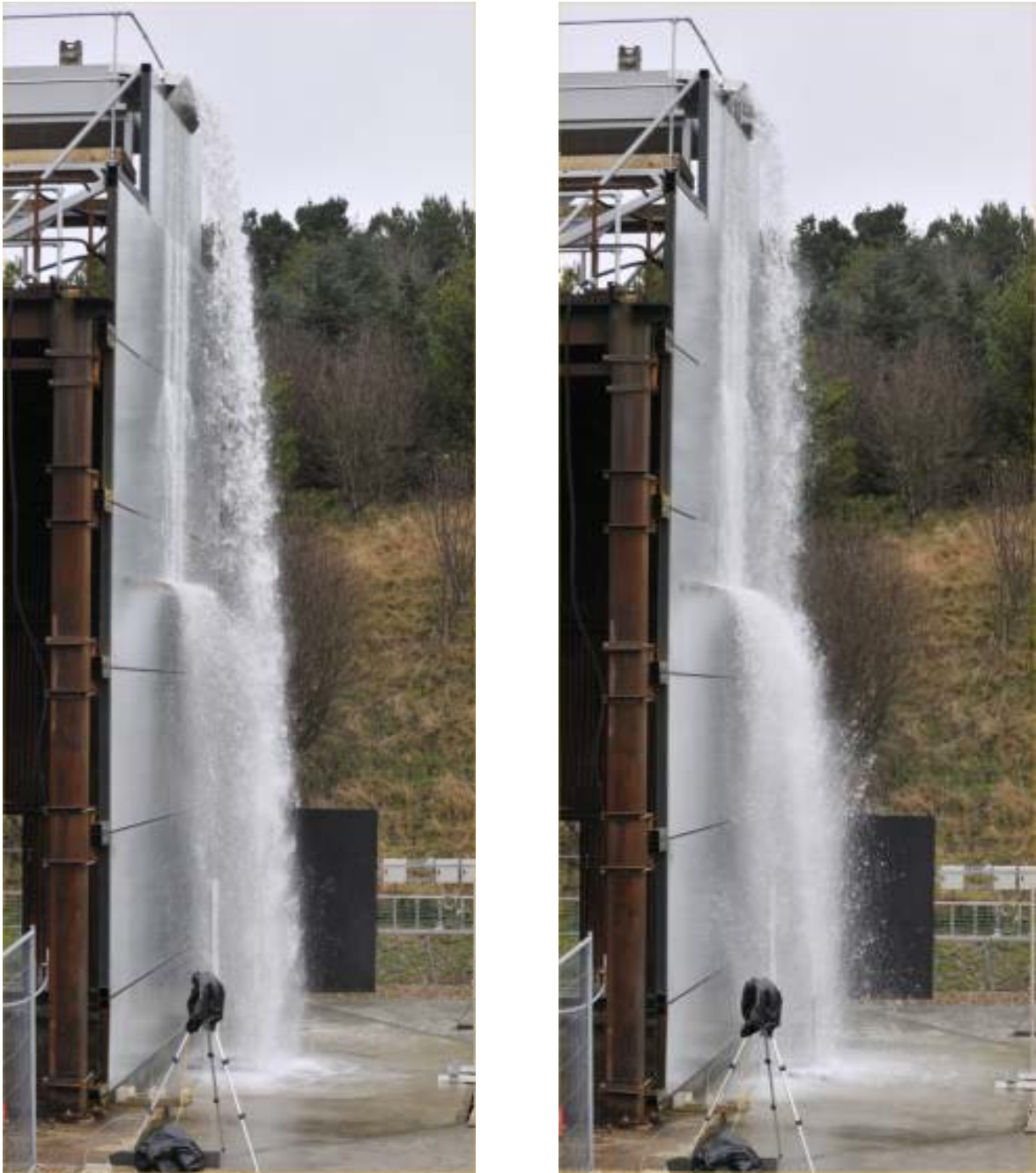


Figure 32: Changes to cascade trajectory with flow rate.

The left hand image shows a high flow rate with the bulk of the flow overtopping the deflector plate and falling as a free cascade. The free cascade has sufficient throw away from the tank wall to largely avoid intersection with the wind girder flow.

The right hand image shows a lower flow rate with the bulk of liquid running down the wall. The degree of projection of the windgirder flow is increased and the throw of the free cascade reduce so that the two cascades intersect.

7.1 TEST 13 – A BIFURCATED CASCADE IN VERY STABLE CONDITIONS

Figure 33 shows the cascade structure and resulting vapour cloud during Test 13.



Figure 33: Cascade structure and vapour cloud formation during Test 13 (15 kg/s hexane).

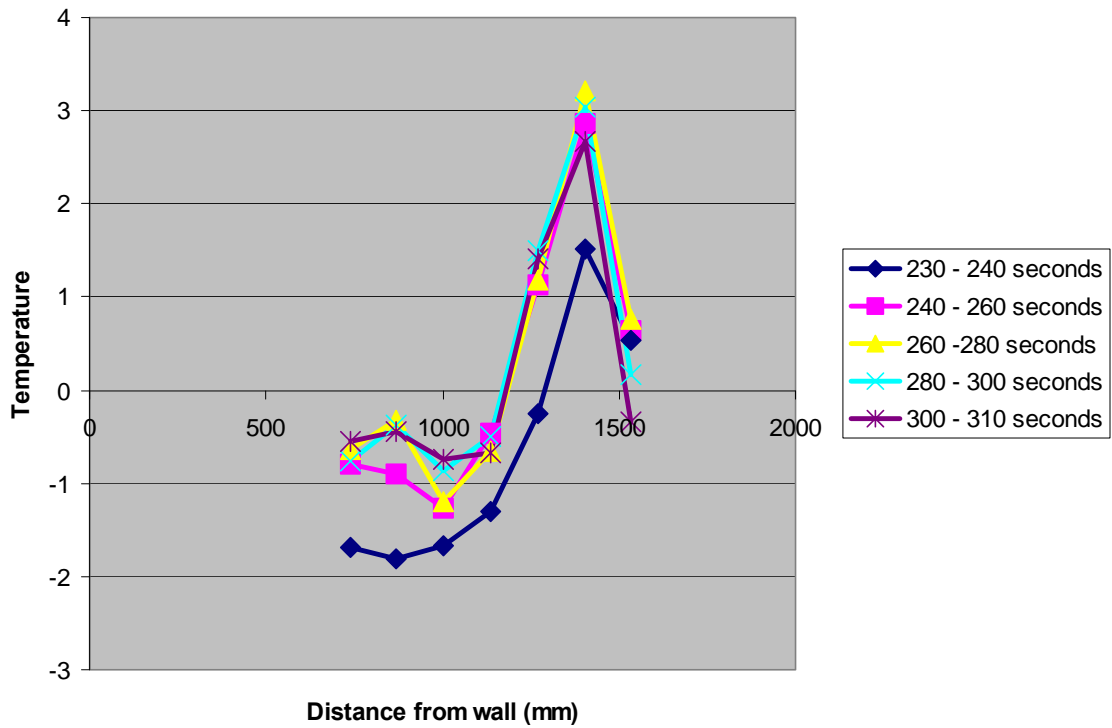
This test was carried out very early on a winter morning in a very strong inversion layer. The atmosphere had cooled overnight and the relative humidity was high. Even slight decreases in temperature triggered condensation of atmospheric moisture, which made the cloud visible over a wide area.

The strongly stable thermal gradient in the atmosphere meant that there was no wind and the cascade flow was extremely stable throughout. This can be appreciated from results shown in Figure 34. Careful examination of the liquid temperature profiles shows that the average trajectory of the main (free) cascade did not vary by more than a few tens of millimetres over a period of a minute or more.

The flow could be divided into two distinct parts. One was a free cascade that behaved in a very similar manner to the free cascade flows described in the previous sections. This main cascade was again only around 350-400 mm wide (Figure 35).

In addition there was a weaker, more diffuse flow from the wall flow deflected by a windgirder halfway down the tank. The trajectory of this second flow lay mostly between the main cascade and the wall. The liquid mass flux density was lower in the windgirder flow and consequently more air was entrained - in proportion to the liquid mass flow. The higher air fractions led to reduced liquid and vapour temperatures (Figure 36). Despite the reduced distance of fall the windgirder cascade was somewhat wider than the free cascade.

Variation in liquid temperature profile with time



Variation in vapour temperature profile

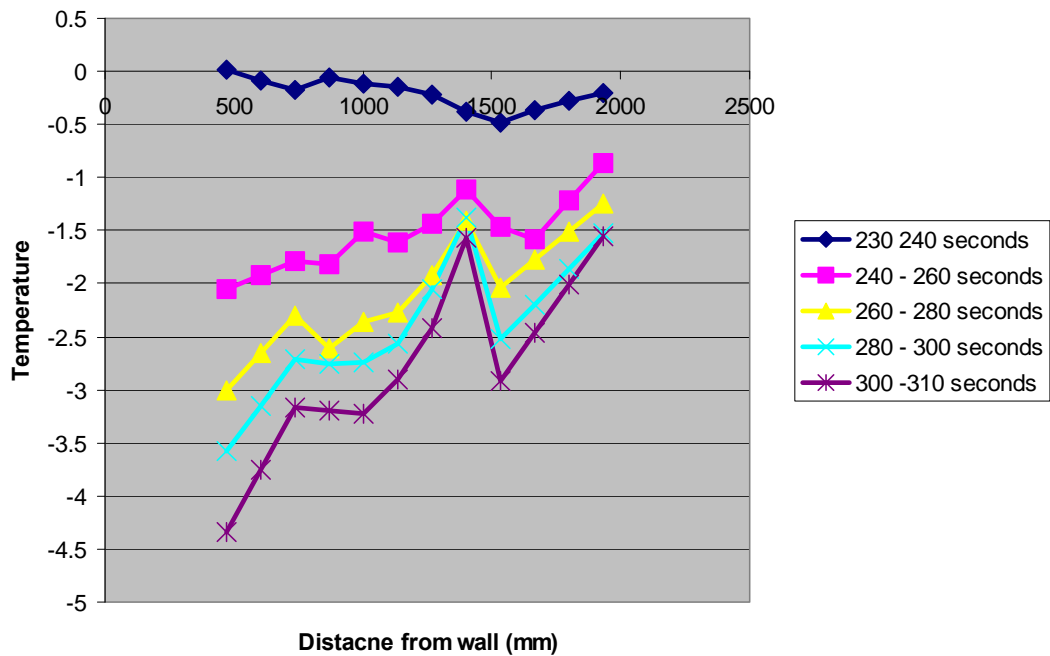


Figure 34: Averaged liquid and vapour temperature profiles in Test 13

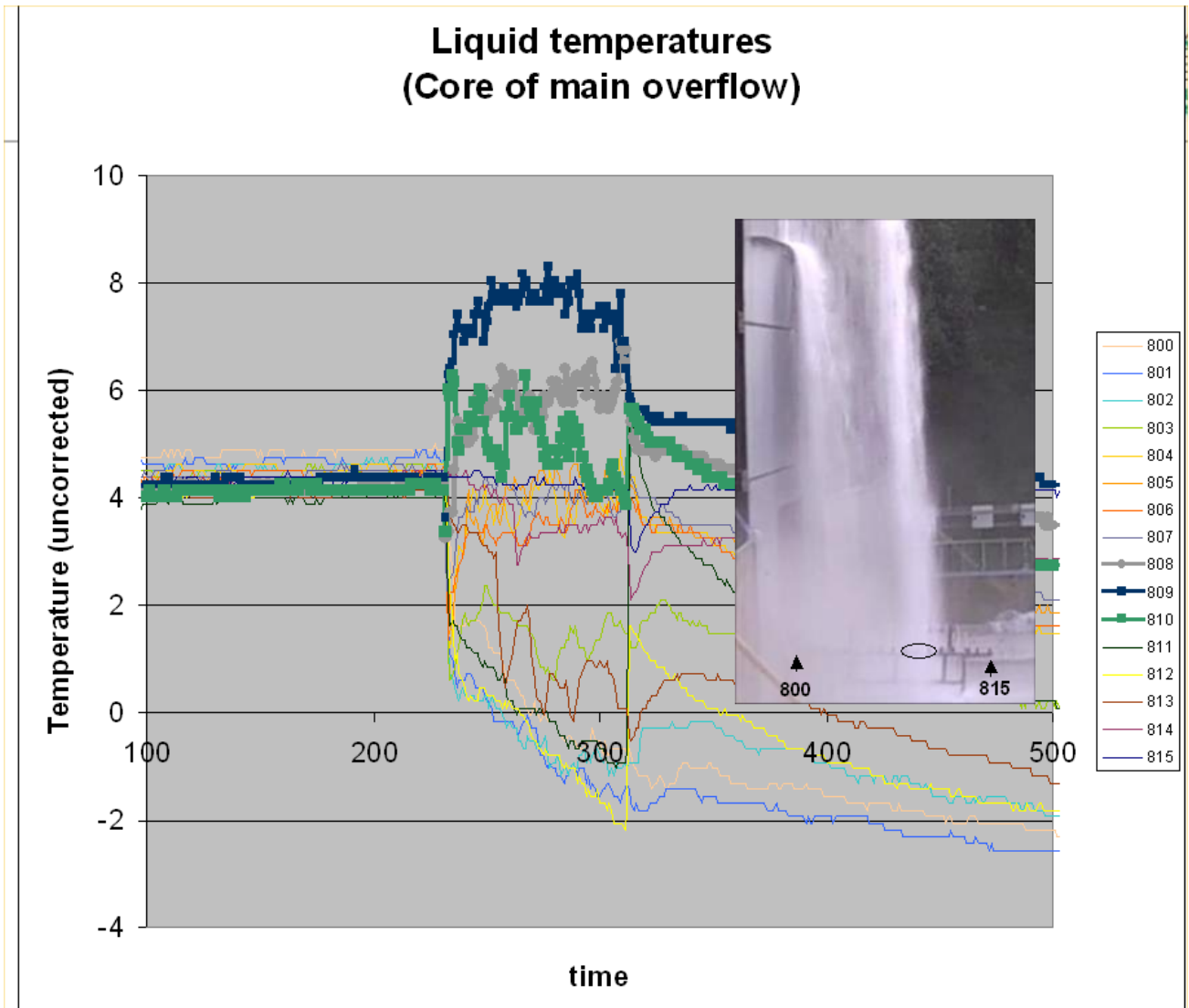


Figure 35: Example time series results from Test 13.

Highlighted traces are from the main cascade – as indicated by the inset panel

The results indicate a high degree of cascade stability.

Liquid temperatures (Core of windgirder flow)

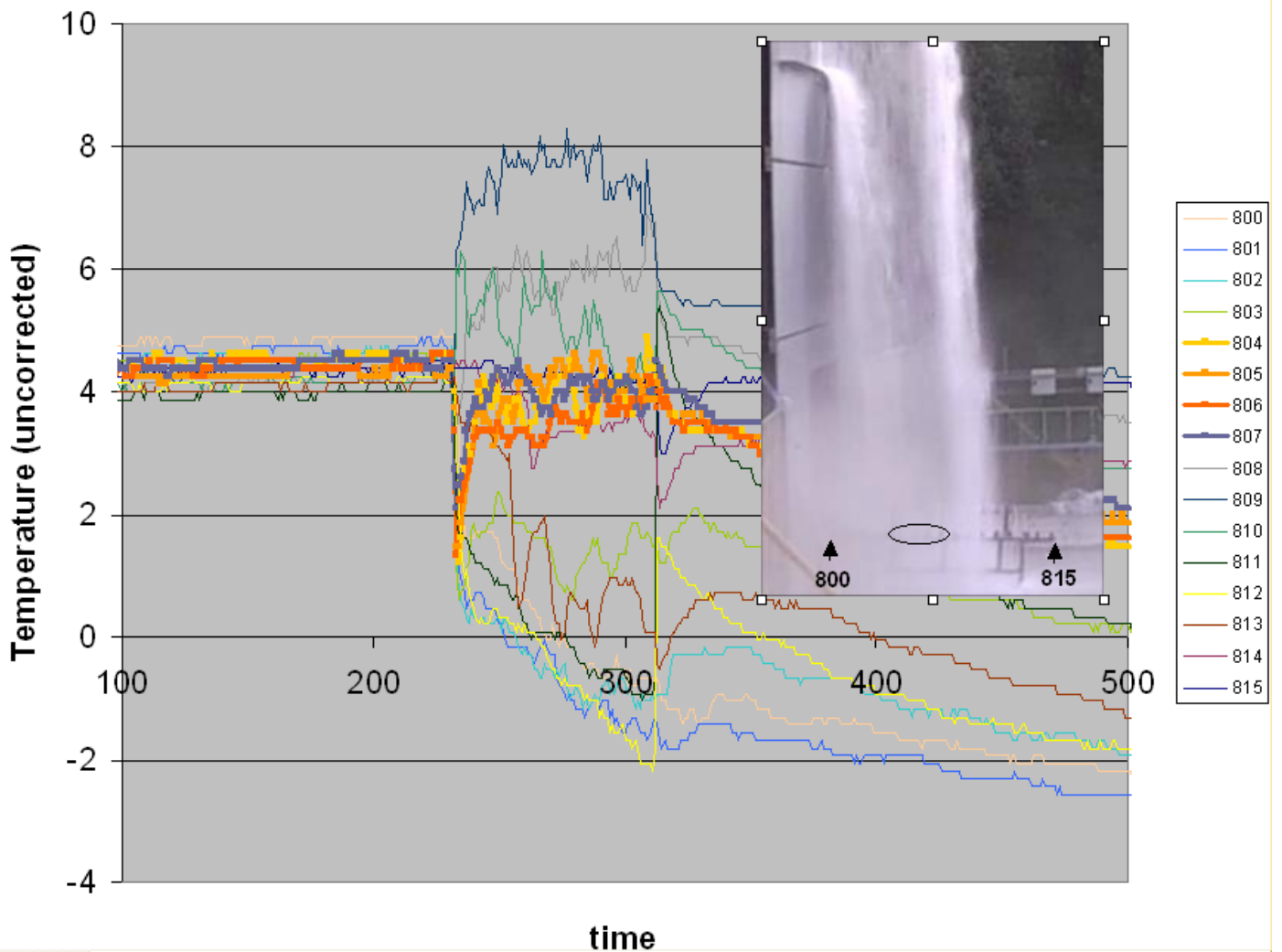


Figure 36: Further example time series from Test 13.

Highlighted traces are from liquid pots in the wind girder cascade – as indicated by the inset panel

The results indicate a high degree of cascade stability.

Wetted TC temperatures close to impact point

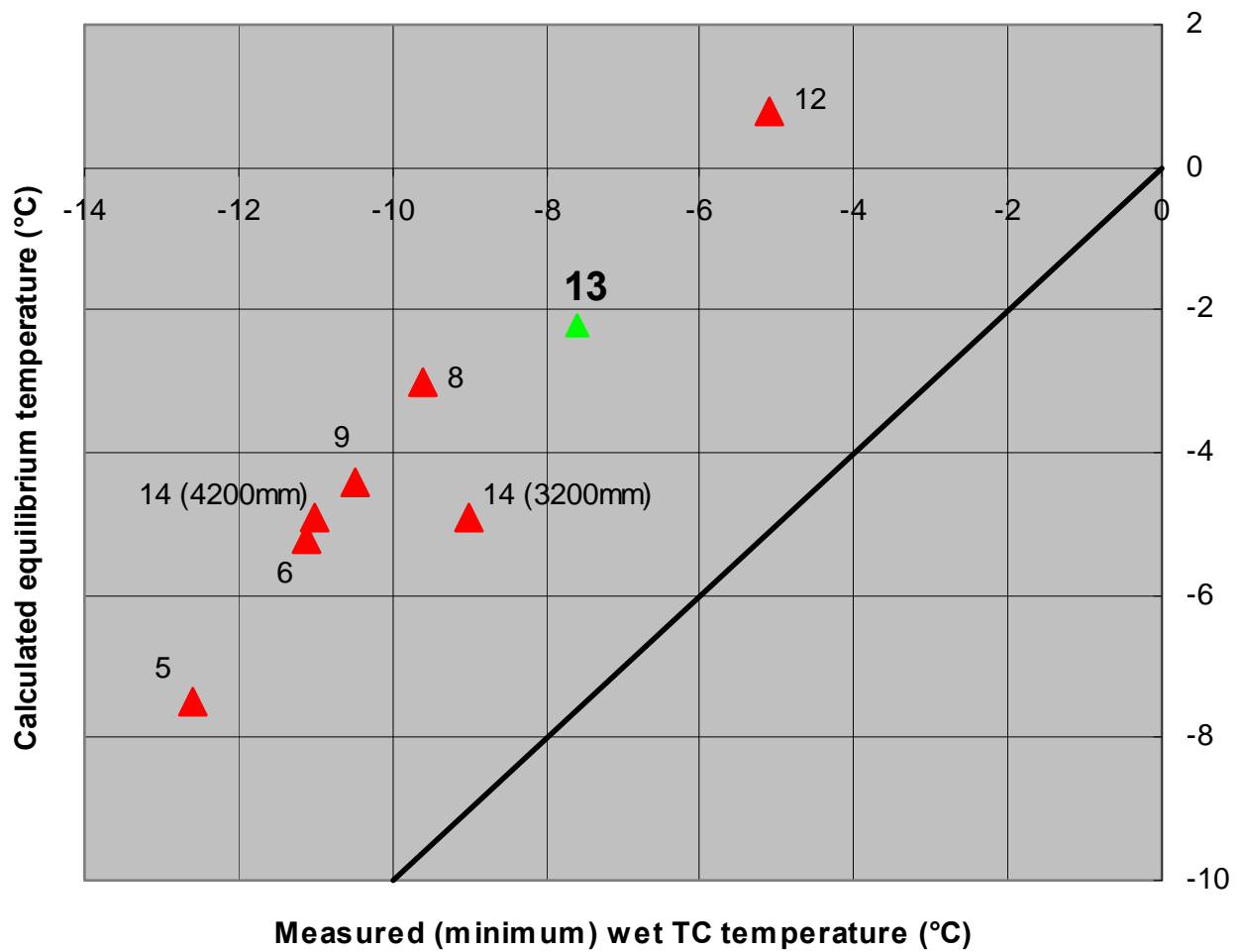


Figure 37: Minimum recorded wet thermocouple temperatures

For Tests 5 –13 the thermocouple elevation is 250mm and distance from wall 3200mm

For Test 14 the thermocouple elevations are 150mm distance from wall 3200/4200mm.

Red symbols are single free cascades. Green symbol (Test 13) is a bifurcated cascade. Equilibrium temperatures are calculated on the assumption of a cascade cross-section of 0.6 m^2 in every case.

Figure 37 compares the measured wet thermocouple temperatures in a range free cascades with Test 13. At least close to the impact point for the main (overtopping) cascade the flow from the wind girder does not appear to significantly disturb the outflow from the main cascade. This is perhaps not surprising as in this case the partitioning of the flow at the top of the tank favours the free cascade.

It is interesting that the change in thermocouple elevation in Test 14 has a noticeable effect on the wetted temperature. Presumably air ratios are higher closer to the top of the flow and where there are still droplets this lowers the temperature. Moving further away (to 4200mm) at lower elevation also increases the air ratio and lowers the temperature.

One important effect of the inner wall flow cascade is probably to increase the strength of the vapour current driven sideways. Vapour flow temperature recorded by the instruments on the centreline in Test 13 show a strong stable flow close to the main impact point but this weakens much more rapidly than one would expect based on the results for free-cascades (Figures 38 and 39). One part of the explanation for these results is an interaction between the forward vapour flow and strong gravity currents reflected from the sides of the (asymmetric) valley where the rig is located. This type of flow is very clear in video records and may displace the weakening forwards vapour current from the centreline.

The videos also show that a noticeable backflow towards the wall becomes established a few tens of seconds into the release and then dies away again. This backflow apparently occurs only at low level and is driven by the release rather than an external wind as the trajectory of the discharge remains stable. Figure 40 shows measurements of thermal gradients prior to test. The first air entrained by the vapour current is colder than that which is subsequently drawn down. There is therefore a tendency for the material in the first part of the vapour current to run back down the valley towards the wall reversing later forwards vapour currents where they are weak enough. More comprehensively instrumented tests (in neutrally buoyant conditions) are probably needed to make sense of the development of vapour currents driven by bifurcated cascades.

The problem of bifurcated cascades would also be a useful application of CFD. If a code can reliably capture the behaviour of a single cascade test case it is reasonable to use it to explore the effects of dividing the release and impacting the two resulting cascades at different places.

Normally bifurcation of the liquid release and extra spreading induced by impact with the wind girder will increase the cross sectional area of the release. The mass flow of air will increase along with the total rate of vaporisation. Maximum concentrations in the vapour current will however generally fall.

The general lessons from single free cascades would be expected to apply to each part of the bifurcated cascade separately: with vaporisation roughly corresponding to the equilibrium level based on cascade air entrainment. The vaporisation would be topped up with small but significant amounts of fine splashed spray – probably at a level of about 1% of total mass flow.

In practical assessments it may be difficult to specify the partitioning of liquid between free cascade and wall streams. This is very sensitive to the exact design of the deflector plate and tank top. The trajectory and degree of spreading of the wind girder spray will also be sensitive to tank design.

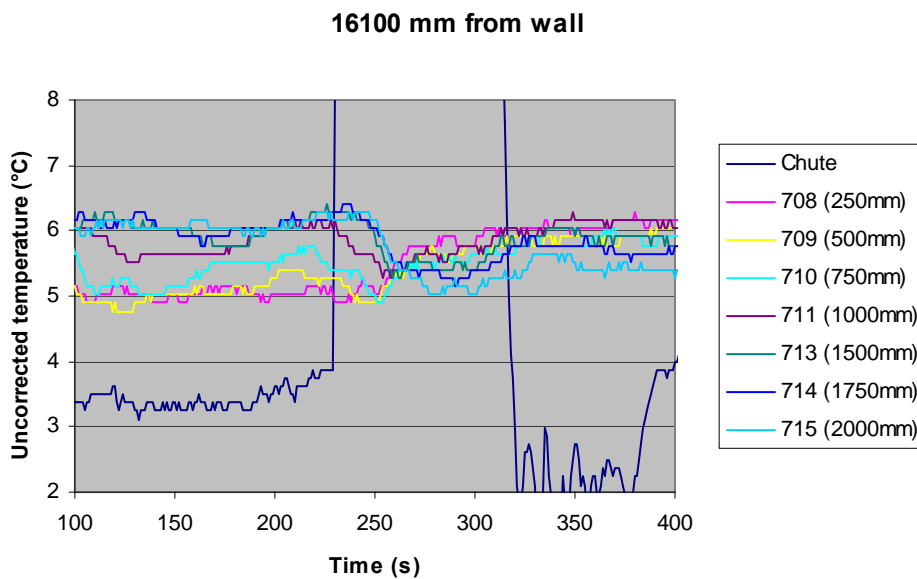
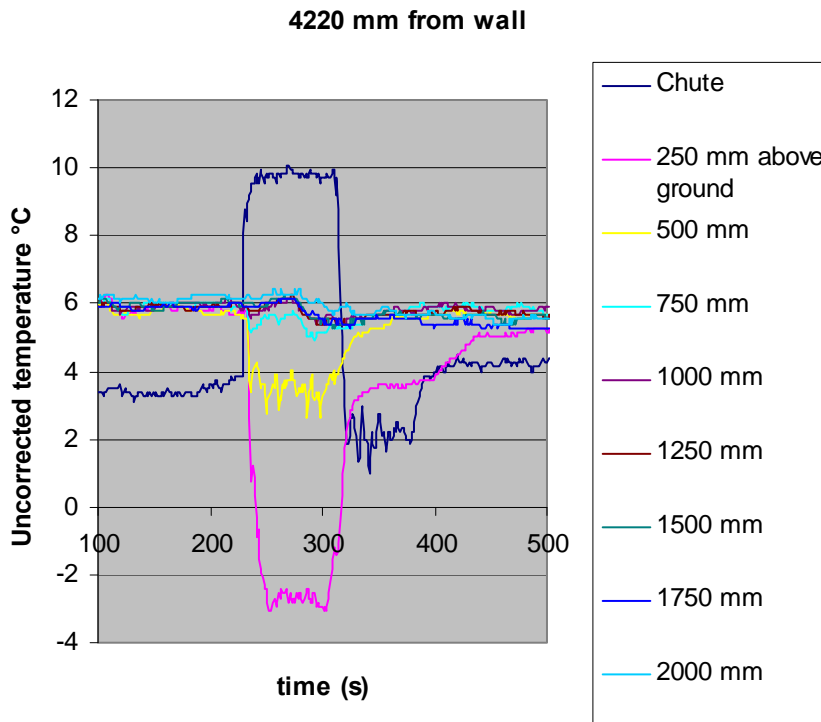


Figure 38: Contrast between vapour current measurements close to the cascade (above) and at distance. The vapour current is initially well defined and stable but does not penetrate far from the base of the tank. The stable temperature gradient over grassy parts of the site is apparent in the lower plot. The action of the cascade at distance in this case is actually to bring warm air down to ground level. These results should be compared with Figure 19 and Fig App2.14

The forward impetus of bifurcated cascades is clearly much reduced and this is particularly significant if there is a strongly stable temperature gradient.

Dilution of cold current

Reduced temperature drop = $T_{\text{drop}}(\text{air measured}) / T_{\text{drop}}(\text{liquid measured})$

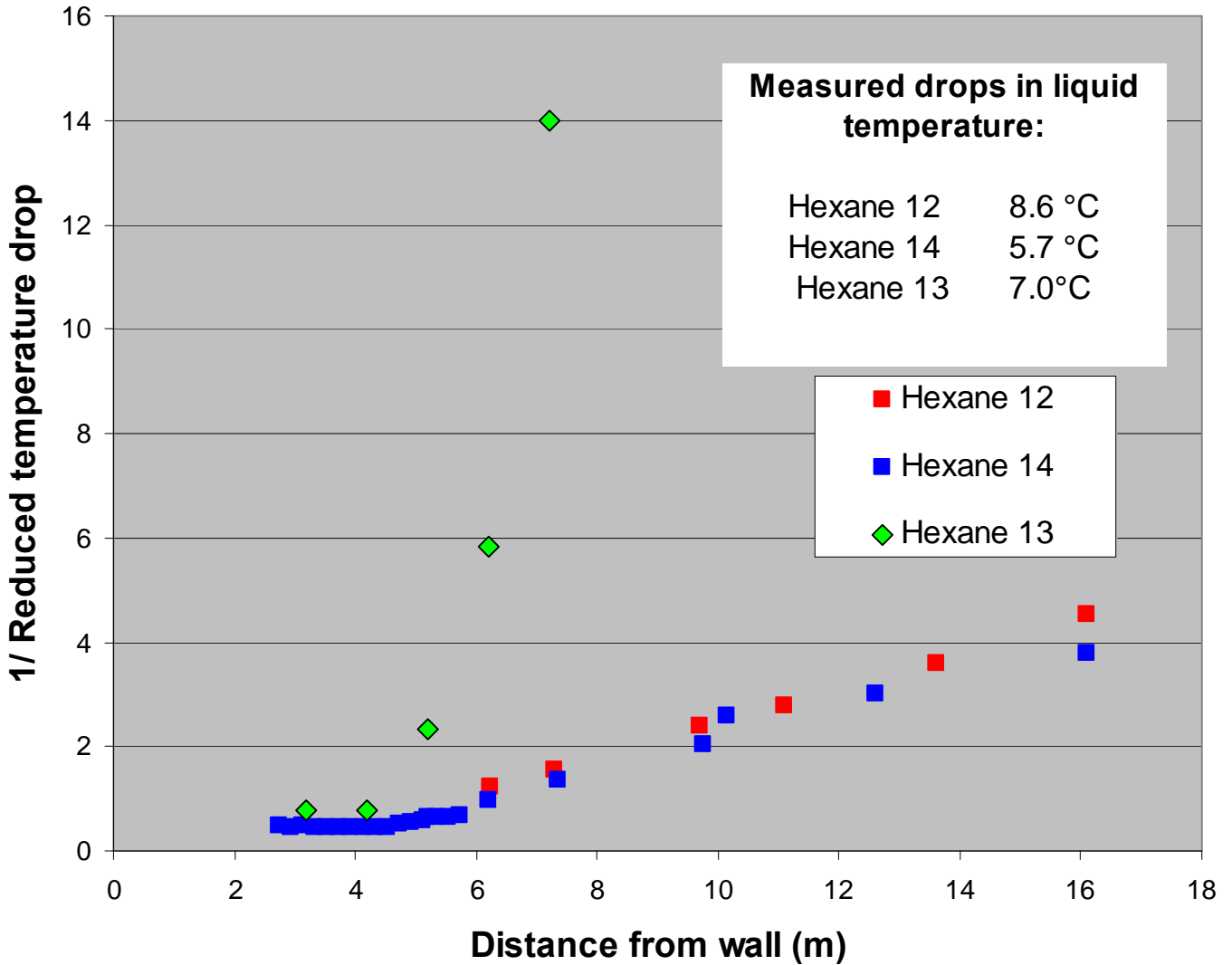


Figure 39: Contrast between vapour current measurements in free and bifurcated cascades.

Very close to the impact point the temperature drops are similar. The forward impetus of bifurcated cascades is however clearly much reduced and it appears that the flow can be completely stalled by a strongly stable cold layer at ground level.

Hexane 13: Average temperature profile before test

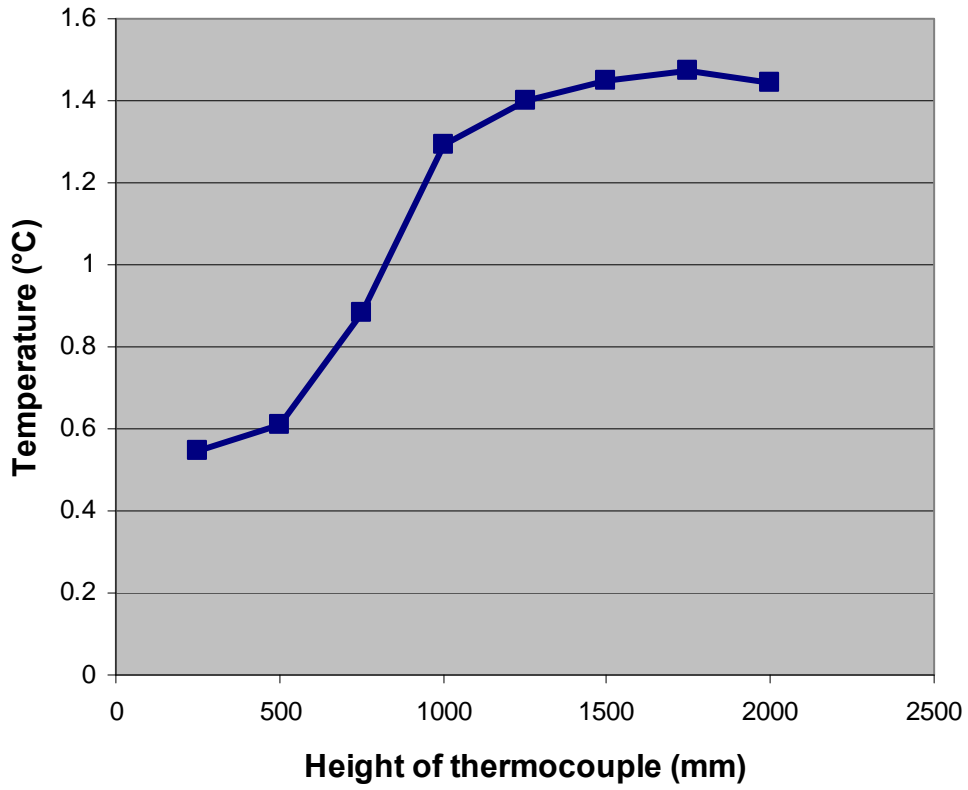


Figure 40: Temperature variation over grassy parts of the test area (greater than 10m from the wall)

8. CFD MODELLING

Throughout the duration of the project, CFD modelling was undertaken in conjunction with the experimental programme. CFD modelling can be used to explore aspects of vapour cloud generation and dispersion not readily achieved experimentally. In particular, it can be used to help understand the longer term effects of the accumulation (or recirculation) of vapour within bunds. This is difficult to analyse using alternative methods, since it is inherently a transient process, with the liquid spilling into a vapour layer of increasing depth. However, the CFD modelling cannot be undertaken in isolation as it requires validation data from the experimental programme. Therefore a simultaneous programme of experiments and simulation was undertaken to enable model validation and insight into vapour cloud generation from liquid cascades. The following sections describe how the CFD model was constructed, validated and used to extend the scope of the experimental results.

8.1 THE CFD MODEL

The general-purpose CFD software, CFX 12.1 was used to model the release tower, liquid cascade and vapour current. The approach taken was similar to that used previously in the preliminary investigation by Gant and Atkinson (Reference 7) and Coldrick et al. (Reference 3). The flow of air and vapour was modelled using an Eulerian model, which involved a computational mesh that was fixed in space through which the gases flowed. Momentum, mass and energy conservation equations were solved in each mesh cell to find the velocity, temperature, pressure and concentration distributions. The spray of droplets was modelled using a Lagrangian approach in which the paths of discrete computational particles were tracked through the flow domain from their injection point until they hit a solid surface, escaped the domain or evaporated completely.

The exchange of momentum, mass and heat between the Eulerian phase and Lagrangian particles was two-way. For momentum, particles falling through the air were subjected to drag forces, and their trajectories were affected by turbulent perturbations in the air. The air was also affected by the drag of the droplets and was entrained into the spray. Two-way coupling was important in determining evaporation rates, where the vapour concentration in the gas phase affected the rate of evaporation from the droplets and vice versa. Droplet evaporation led to a temperature decrease which affected the saturation vapour pressure and hence the calculated evaporation rate. Coupling between the two phases was achieved by introducing source terms derived from the Lagrangian solution into the Eulerian transport equations. The overall CFD solution was obtained by iterating between the Eulerian and Lagrangian models.

In previous simulations reported by Coldrick et al. (Reference 3), the cascade of liquid was modelled as a collection of particles injected from slots on the front face of the release tower. The current study aimed to examine the effect of various cascade parameters more closely and therefore a different approach was taken to release the spray droplets. The release tower was approximated as a rectangular box located on a flat surface as shown in Figure 41. The flow domain included a $30 \times 30 \times 20$ m section of atmosphere to account for expected air movements. A projection, rather like a short diving board, was positioned at the top of the release tower. Particles were then injected downwards from a horizontal rectangular area in space at the end of the diving board using a custom droplet-injection routine. This arrangement allowed for variation of the width and depth of the cascade and its offset from the release tower. Particles were injected uniformly at randomly assigned locations within the specified area at each time step in the simulation.

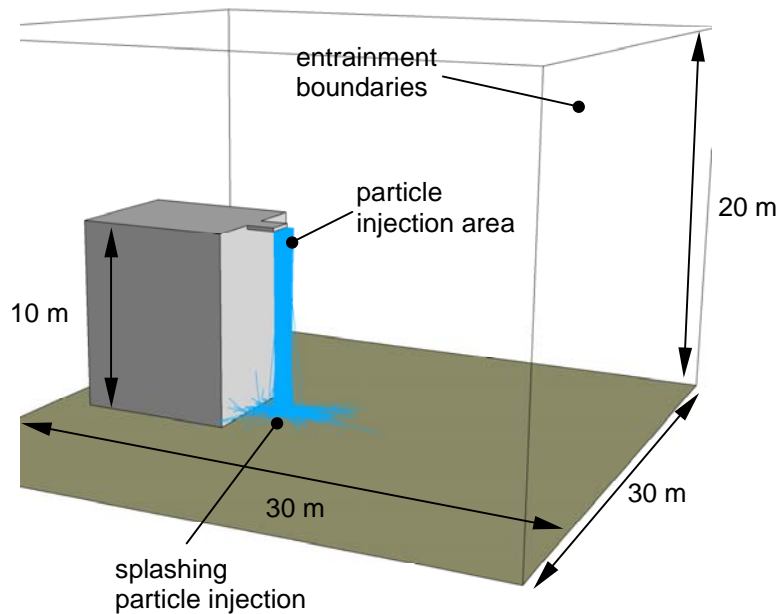


Figure 41 Computational geometry

An unstructured computational mesh was used with cells more densely clustered near the release points, along the trajectory of the spray particles and close to the floor. Near the liquid cascade, cell sides were typically a few centimetres across, whilst in the far field they were around one metre or more. Tetrahedral cells were used in the majority of the flow domain, whilst prism-shaped cells were used near the ground to increase the number of cells in the vertical direction and resolve the thin, dense, gravity current.

The open boundaries at the domain sides and top (representing the atmosphere) were set as entrainment boundaries, allowing the air velocities to freely develop whilst maintaining a set hydrostatic pressure. The 20 m domain height means that hydrostatic pressure has a significant effect on the density. Rather than specifying a uniform constant pressure, an analytical profile was used.

Turbulence was modelled using the industry standard SST model (Reference 8). At the start of the simulations, when the liquid first begins to cascade from the tank, it was assumed that the air velocity was zero everywhere (i.e. the air was quiescent). A very low but finite initial turbulence level was also specified: an initial turbulence intensity of 5% (based on a reference velocity of 0.01m/s) and a ratio of the turbulent viscosity to the fluid viscosity of 10. A non-Boussinesq approach was adopted to model buoyancy effects, which is suitable for modelling a wide range of density variations. The effect of density variations on the flow turbulence was accounted for using standard buoyancy corrections in the turbulence transport equations, for details see Reference 9.

Gant and Atkinson (Reference 7) noted previously that splashing droplets at the base of the cascade may be of importance in altering the vapour current properties. Splashing has the effect of reintroducing droplets at the base of the cascade. The splashing models available in CFX are designed for applications such as internal combustion engine fuel injection and limited success was found in using them for the current application. Instead, the effects of splashing were

accounted for by a secondary injection of particles at the base of the cascade, with a prescribed size, mass flow, temperature and velocity.

During the course of the transient CFD simulations, several outputs from the model were monitored: the total vapour volume, cascade vapour temperature and vapour current temperature. The total vapour volume was calculated as the volume integral of vapour in the domain added to the time integral of the vapour leaving the domain through the open boundaries. Vapour temperatures were monitored at locations corresponding to the measurement locations. Cascade liquid temperatures were also obtained at the end of the simulation period by post-processing the droplet temperature, which were stored as part of the particle-tracking information. The equivalent liquid pot temperatures were obtained by exporting the location, temperature and mass of each particle for the entire period of the release. The data were then filtered to determine those particles whose positions corresponded to the position of each liquid pot. The temperatures of all the particles in each pot were then mass-averaged to give the liquid pot temperatures for the steady state period of the release. Additionally, a mass-averaged liquid temperature for all droplets for the entire simulation was obtained for all of the droplets at a location just above the ground, at the base of the cascade.

8.2 SENSITIVITY ANALYSIS ON THE CFD MODEL

A sensitivity analysis was undertaken to examine the effect of various numerical model input parameters on the resulting flow predictions. These input parameters included: the mesh size, computational time-step, number of iterations per time-step, particle injection speed and number of particles. It was necessary to set a particle injection speed in the model in order to introduce new spray droplets into the flow domain. A low velocity was used for this since, in reality, a tank overflowing release does not impart a significant initial downward momentum to the liquid, which is instead primarily gravity-driven.

A full factorial sensitivity study of these five input parameters would have required at least $2^5 = 32$ simulations. Whilst this type of approach has been used for CFD simulations previously by Cervantes and Engström (Reference 10), it was not feasible for the present application, since a single simulation typically required around one day to compute. To reduce the total number of simulations required and maximise the information gained, an experimental design technique was used, similar to that tested by Hicks and Turner (Reference 11) and Sacks et al (Reference 12). Each of the inputs was set at two levels and a fractional factorial design (see Hicks and Turner, Reference 11) was used to reduce the number of simulations required to 8. Table 3 lists the high and low values of each variable and Table 4 gives the settings used for the 8 runs. Other computational inputs are listed in Table 5. The output variables examined in these tests were the total vapour volume, the average liquid temperature and the average vapour temperature at the base of the cascade.

Table 3 High and low values of the chosen simulation parameters

<i>Parameter</i>	<i>Low value</i>	<i>High value</i>
Mesh nodes (1000's)	148	60
Timestep (s)	0.05	0.1
Particle inlet speed (m/s)	0.5	1
Number of iterations	5	9
Number of particles	500	1000

Table 4 Arrangement of simulations for the fractional factorial experiment

<i>Run</i>	<i>Mesh nodes (1000's)</i>	<i>Timestep(s)</i>	<i>Inlet speed (m/s)</i>	<i>Iterations</i>	<i>No. of particles</i>
1	148	0.05	0.5	5	1000
2	148	0.05	1	9	500
3	148	0.1	0.5	9	500
4	148	0.1	1	5	1000
5	60	0.05	0.5	9	1000
6	60	0.05	1	5	500
7	60	0.1	0.5	5	500
8	60	0.1	1	9	1000

Table 5 Other computational inputs for the fractional factorial design

<i>Parameter</i>	<i>Setting</i>
Hexane flowrate (kg/s)	11.8
Air temperature (°C)	6
Liquid temperature (°C)	6.4
Turbulence model	SST
Turbulence intensity (%)	5
Eddy viscosity ratio	10

Results of the fractional factorial sensitivity analysis are shown in Figure 42. The effect of each input variable was calculated from the difference between the high and low values for each input parameter, as a percentage of the mean over all eight simulations. The largest effect was clearly the mesh size, which accounted for roughly 20% of the total variation. As a result of this, an independent test of mesh sensitivity was carried out to determine a suitable mesh size for the simulations. The other inputs tended to have small effects on the three output variables.

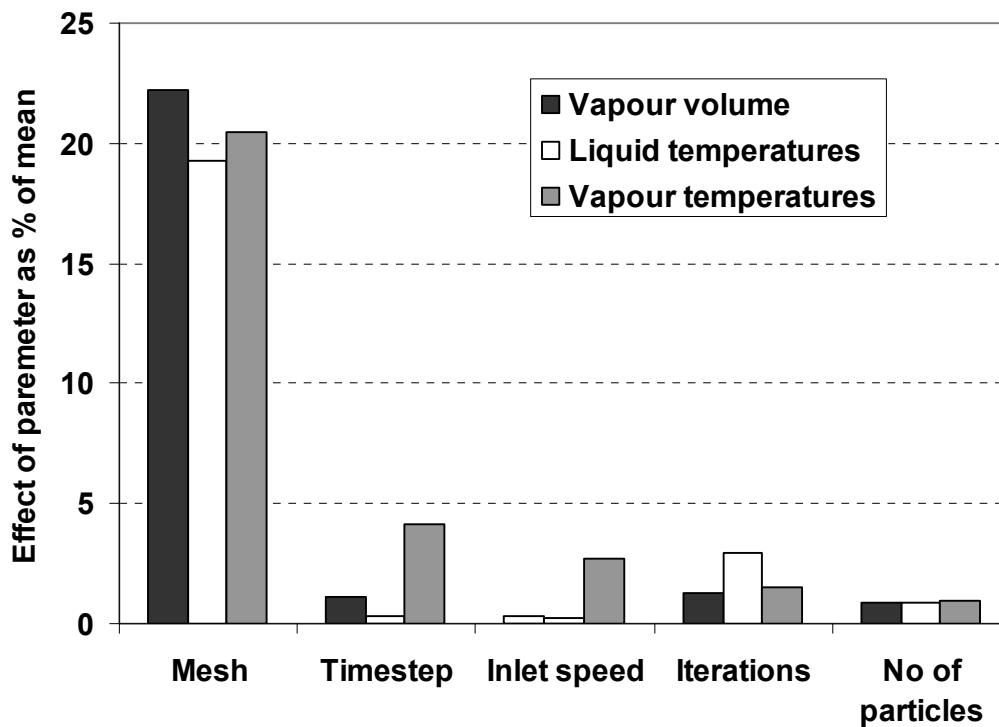


Figure 42 Relative sensitivity to numerical inputs

8.3 MODEL VALIDATION

A number of physical input parameters to the CFD model were the subject of significant uncertainty. For a given release rate of liquid from an overfilling tank, it is difficult to establish from theoretical considerations alone the trajectory of the droplets and initial spreading rate of the spray. The precise details of the resulting flow behaviour are a complex function of the tank top design (or spill chute) and the primary breakup mechanism, from a continuous liquid stream into fluid ligaments and spray droplets. Similarly, the nature of splashing at the base of the cascade is complex and the proportion of re-suspended liquid, its trajectory and size spectrum, cannot easily be quantified without recourse to detailed experiments.

To address these issues, exploratory simulations were performed to adjust the CFD model to fit the experimental data. These simulations concentrated on the physical (as opposed to the numerical) aspects of the model, and included tuning parameters such as the cascade inlet dimensions, droplet size distribution and splashing conditions (further details are provided in the next section). The model parameters were systematically varied within reasonable ranges until a good fit with the data was obtained. In the first step, the cascade dimensions in the CFD model were specified to match the behaviour observed in the experiments. Then the initial size spectrum of the droplets was specified, using a Rosin-Rammler distribution. This size distribution is specified by two parameters: a characteristic diameter (δ) and an index that controls the spread in droplet sizes (γ). It was found that the average liquid temperature in the cascade was primarily controlled by δ , but was relatively insensitive to changes in γ . Therefore, simulations first concentrated on finding the value of δ which gave the correct average liquid temperatures. Then γ was adjusted to match the vapour temperatures in the cascade. Once the

liquid and vapour temperatures in the cascade were predicted well by the CFD model, the splashing conditions were adjusted in order to obtain good agreement with the measured temperatures of the vapour current downstream from the splash zone. Droplets were injected close to ground level and followed trajectories in the lower part of the vapour current. Due to the specification of the initial trajectories and prescribed droplet size, reduced mixing across the flow by large eddies was observed in the CFD model. In these conditions vaporisation of droplets was reduced and their lifetime in the flow controlled by settling-out. Substantially larger mass injection rates (as a proportion of the total mass flow) than the experimental values were required to reproduce the total evaporation rate and consequent cooling effect.

The experiments used for these comparisons were Test 9 and Test 12, having different release rates and ambient conditions. The results presented below are for the simulations that were found to best fit the data, denoted “Case A” and “Case B”, the conditions for which are given in Table 6.

Table 6 Computational settings for the two best fit simulations

<i>Parameter</i>	<i>Case A</i>	<i>Case B</i>
Test	9	12
Air temperature (°C)	6	10
Liquid starting temperature (°C)	6.4	12.6
Mass flow (kg/s)	11.8	15
Particle size in cascade	2 mm, $\gamma = 3$	2 mm, $\gamma = 3$
Splashing particle mass flow (% of liquid flow)	10	10
Splashing particle size	0.1 mm	0.1 mm

The predicted mass-averaged liquid temperatures for Case A across the depth of the cascade are shown in Figure 43. These were obtained for the period between 10 and 60 seconds after the start of the release, when the flow had reached a steady state. The solid line represents the mass average temperatures and error bars indicate the maximum and minimum droplet temperatures obtained at each location. The mean liquid temperatures (number weighted, rather than mass-averaged) are also shown with a dotted line. A single value from the experiments is plotted as the horizontal dashed line. This corresponds to the average temperature from a single liquid pot which was reliably being impacted by the cascade and therefore corresponds to the mass average liquid temperature at the cascade centre. Due to the ratio of surface area to volume, large droplets tend to stay relatively warm, whereas small droplets can reach very low temperatures. At the edges of the cascade, the vapour concentrations are low and hence droplets can readily evaporate. In the core of the cascade, the vapour concentrations are higher, evaporation is more limited and hence droplet temperatures tend to be higher. Therefore, at the edges of the cascade, relatively few droplets were collected and these tended to be very small and cold.

The bulk liquid temperature given by the large mass of liquid at the centre of the cascade in Figure 43 provides an indication of the overall degree of evaporation. However, a small proportion of the injected mass was contained in very fine droplets. Although these fine droplets contributed to the total vapour production, some of their effect was not registered in Figure 43, since a proportion of these droplets were either carried away or evaporated completely before they could arrive at the measuring point. The liquid temperatures should therefore not be relied

upon solely to determine the total amount of evaporation. Figure 3 also highlights the difficulty faced in assessing the degree of saturation of the vapour in the cascade. Small, cold droplets may not be able to evaporate whilst larger, warm droplets can still evaporate, although their contribution will be limited, due to their smaller ratio of surface area to volume.

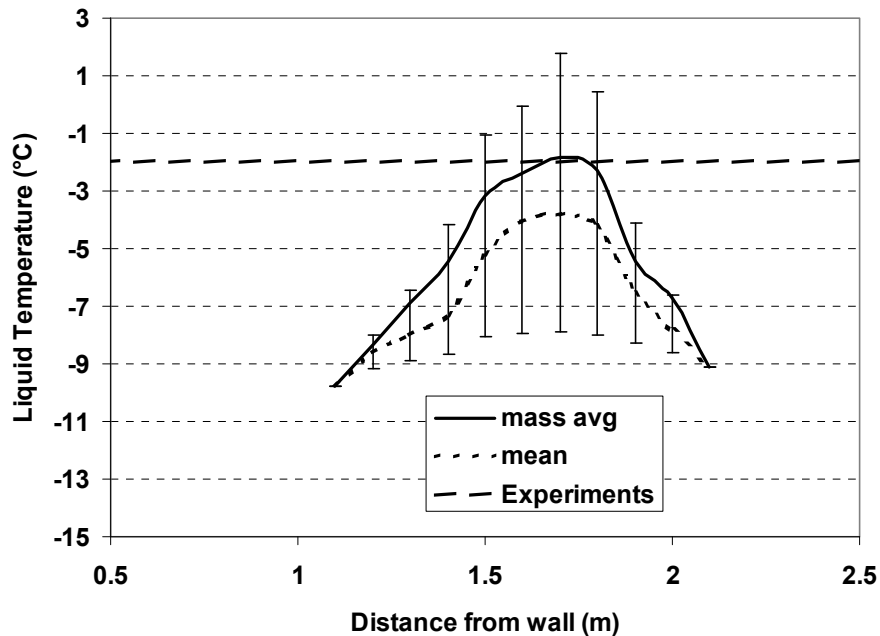


Figure 43 Averaged droplet temperatures across the depth of the cascade

The predicted and measured minimum vapour temperatures within the cascade are shown in Figure 44. In the first 20 seconds of the release, the profiles exhibit different behaviour, with the CFD model showing an immediate temperature drop followed by a recovery to a steady state whereas in the measurements there was a more gradual decline to the steady state. The sudden initial temperature drop in the CFD model results was caused by the droplets falling initially through fresh air. In this short period, significant evaporation took place and therefore the predicted fresh temperatures were low. The gradual decrease in the measured temperatures is considered to result from a time delay related to the thermal mass of aspirated thermocouples and flow recirculation effects within the devices. The gradual reduction in temperatures also appeared to be linked to a recirculation of cold vapour in the region behind the cascade. This effect took up to 20 seconds to become established fully. Tests with the CFD model suggested that the significance of the flow recirculation effects was dependent on the proportion of fine droplets present. In the experiments, it was likely that the droplet size spectrum changed over time. Very fine droplets were probably produced initially, when the relative velocity between the falling droplets and the quiescent ambient air was greatest. The recirculation of these fine droplets within the region between the cascade and the tank wall, may have then led to the gradually declining vapour temperature in the cascade. Such subtle effects cannot easily be accounted for in the CFD model, which uses a fixed droplet size spectrum that was tuned to obtain the correct steady-state temperatures.

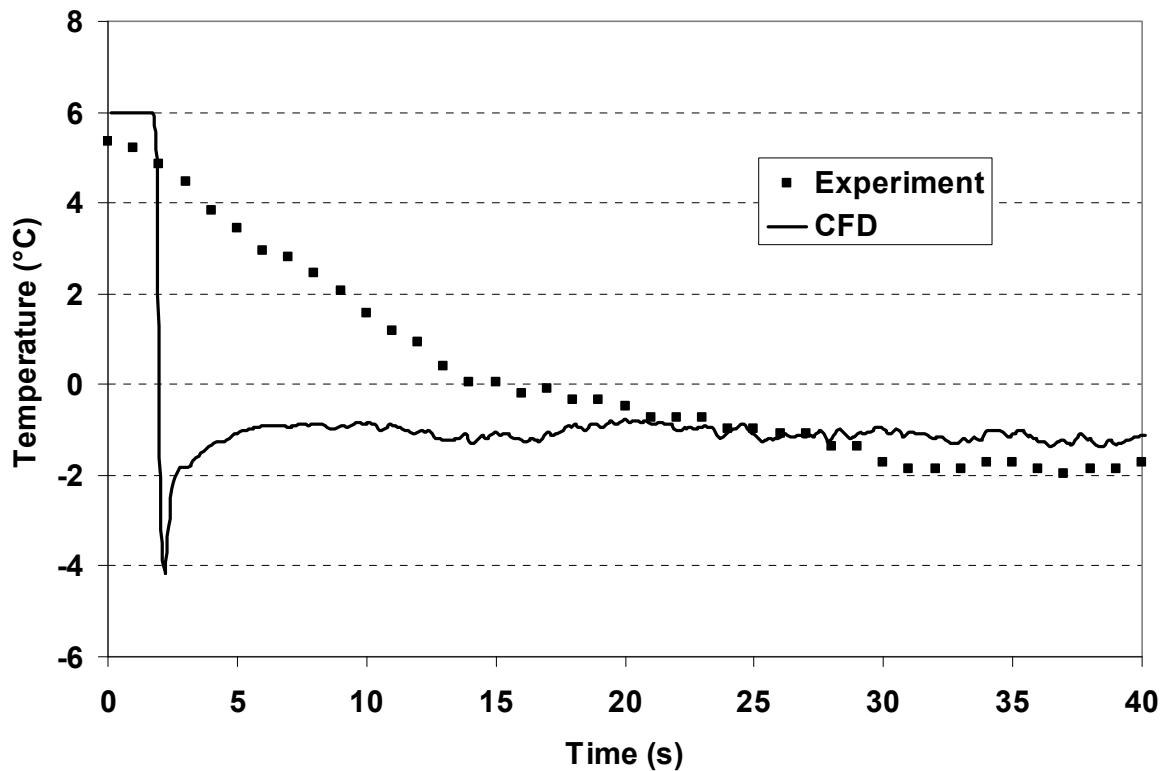


Figure 44 Vapour temperatures at the centre of the cascade

The predicted and measured vapour temperatures at a position 0.5 m from the ground and 5 m from the release tower are shown in Figure 45. The arrival of the cold vapour current is clearly evident in the experimental trace and visible as a slight dip in the CFD profile. The CFD temperatures then undergo a rapid cooling after around 10 seconds. The reason for the lag in the predicted temperature drop is not clear but is likely to be due to assumptions made in the prescription of the splashing droplets in the model. Despite these differences, the predicted steady-state temperature is within one degree of the measured value. The temperature profiles at the 5 m mast were used as a benchmark to adjust the splashing droplet size and mass flow.

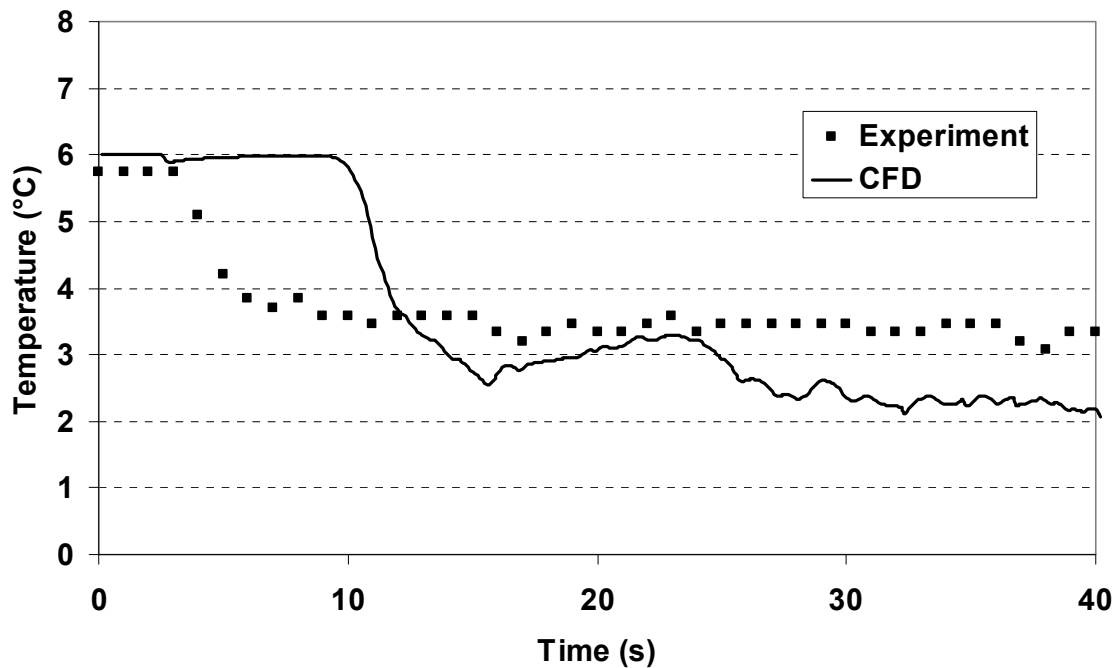


Figure 45 Vapour temperatures 5 m from the wall and 0.5 m from the ground

8.4 IDENTIFICATION OF IMPORTANT PARAMETERS

The exploratory process of fitting the CFD model to the experimental data resulted in an increased understanding of the vapour generation processes. Coupled with this, the previous systematic variation of model input parameters resulted in a large results dataset. This dataset was used to examine the relative importance of several input parameters as follows:

Droplet size – Simulations were performed with both a mono-sized droplet spectrum and a Rosin-Rammler size distribution, in which a representative diameter and spread were specified.

Number of particles – Whilst the number of particles was investigated previously (see Section 8.2), this factor was revisited once the particle size distribution that best fitted the measurement data was found. It is a potentially important parameter, since a particle size distribution usually requires the simulation of a greater number of particles than if a mono-sized droplet spectrum is used. The sensitivity of the results to the number of computational particles was assessed both for those injected in the cascade and those in the splash zone.

Turbulent dispersion – As droplets pass through the air, their trajectory may be affected by turbulent perturbations or localized eddy motion. This was accounted for in the CFD model by using the particle turbulent dispersion model of Gosman and Ioannides (Reference 13). Tests were performed without this model to examine the sensitivity of the results to the effect of turbulent dispersion.

Wall heat transfer – The vaporisation rate could potentially be influenced by heat transfer from the ground and the release tower walls. Simulations were performed with different thermal boundary conditions on these surfaces to assess the degree of sensitivity in the model predictions. Tests were performed using constant temperature walls, adiabatic walls or a model that accounted for heat transfer through the concrete floor at the base of the cascade.

Droplet breakup – Simulations were performed using the droplet breakup model of Rietz and Diwakar (Reference 14) in conjunction with an initial droplet size distribution. The model accounted for aerodynamic breakup of particles as a function of the particle speed relative to the surrounding gas phase.

Cascade dimensions – The cascade dimensions were initially specified in the CFD model using photographs taken during the experiments. In addition to this, simulations were carried out using a range of cascade heights, widths, depths and offsets from the release tower wall.

Splashing droplet size and mass flow – Splashing droplets at the base of the cascade were represented by a separate vertical injection of spray particles with an initial temperature equal to the average temperature of cascade particles striking the ground. The influence of splashing droplets was assessed by varying their initial size and mass flow.

For these sensitivity tests, the model outputs used for the comparison were again the cascade liquid and vapour temperatures and the total amount of vapour produced over the simulation period. Due to the large number of variable parameters, a full parametric study was not undertaken and the dataset did not include a full breakdown of the effects of varying one parameter at a time. Results were therefore examined using the coefficient of variation (CV), defined as the ratio of the standard deviation (σ) to the mean (μ):

$$CV = \frac{\sigma}{\mu}$$

The coefficient of variation is a means for comparison of the relative effects of each of the inputs on each of the outputs. Figure 46 shows the coefficient of variation for the three output parameters for a number of input parameters. The total vapour volume was almost equally affected by the cascade droplet size, the splashing droplet size and mass flow, but the largest influence was from the cascade dimensions. Including a model for turbulent dispersion had the effect of increasing the spray width, and therefore had a significant effect on the total vapour volume. The wall heat transfer treatment had a relatively small effect, indicating that the production of vapour was governed by mixing with ambient air, rather than heat transfer from neighbouring solid surfaces. The overall vaporisation rate was largely uninfluenced by the numbers of particles.

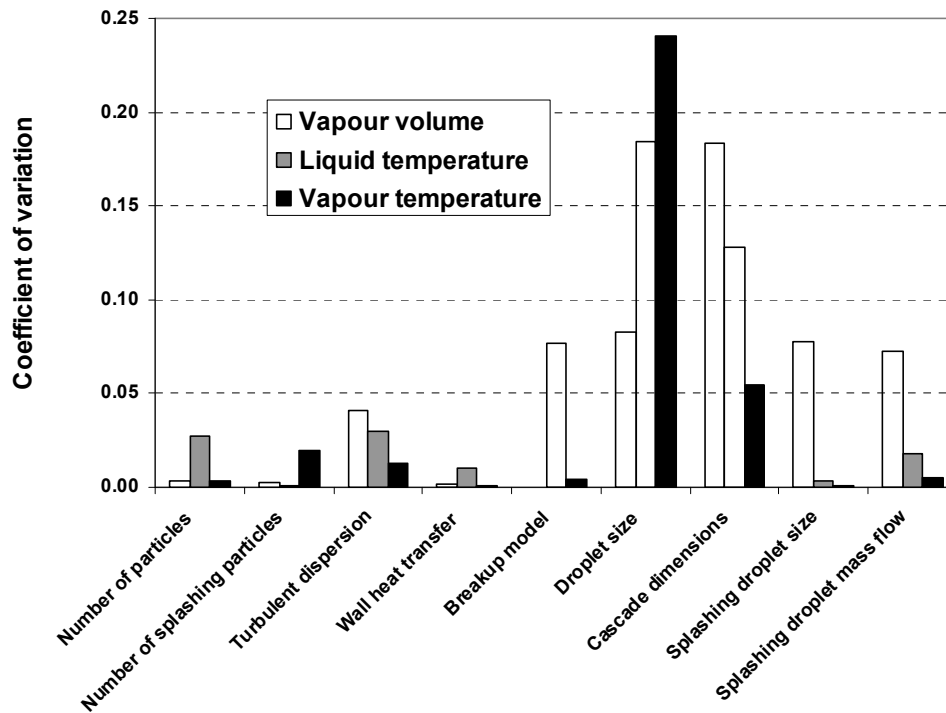


Figure 46 Sensitivity of the model to inputs

The cascade liquid and vapour temperatures were mainly a function of the droplet size within the cascade, and the cascade dimensions. This was expected, since the temperatures were linked directly to the effectiveness of mixing between air and liquid within the cascade. Spreading the particles over a larger area increased the available air for mass transfer, and similarly, decreasing the particle size resulted in a greater surface area for mass transfer. The liquid temperature appeared to be affected by the number of particles in the cascade. This was a symptom of the method of assessing the liquid temperature: more particles resulted in an increased likelihood of collecting particles in the liquid pots in the model, and an improved statistical measure of the mean liquid temperature. The vapour temperature was insensitive to the number of droplets in the cascade, but sensitive to the number of splashing particles. This is likely to have been due to very small splashing particles being caught in the flow recirculation behind the cascade and then re-entrained into the cascade flow. The more particles that were injected, the greater this effect had on the results. The model results shown subsequently used the maximum number of droplets that were practical, given the computing resources available.

8.5 EFFECT OF SPLASHING DROPLETS

The effect of splashing droplets is readily illustrated by examining the vapour current properties with distance from the tower wall. Figure 47 shows the vapour current temperature and concentration on a line extending 10 m perpendicular to the release tower wall, at 0.15 m height from the ground. The values shown were extracted towards the end of a simulation once a steady state had been reached. Three simulations are presented: 1.) without splashing, 2.) splashing with a fixed post-impingement droplet diameter of 0.1 mm monosize droplets, and 3.) splashing with a post-impingement droplet size spectrum specified using a Rosin-Rammler distribution with $\delta = 1$ mm and $\gamma = 1.5$. Splashing mass flow rates for Cases 2 and 3 were 10%

and 50% of total liquid flow released from the tank, respectively. The peak concentration and lowest temperature shown for the non-splashing case correspond to the location of the center of the cascade. Concentrations and temperatures show opposite trends, since dilution and temperature rise are interlinked and there is very little additional vaporization outside of the cascade for the non-splashing case. For both cases with splashing droplets, the vapour temperature surrounding the cascade is approximately equal to the splashing droplet temperature. A slightly higher initial concentration is obtained for Case 3 in the region of the cascade. This is likely to be due to the presence of some very fine droplets that evaporate readily. Outside of the splashing zone, there is an immediate increase in temperature for this case. For Case 2, the monosize 0.1 mm droplets produce some further evaporation outside of the splash zone, and hence a further temperature drop, before the vapour current begins to be warmed by entrainment of fresh air. This appears to be due to a greater proportion of the droplets being carried downstream by the vapour current for this case. It is interesting to note that the two splashing droplet sizes and mass flows used ultimately resulted in the same concentration being produced. The different prescriptions of splashing droplets were found to result in similar velocity fields along the vapour current. For the effect of splashing relevant to this problem, the fluid mechanics and thermodynamics of the vapour current are effectively uncoupled. Similar velocity fields imply similar levels of mechanical mixing independently of the temperature and concentration fields.

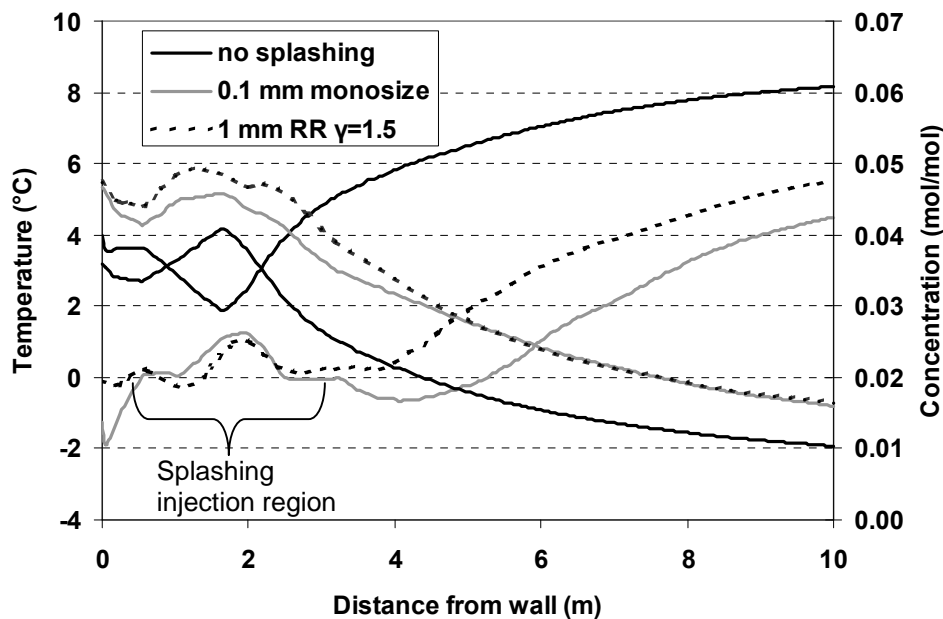


Figure 47 Concentration and temperature on a line extending from the tank wall at a height of 0.15 m from the ground (concentrations showing a downward trend)

Many more splashing simulations have been performed than are presented here, which showed that the concentrations and temperatures in the vapour current are sensitive to both the proportion of released liquid mass flow rate that is splashed back into the air, and the size spectrum of the splashed droplets. Further investigation is required to fully understand these effects and to develop a generic splashing model. Previous work on this subject, in the context of internal combustion engines, was reported by Bai et al. (Reference 6). They showed that

splashing on a wetted wall could potentially result in the reintroduction of 110% of the liquid mass flow rate, and hence substantially increased vapour production.

8.6 SIMULATIONS WITH GASOLINE

The experiments and simulations presented above used pure hexane to represent the complex multi-component substance, gasoline. This approach greatly simplified the analysis because no account had to be made for preferential evaporation of lighter fractions. This section presents the results of a single simulation which was carried out using a four-component gasoline mixture. The four-component mixture was used by Gant et al. (Reference 15) in simulations of dispersal of the Buncefield vapour cloud. Although this mixture is still a simplification of real gasoline, it offers insight into the nature of multi-component fuel vaporization. The four-component mixture is composed of butane, pentane, hexane and decane in the proportions given in Table 7. Simulation of this mixture required modification of the droplet evaporation model in CFX to include the effects of Raoult's Law. The composition of the splashing droplets was also modified to reflect the loss of lighter fractions in the cascade, and the greater proportion of heavier fractions in the splashed droplets. The composition was obtained by simulating a gasoline release without splashing and then mass-averaging the fraction of each component for all of the droplets at the base of the cascade. Splashing droplets were then injected with this modified composition at the base of the cascade (details are given in Table 7).

Aside from the material change, the conditions simulated were the same as those used for Test 12 (Case B in Table 6). Outputs of vapour volumes were therefore directly comparable. The vapour volumes for the gasoline simulation were obtained in the same way as for the hexane simulations as the integral of vapour volume in the domain added to the integral of the vapour volume leaving the domain through the sides. The volumes for each component were then summed to give a total. Figure 48 provides a comparison of the vapour volumes for the hexane and gasoline simulations. The solid lines represent the integral of material flowing through the sides of the domain and the dashed lines represent the total vapour volume produced by the two materials. In both cases, material begins to flow out of the domain after approximately 15 seconds. The fact that the vapour current is driven by the kinetic energy within the cascade means that the hexane and gasoline vapour currents will tend to have similar flow behaviour in the near field. Comparison of the total vapour volume shows that a substantial increase is obtained with gasoline; approximately 50% greater vapour volume is achieved.

	<i>Mass Fraction in cascade (% w/w)</i>	<i>Mass Fraction in splashing droplets (% w/w)</i>
Butane (C ₄ H ₁₀)	9.6	3.5
Pentane (C ₅ H ₁₂)	17.2	14.5
Hexane (C ₆ H ₁₄)	16.0	16.9
Decane (C ₁₀ H ₂₂)	57.2	65.1

Table 7 composition of cascade and splashing droplets

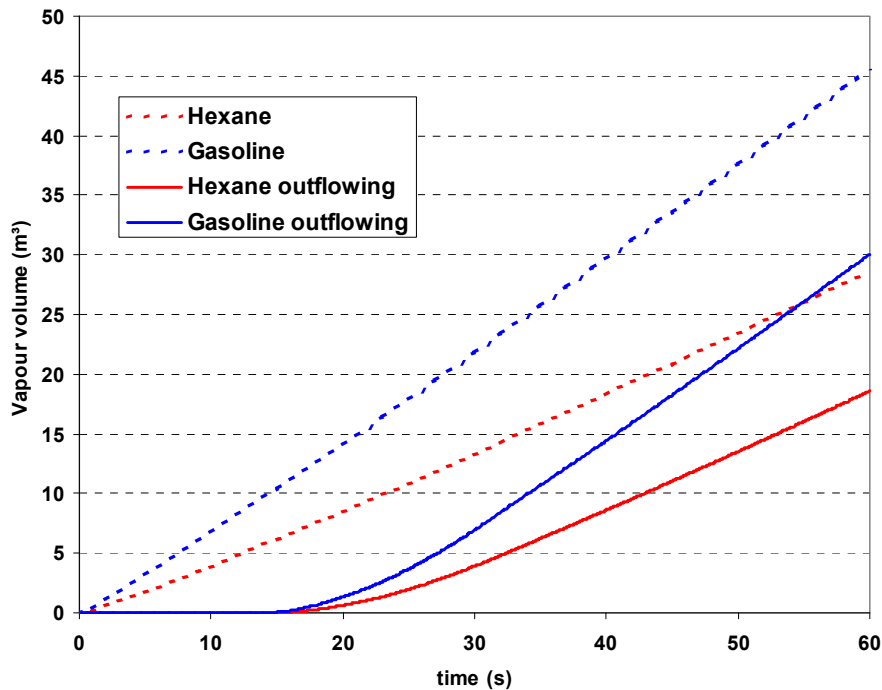


Figure 48 comparison of vapour volumes produced by hexane and gasoline

8.7 DISCUSSION OF RESULTS

The previous sections have presented CFD simulations of tank overfilling releases and have examined the model sensitivity to its input parameters. Two cases have been developed which show good agreement with the vapour and liquid temperatures measured in the experiments (Table 6). On the basis of liquid and vapour temperatures, it is possible to infer a vapour concentration produced by an isolated cascade. A method for doing this is presented in Coldrick et al. (Reference 3) using bulk liquid and vapour temperature changes. However, the current simulations include splashing droplets such that it is not possible to obtain bulk temperature changes. A more reliable estimate of vapour concentration is obtained when the simulations include some form of constraint such as a bund. Furthermore, in a real tank overfilling release, the presence of such obstructions close to the tank would lead to a vapour layer building up over

time (as demonstrated at Buncefield). These bundled simulations are presented in the following section.

9. MODELLING OF VAPOUR ACCUMULATION

In this section, a further set of simulations are described in which the validated model is used to examine the effects of various bund configurations on the vapour concentrations. The effect of multiple adjacent release points – as encountered on a circular tank (see Reference 7) – is also considered. Figure 49 shows the geometry used for these simulations, consisting of a 20 m diameter circular tank located centrally within a bunded area, with eight release points equi-spaced around the tank roof. Computing requirements for the simulations were reduced by taking advantage of symmetry, and only one quarter of the flow domain was modelled. The section of the geometry used for the model is indicated by the wireframe in Figure 49. Two injection locations were specified, with the injection parameters corresponding to those used previously for Case B (see Table 6). Three simulations were performed without a bund, and four simulations were performed with different bund configurations, as listed in Table 7. In the first simulation without a bund (Case C), an unobstructed ground plane was modelled and the vapour was allowed to escape the flow domain unimpeded. In the other two simulations without a bund, a wall was placed at the edges of the flow domain to simulate the effect of a gradually accumulating vapour layer. The wall was 4 m high in Case H and 2.5 m high in Case I. A number of outputs were monitored over the course of the simulation period. These included the average vapour concentration within the bund, the concentration of material flowing over the top of the bund and the concentration of vapour just outside the bund. Simulations were continued until the average vapour concentration within the bund reached a steady state.

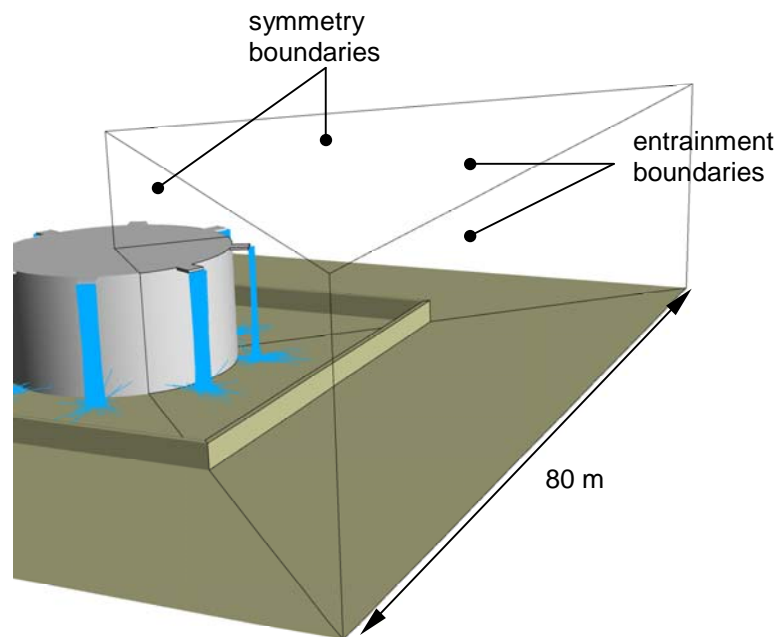
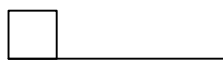
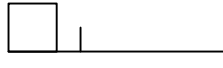
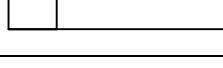
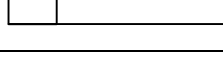


Figure 49 Computational geometry for Cases C to H. The triangular section identified by the wireframe was modelled.

Table 8 Configurations for the circular tank simulations

<i>Simulation</i>	<i>Configuration</i>	
Case C	no bund	
Case D	bund at 5 m	
Case E	bund at 10 m	
Case F	bund at 15 m	
Case G	sloping bund at 5 m	
Case H	no bund, 4m wall surrounding domain	
Case I	no bund, 2.5m wall surrounding domain	

9.1 EFFECT OF ACCUMULATION ON CASCADE PROPERTIES

Figure 50 shows the liquid temperature profiles for five of the cases given in Table 8, presented alongside the results for the single release Case B. The liquid temperature profiles are taken as the average over the steady-state period of the release, from 10-60 seconds. It can be seen that the different bund configurations have minimal effect on the liquid temperature profiles. The cascade vapour temperatures (Figure 51) show that the presence of adjacent release points leads to a small reduction in vapour temperature within the cascade, generally less than one degree, as compared to the case with the single release (Case B). This may be in part due to additional cold vapour being available at the sides of the cascades. As vapour begins to accumulate within the bund, an increasing amount of cold material is recirculated back into the cascade. This manifests itself as a slight reduction in the liquid and vapour temperatures in the cascade. Table 9 shows the differences in the averaged liquid and vapour cascade temperatures between the first 60 seconds and the last 60 seconds of each simulation. Both liquid and vapour temperatures undergo a small reduction, as a result of the recirculation.

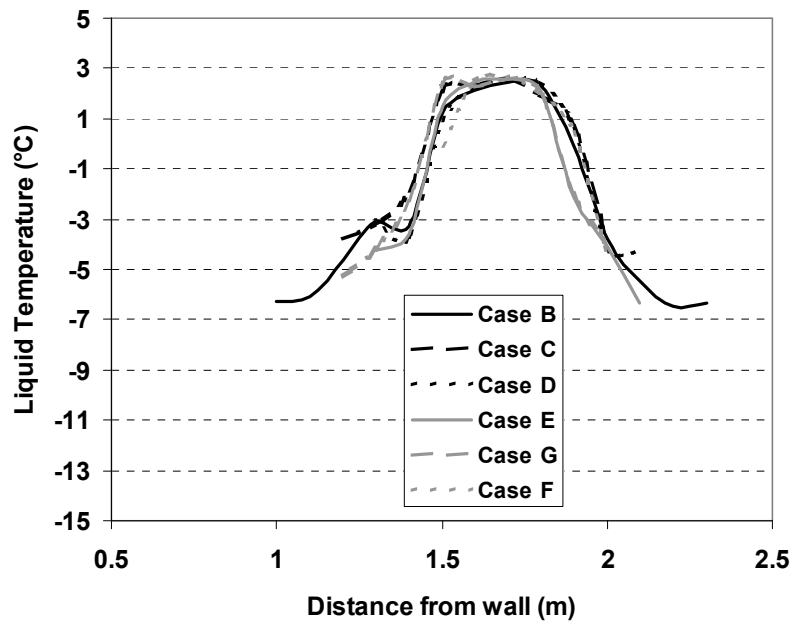


Figure 50 Liquid temperatures for the initial 10-60 second period of each simulation

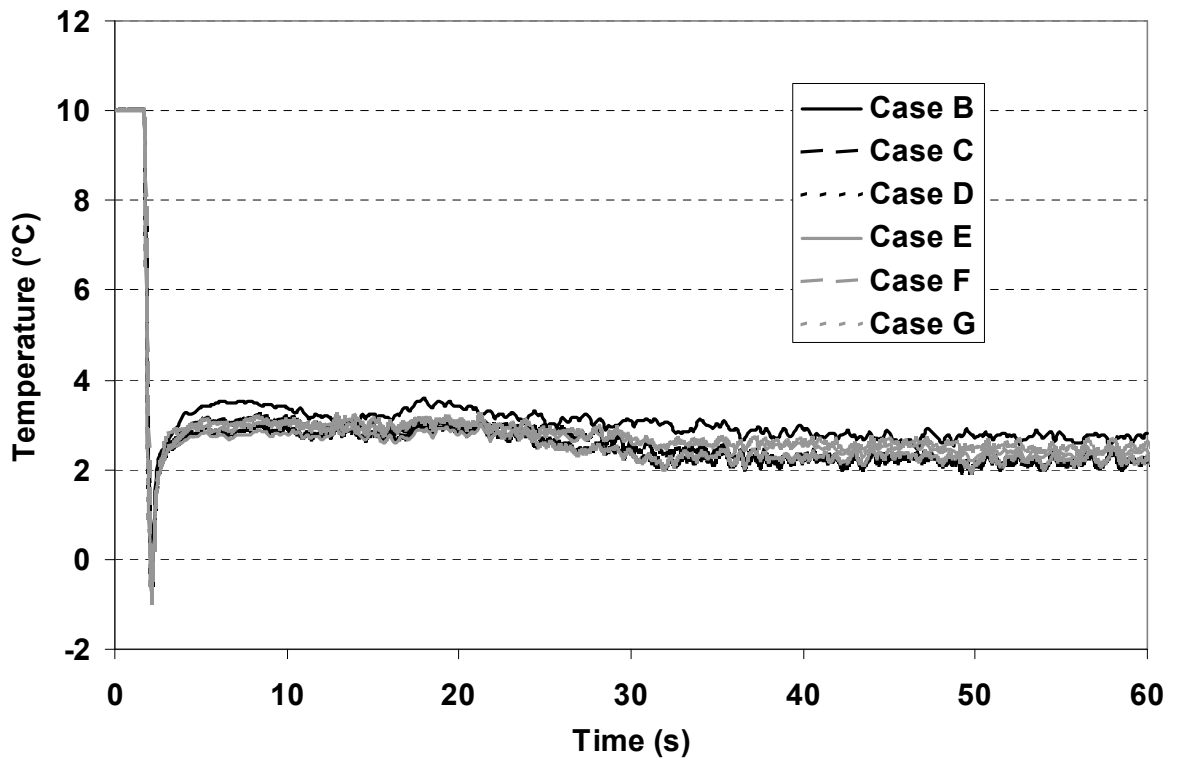


Figure 51 Vapour temperatures at the centre of the cascade

Table 9 Cascade vapour and liquid temperature between the start and end of the simulations

	<i>Temperature difference (start-end) (°C)</i>	
	<i>Vapour</i>	<i>Liquid</i>
Case C	0.3	0.5
Case D	0.2	0.9
Case E	0.3	0.4
Case F	0.3	0.1

9.2 RESULTS

For the simulations with bunds (Cases D, E, F and G), the average concentration within the bund was defined as the volume integral of concentration for all cells within the bund (below the bund height), divided by the total volume of the bund. The average temperature was similarly defined. In all of the cases modelled, the bund height was 2 m. Figure 52 shows the development of the average concentration and temperature over time for the four cases. Cases E, F and G all eventually led to similar steady state concentrations of around 0.025 mol/mol, despite the bund wall being spaced at different distances from the tank, or for the bund to have a sloping rather than a vertical wall. However, Case D produced a slightly higher steady state average concentration of 0.028 mol/mol. The bund wall was located closest to the tank for this case, and the higher concentration resulted from the vapour current inside the bund having little opportunity for dilution. For all four cases, the behaviour observed in the average concentration was mirrored in the temperature profiles, all exhibiting a drop of approximately 6 °C. The relationship between the average concentration within the bund and that of the material flowing over the top of the bund wall is illustrated in Figure 53 for Case E (bund at 10 m). At a point on top of the bund wall directly opposite the cascade, the peak concentration was slightly higher than the average within the bund as this was where the body of the vapour current passed over the bund wall. On top of the bund wall in between the two cascades, the vapour concentration matched the average inside the bund. This behaviour was observed for all of the bunded spills, indicating that the steady state mean concentration within the bund is a good approximation for the vapour source term arising from a spill into a bund.

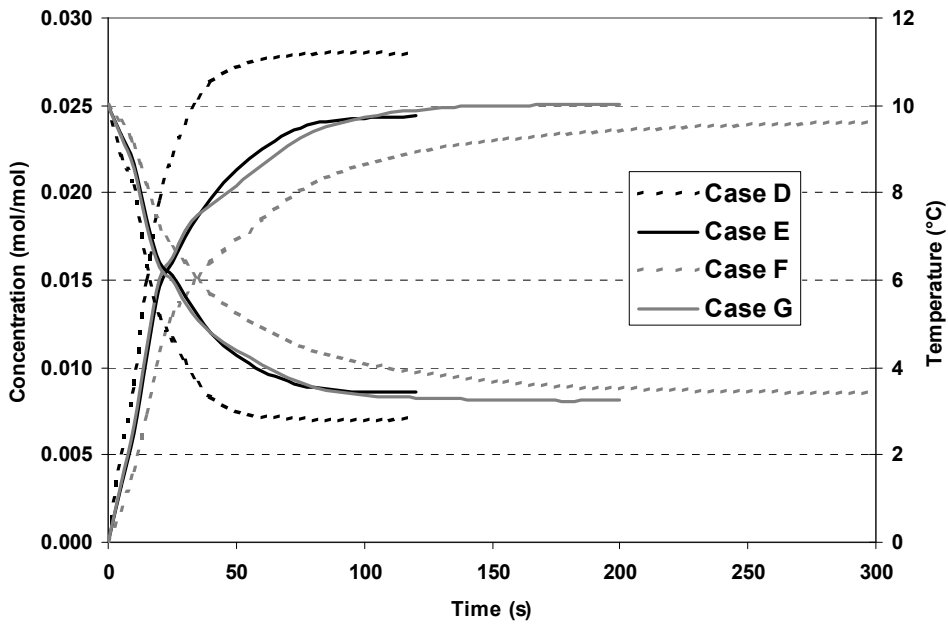


Figure 52 Average vapour concentration and temperature within the bund (ambient temperature is 10°C)

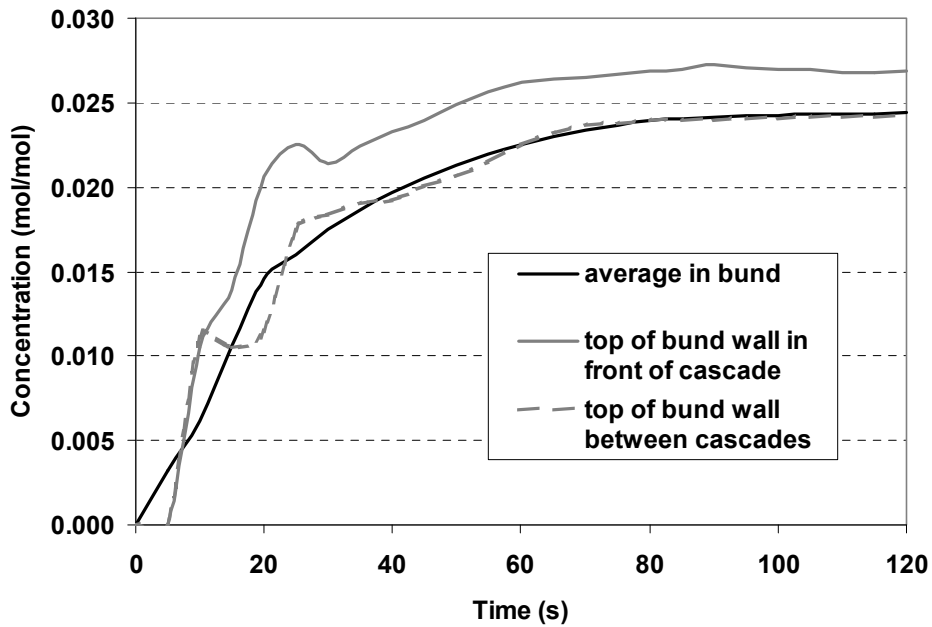


Figure 53 Average vapour concentration in the bund and average vapour concentration flowing over the bund wall (Case E)

The shape of the vapour clouds produced by the different bund configurations are shown in terms of isosurfaces at the Lower Flammability Limit (LFL) concentration for hexane of 0.012 mol/mol in Figure 54. The isosurfaces are coloured with height from the ground up to a maximum of 2 m, (corresponding to the bund height). The images are mirrored in the symmetry planes and a section of the isosurface has been removed to show the bund geometry. In each case, rapid entrainment into the vapour current close to the cascade impact point draws fresh air down into the vapour layer, causing a deformation of the isosurface. For Case D, and to a lesser extent Case E, the high-momentum stream of vapour produced by the cascade leads to a deformed surface of the vapour layer even outside the bund, whereas in Cases F and G it is more uniform.

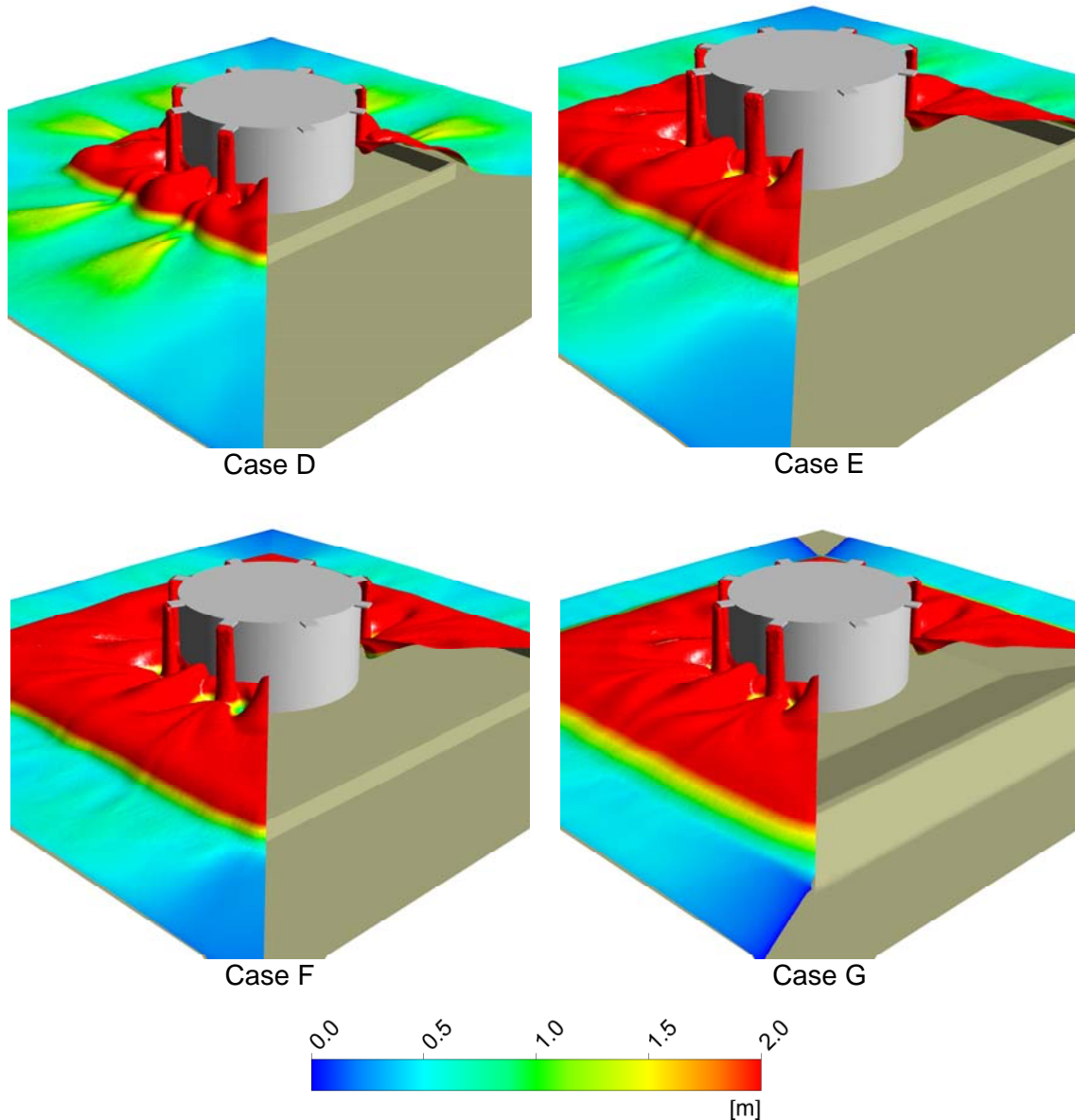


Figure 54 Isosurfaces of vapour concentration at the LFL. The surfaces are coloured according to height from the ground, up to a maximum of two metres

The deformation of the vapour layer is illustrated further in Figure 55, which shows the concentration on a cross section through the vapour layer for each of the four cases. The contour plots are coloured up to a maximum concentration of twice LFL (0.024 mol/mol) for illustration, though higher values than this were achieved in the cascades. The results are shown in the steady state period of each simulation, corresponding to the time when the maximum depth and concentration were reached. In all four cases, the banded volume has filled with dense vapour and this is flowing over the bunds in a layer approximately 1 metre deep. Toward the cascade, the displacement of the vapour layer by the entrained air is evident in the lower concentrations immediately in front of the cascade.

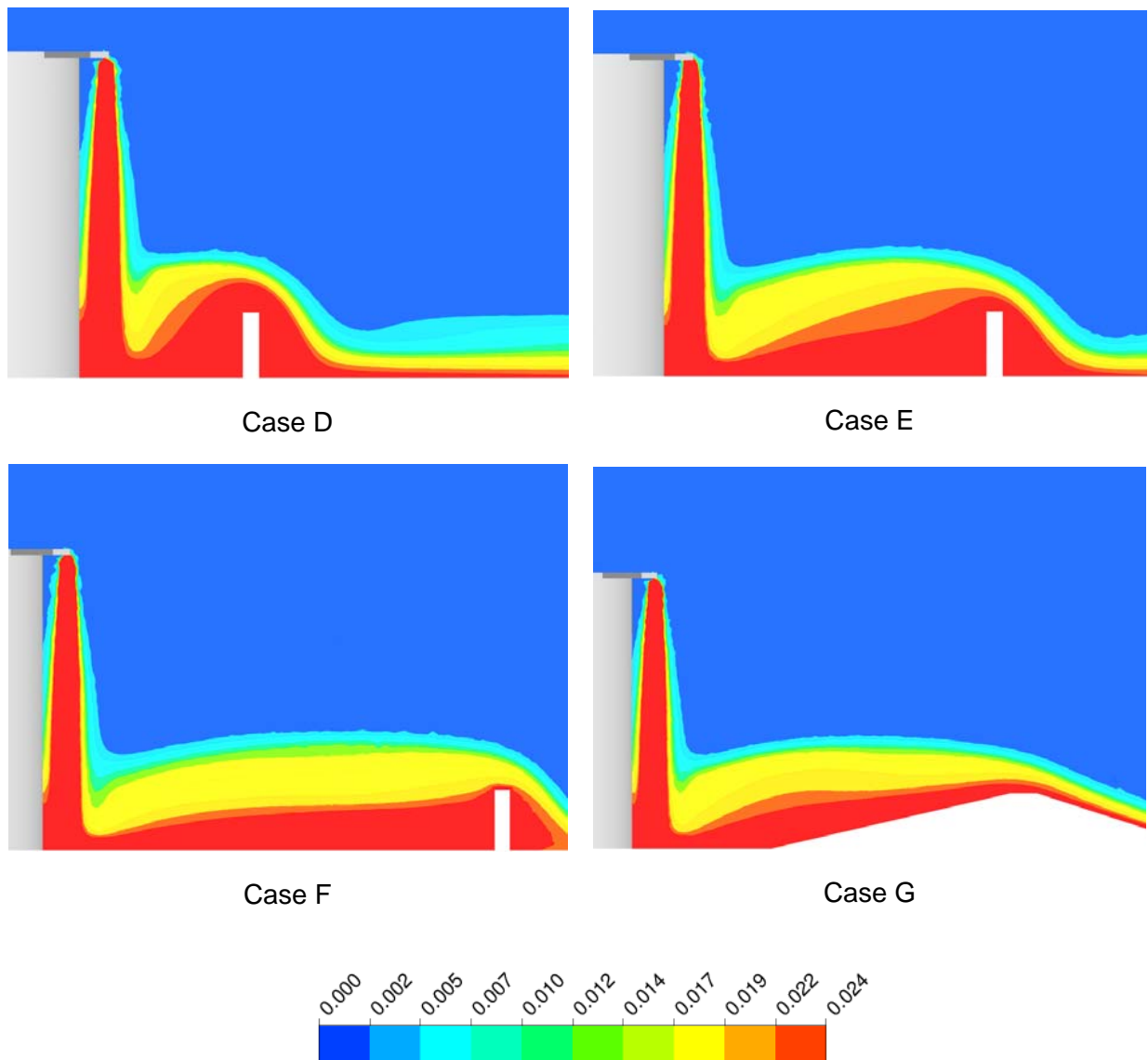


Figure 55 Contour plots of concentration (mol/mol) up to twice LFL on a plane extending from one of the cascades out to the bund.

9.3 EFFECT OF ACCUMULATING VAPOUR LAYER

In an overflowing incident, vapour is not necessarily free to travel away from the immediate vicinity of the tank. Topographical features and obstacles may result in an increasingly deep layer accumulating and surrounding the tank. This was observed in the Buncefield incident where the CCTV records showed a mist increasing in depth over a 23 minute period to around 4 metres in the area adjacent to the bund in which the tank was overflowing (Reference 15). Simulations reported by Coldrick et al. (Reference 3) examined the effect of an accumulating vapour layer on the concentration of material overflowing from the bund. This effect was examined further in the current study using the Case H and Case I arrangements (see Table 8), in which there was no bund but a wall was placed at the flow domain boundaries. During the course of the simulation, the average vapour concentration within the “tray” and the depth of the layer corresponding to $\frac{1}{2}$ LFL (a concentration of 0.006 mol/mol) were monitored. The former quantity was calculated from the integral of all computational cell volumes with concentration over $\frac{1}{2}$ LFL, divided by the total area of the ground. The simulations were continued until the concentration reached a steady state. For the 4 m deep Case H, this required approximately 15 minutes simulation time, corresponding to 17 days computer run time using a four-processor workstation

Results for the 4 m wall simulation (Case H) are shown in Figure 56. The vapour depth is relatively quickly established, taking 200 s to reach a depth of just over 4 m. At this point, vapour begins to spill over the outer wall. The average concentration within the 4 m tray increases steadily over time, levelling out after around 13 minutes. The recirculation process reaches a steady state, giving a final concentration of 0.035 mol/mol or approximately three times the LFL. The increased concentration obtained in comparison to the banded spills is caused by the increased layer depth of 4 m as opposed to 2 m. An increased layer depth results in a larger proportion of vapour being recirculated into the cascade and hence a higher concentration. However, the maximum concentration is always limited by the entrainment of fresh air that is pulled downwards into the vapour cloud by the cascade. This is illustrated in Figure 57 showing an isosurface at twice the LFL, coloured according to the height from the ground. Twice LFL has been used for illustration purposes of the higher average concentration achieved in this case. In the region immediately surrounding each cascade, the vapour layer is clearly displaced by the downward motion of the entrained ambient air. Figure 58 is a contour plot of concentration on a plane through the cascade. The contours are shown up to a maximum of 0.05 mol/mol, and the lower concentration immediately surrounding the cascade is evident. Figure 58 also demonstrates the sharpness of the interface between the dense vapour layer and the surrounding atmosphere.

Results for the 2.5 m wall simulation are shown in Figures 59 to 61. Due to the smaller volume, a steady state concentration is reached in roughly 12 minutes. The shallower depth also results in a slightly lower average concentration of approximately 0.024 mol/mol. This is illustrated in Figure 60, which shows the isosurface at the LFL (rather than twice the LFL). The shallower layer depth is also shown in Figure 61 and is fairly well defined at around 4 m – this is comparable to that observed during the Buncefield incident. In the cascade, concentrations of approximately 0.05 mol/mol are evident which is roughly twice the average concentration of the vapour layer.

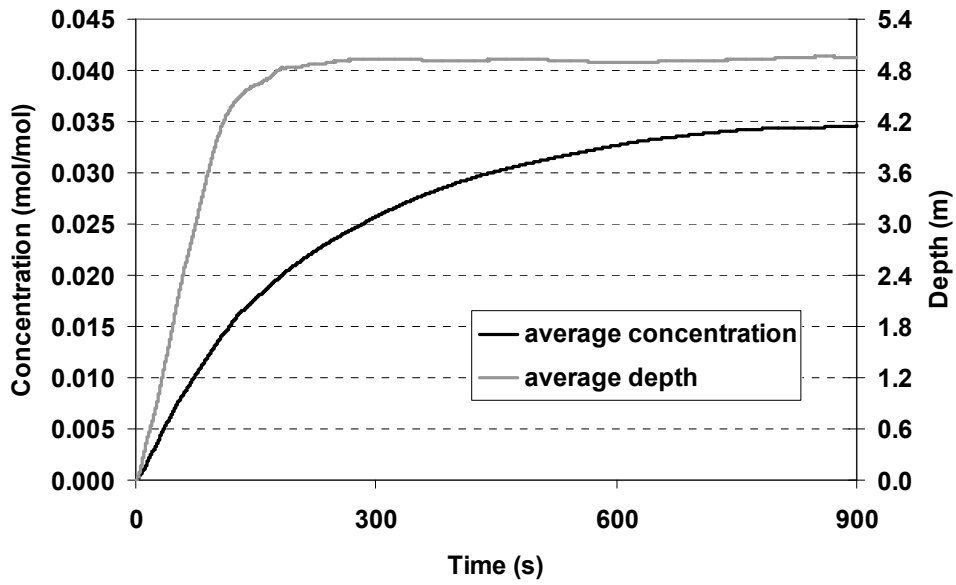


Figure 56 Average concentration of the accumulating layer and depth to ½ LFL

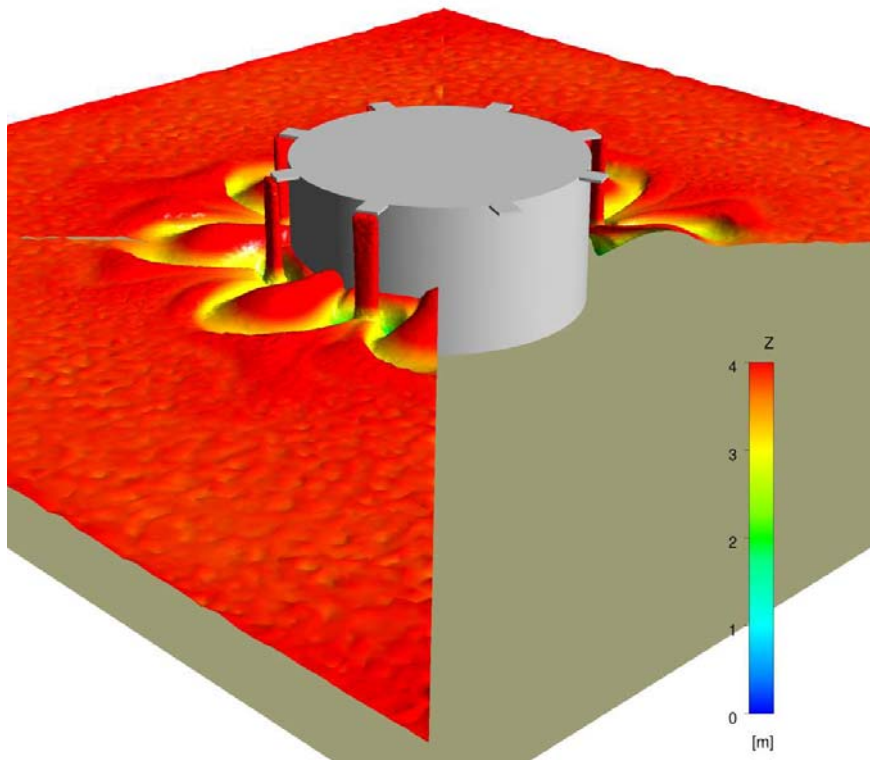


Figure 57 Isosurface at twice the LFL after 10 minutes. The surface is coloured according to height from the ground, up to a maximum of four metres

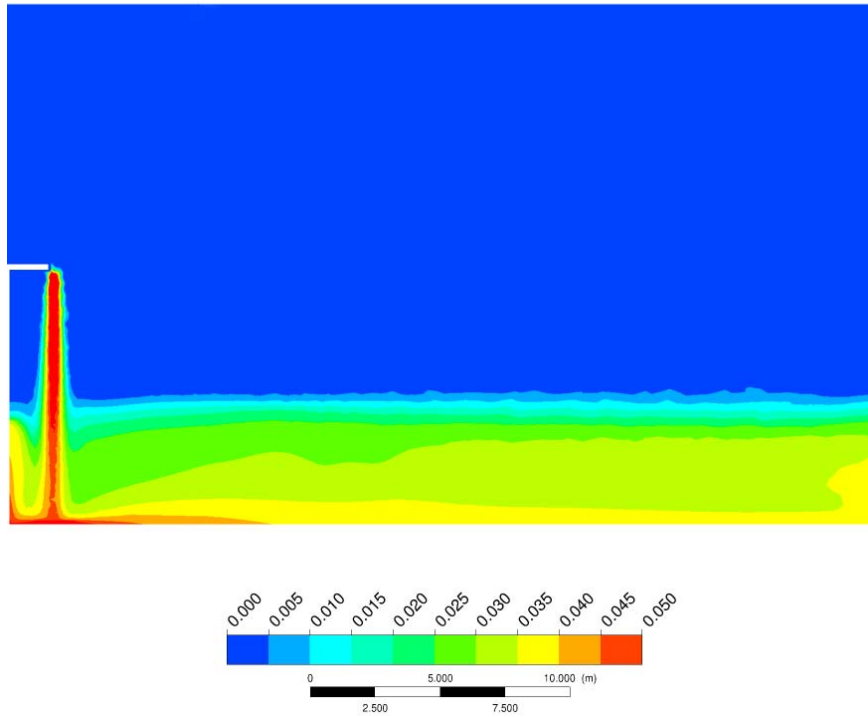


Figure 58 Contour plot of concentration on a plane through the cascade

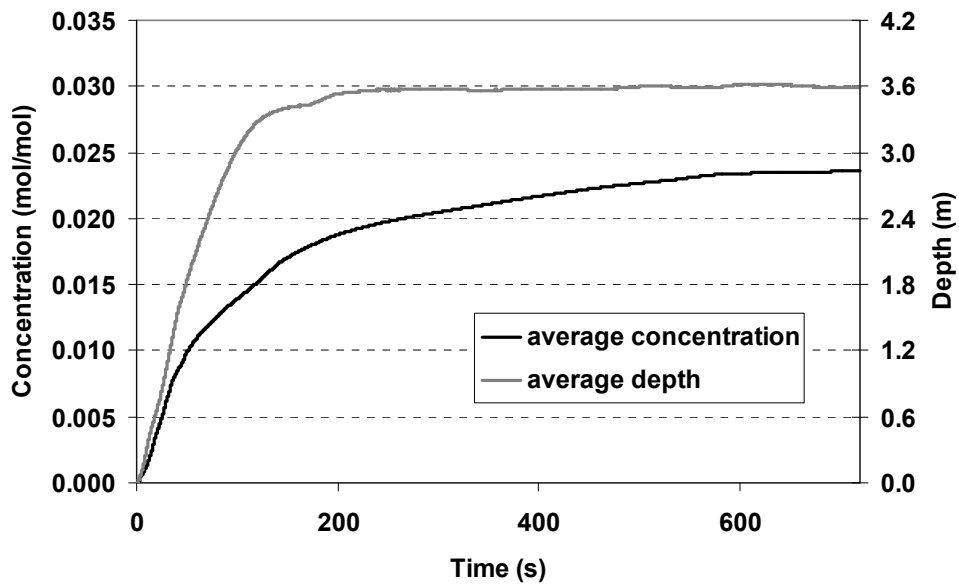


Figure 59 Average concentration of the accumulating layer and depth to $\frac{1}{2}$ LFL

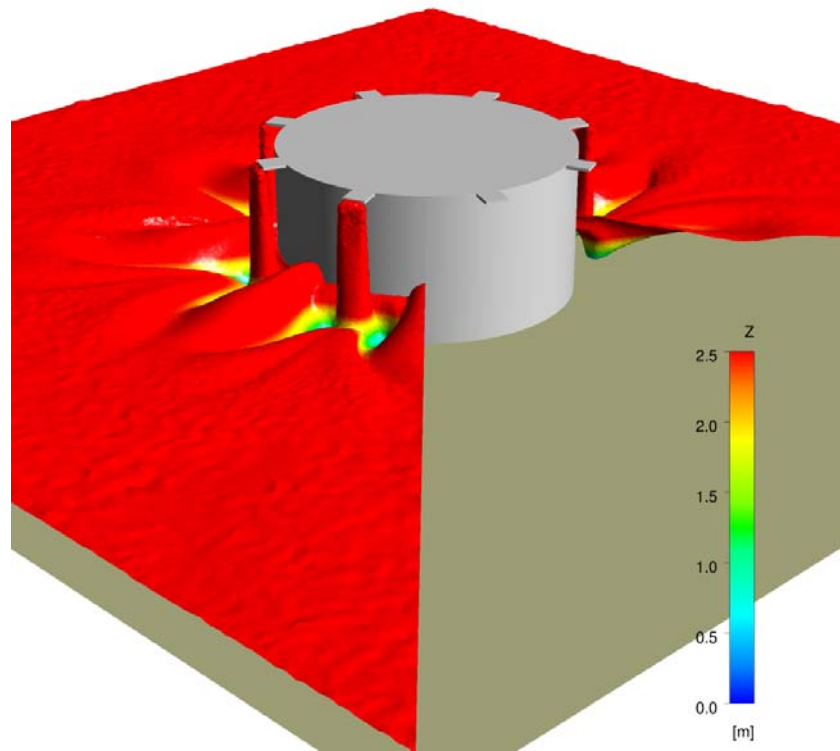


Figure 60 Isosurface at the LFL after 10 minutes. The surface is coloured according to height from the ground, up to a maximum of 2.5 metres

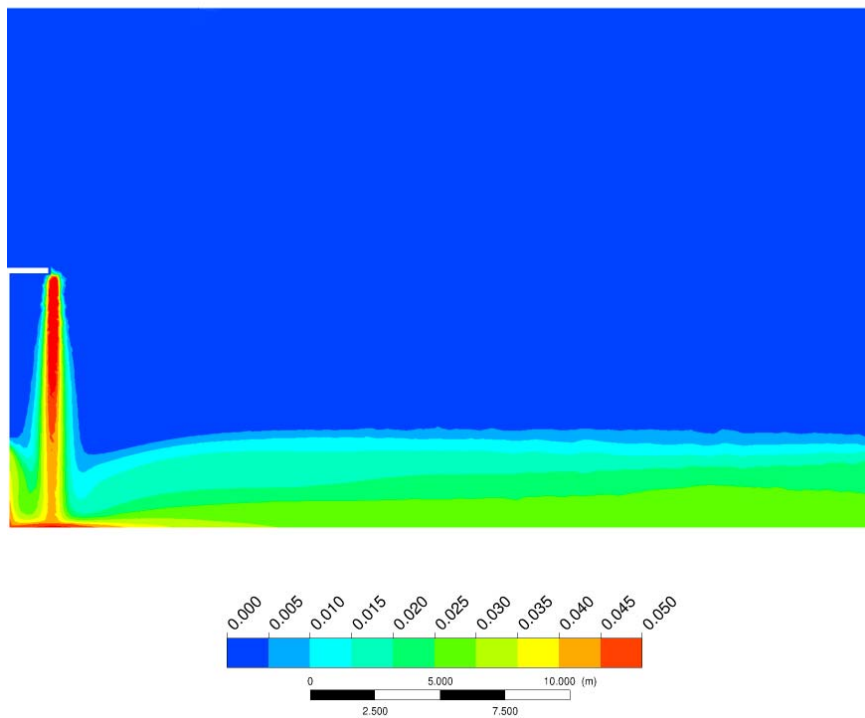


Figure 61 Contour plot of concentration on a plane through the cascade

The effect of the accumulating layer on the vapour current is shown in Figure 62. The Figure shows the temperature on a line 0.15 m from the ground extending from the tank wall, through the cascade to the outer wall. At 20 s, the core of the cascade is relatively warm. However, the vapour current is cool due to the effects of the initial mass of fluid travelling through fresh air and evaporating readily. By 40 s, the current has travelled to the outer wall and the layer is beginning to accumulate, lowering the temperature in the cascade. At 600 seconds, the layer is reaching a steady state such that the entire length from the tank has cooled by approximately 2 degrees.

The long term simulations illustrate the use of CFD in extending our understanding of accumulation beyond the times achievable in the experiments. The latter two simulations show this, with tens of minutes required to achieve a steady state.

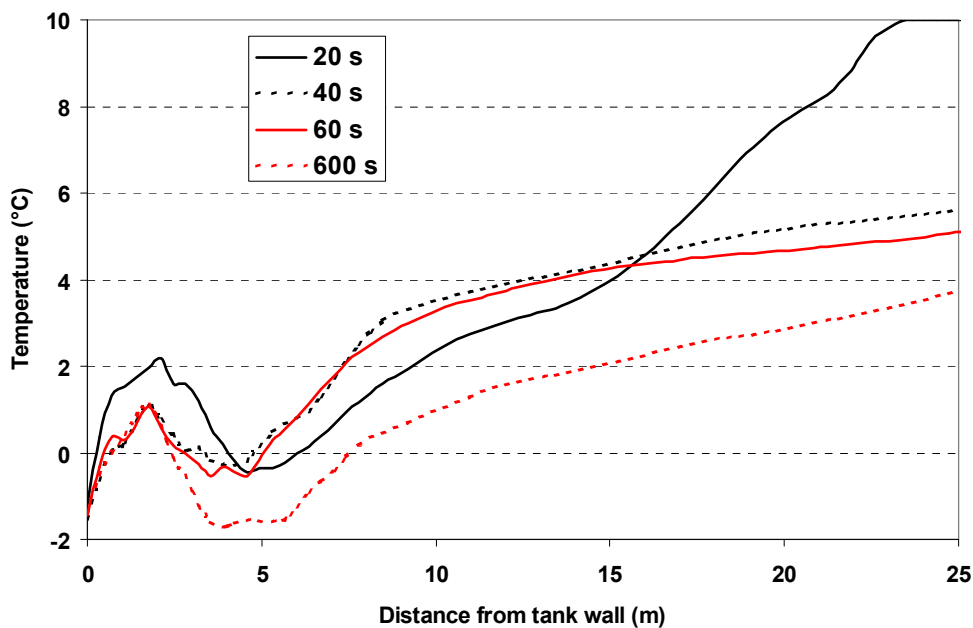


Figure 62 Temperature profiles on a line 0.15 m from the ground and extending from the tank wall, through the cascade and vapour current to the outer wall

9.4 SUMMARY

CFD models of evaporating liquid cascades have been developed and validated using data from a series of large-scale experiments. Predictions from the CFD models have been compared to measurements of the liquid and vapour temperatures at the base of the cascade and the temperature of the vapour current moving away from the base of the cascade.

Sensitivity studies have shown that the total amount of vapour produced by the liquid cascade is strongly influenced by the cascade dimensions, the droplet size distribution and the presence of splashing at the base of the cascade. The liquid and vapour temperatures in the cascade itself were found to be primarily affected by the cascade dimensions and droplet size distribution, and were unaffected by splashing. Heat transfer from surrounding surfaces was found not to influence the results significantly, i.e. vaporisation was largely driven by mixing of the liquid droplets with the entrained ambient air. The presence of splashing droplets was found to

contribute significantly to the overall vapour production. Splashing droplets are effectively a means of vaporising additional liquid into the current leaving the cascade.

The effect of a gradually deepening vapour layer, was shown to increase the re-entrainment of vapour into the cascade. However, the fresh air was still drawn into the upper portion of the cascade, which limited the maximum concentration produced in the vapour layer.

10. REFERENCES

1. Buncefield Major Incident Investigation Board (2007). *The Buncefield Incident – 11th December 2005- the final Report of the Major Incident Investigation Board*. Volume 1. ISBN 978 07176 6270 8 (www.buncefieldinvestigation.gov.uk).
2. Atkinson G., Gant S., Painter, D., Ungut A. and Shirvill, L. (2008) “*Liquid dispersal and vapour production during overfilling incidents*” IChemE Hazards XX Conference (UMIST).
3. Coldrick, S., Atkinson, G. and Gant, S.E., (2011), “*Large scale evaporating liquid cascades – an experimental and computational study*” IChemE Hazards XXII Conference (Liverpool).
4. Eldin Wee Chuan Lim, Swee Heng Koh, Liang Kuang Lim, Siew Hoon Ore, Bee Kiat Tay, Yifei Ma and Chi-Hwa Wang, (2008), “*Experimental and computational studies of liquid aerosol evaporation*”, Journal of Aerosol Science Vol 39, p618-634.
5. Cussler, E.L. (1997), “*Diffusion: Mass transfer in fluid 3rd Ed.*”, Cambridge University Press.
6. Bai, C.X., Rusche, H., Gosman, A.D., (2002). “*Modelling of gasoline spray impingement*”, Atomization and Sprays 12, 1-27.
7. Gant, S.E., Atkinson, G.T., (2007), “*Flammable vapour cloud risks from tank overfilling incidents*”, Health & Safety Laboratory Report MSU/2007/03 (Available from the Health and Safety Laboratory).
8. Menter, F.R., (1994), “*Two-equation eddy-viscosity turbulence models for engineering applications*”, AIAA J. 32, 1598-1605.
9. ANSYS (2009) ANSYS CFX-12.1 User Guide. ANSYS, Inc., Canonsburg, Pennsylvania, USA.
10. Cervantes, M.J., Engström T.F., (2004), “*Factorial design applied to CFD*”, J. Fluids Eng. 126, 791-798.
11. Hicks, C.R. and Turner Jr, K.V., (1999), “*Fundamental concepts in the design of experiments*” Fifth edition, Oxford University Press.
12. Sacks, J., Schiller, S.B. and Welch, W.J., (1989) “*Designs for computer experiments*” Technometrics 31, 41-47.
13. Gosman, A.D., E. Ioannides, (1981) “*Aspects of computer simulation of liquid fuelled combustors*”, AIAA Paper 81-0323.
14. Reitz, R.D. and Diwakar, R., (1986), “*Effect of drop breakup on fuel sprays*”, Society of Automotive Engineers Technical Paper 860469, SAE Transactions , Vol. 95, Sect. 3, pp. 218-227
15. Gant, S.E., Atkinson, G.T., (2011), “*Dispersion of the vapour cloud in the Buncefield Incident*”, Process Safety and Environmental Protection (in press).
16. Ghosh, S. AND Hunt , (1998), “*Spray jets in a cross-flow*” J.C.R., J. Fluid Mech., Vol. 365, pp. 109-136

11. APPENDIX 1: VAPOUR CLOUD ANALYSIS METHOD

The progress made in understanding the overflow flow of a volatile hydrocarbon in calm conditions described in this report (HSL FP/11/04) and expanded in Buncefield Phase II Dispersion and Explosion of Large Vapour Clouds Project work, to be published in 2013, clearly shows the way in which a practical assessment method can be constructed.

The method described in this Appendix involves a sequence of calculations that could be readily implemented as a spreadsheet, if a number of cases are to be assessed. Alternatively, analysis of a single case could be easily carried out using a calculator.

This is a basic method suitable for general use. Inevitably there are issues where general assumptions have to be made. The most important examples of this are: the specification of the liquid release distribution from a floating roof tank and the effects of site topography on cloud shape. If site-specific data is available, improvements on the general treatment will be possible. If the case is critical such improvements may be necessary.

The method considers the following calculation steps:

1. Air entrainment into the cascade of falling liquid
2. Fuel vapour concentration at the foot of the cascade
3. Additional vaporisation from fine splash products
4. Near-field (within bund) dilution
5. Volume flow rate and concentration of the cloud leaving the bund
6. Idealised hazard ranges for clouds spreading in “zero” wind speed conditions.

11.1 MASS ENTRAINMENT

Air entrainment into a cascade depends primarily on the following variables:

- i. The liquid surface tension
- ii. The liquid mass flow
- iii. The cross sectional area of the cascade(s)
- iv. The height of free fall.

11.1.1 EFFECTS OF SURFACE TENSION

Surface tension determines the fineness of the droplets in the dispersed cascade. Gasoline components, blends and many volatile solvents typically have much lower values of surface tension than that of water (Table 1). Surface tensions of other major components of petrol are fairly similar to hexane.

	Surface tension (N/m)	Density (kg/m ³)
Water	0.0727	998
Hexane	0.0184	667

Table A1: Surface tension of water and hexane (20°C)

A range of large scale experiments with hexane have shown that the droplet size after a fall of 10-15 metres is rather uniform with a median diameter of around 2mm. Detailed measurements of profiles of liquid and gas temperature show **lower** temperatures in the vapour phase than the liquid. This is because smaller droplets have preferentially evaporated – leaving the largest fragments of the final phase of droplet break up. More detail about the development of the cascade droplet spectrum can be found in Gant and Atkinson (2011).

Mass entrainment is reasonably insensitive to droplet diameter so long as this is fairly small. Table 2 shows typical figures for a tank and flow rate similar to that involved at Buncefield.

Modelling of mass entrainment for the VCA method uses a (constant and uniform) value of 2mm for the droplet size throughout the cascade.

Droplet diameter (mm)	Air mass flow (kg/s)
1	95
2	90
3	86

Table A2: Sensitivity of entrained mass flow to droplet size.

11.1.2 EFFECTS OF LIQUID MASS FLOW

This must be specified by the user – obviously for an overfill it is set by the pumping rate and liquid density. Maximum or typical values may be used as appropriate to the assessment.

In fact this choice will not usually be crucial because in general the size of the cloud is not particularly sensitive to the total mass flow. Cloud concentrations are somewhat more sensitive. Table 3 shows the effect of doubling the fuel flow (from 100kg/s to 200kg/s) for a typical gasoline tank.

Overfill rate (kg/s)	Range to which cloud prevents escape (See 11.6) (m)	Hydrocarbon concentration in cloud (% w/w)
100	213	7.7
200	239	9.5

Table A3: Sensitivity of hazard range and cloud concentration to overfill rate

The reason that the entrained air flow is rather insensitive to liquid mass flow is that the liquid flux density is very high. Both liquid droplet and vapour velocities are a significant proportion of the maximum (free-fall) value.

In a typical case the vapour mass flow entrained is proportional to:

$$\text{Air entrained} \propto (\text{Liquid mass flow})^{0.25}$$

11.1.3 EFFECTS OF CROSS-SECTIONAL AREA OF THE CASCADE

The mass entrainment is much more sensitive to the total cross-section of the cascade(s) i.e. the area over which the liquid down flow is distributed. The reason for this follows from the last point in 1.2. An increase in cross-section gives a (larger) cascade that generally still has a high mass flux density. Liquid and vapour velocities are still a good proportion of the free-fall value and the total air-flow increases significantly with area.

In a typical case the mass flow entrained is proportional to:

$$\text{Air entrained} \propto (\text{Cascade cross section})^{0.75}$$

Doubling the liquid flow increases the air mass flow by around 19%. Doubling the cross section of the cascade increases the air mass flow by 68%. Doubling the liquid flow **and** the cross-section of the resulting cascades doubles the air mass flow; which is to be expected, as it could be equivalent to having simultaneous releases from two tanks.

Specifying the cross-section of the cascades is clearly an important part of the analysis but is not straightforward because it depends on the way liquid is released from the tank and this is in turn a function of tank design.

There are three main options for bulk storage of volatile liquids:

1. Vented fixed roof - floating internal deck. This is common for gasoline in the UK and was the type of tank involved at Buncefield.
2. Floating roof tank.
3. Fixed roof tank with PV valve.

11.1.3.1 *Vented fixed roof tanks*

There is a degree of uniformity in design of vented fixed roof tanks (Buncefield tanks). Vents are normally relatively small and separated by approximately 10m around the edge of the roof. There is normally a deflector plate that redirects cooling water applied to the top of the tank onto the walls.

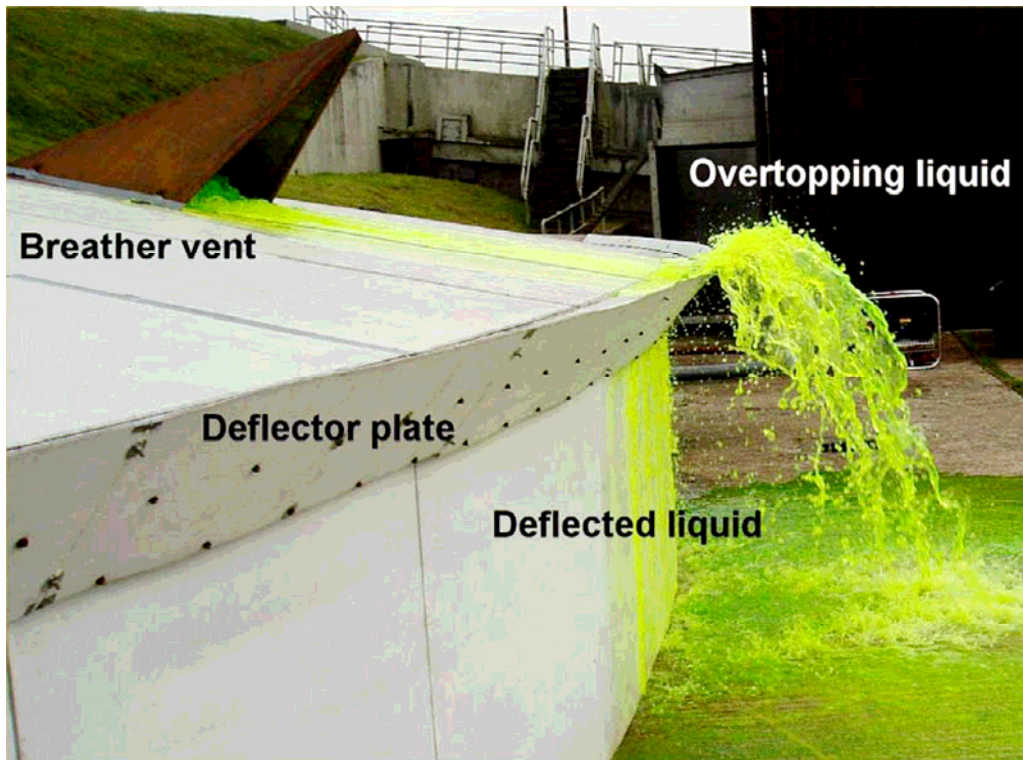


Figure A1: Typical liquid discharge from a vent in a Buncefield-type tank.

Generally part of the liquid released via the vents during an overfilling incident will run straight over the deflector plate and fall to the ground in a “free” cascade from the full tank height. The remainder of the liquid is redirected back towards the wall. Some of this runs down the wall but most falls as a cascade close to the wall (Figure 1). If there is a wind girder the “wall” flow will strike it and be projected outward forming a second free cascade that falls only from the height of the wind girder.

The extent of spread of these cascades has been studied at full scale (Atkinson, G. and Coldrick, S. 2011). The results show that spreading is quite limited. A free cascade from the top of a 10 m high tank is typically only 300-400mm thick at the tank foot (measured away from the wall). The typical length of the flow over deflector plate (around the tank perimeter) is around 1.5m for a Buncefield type tank and this hardly changes as the cascade falls.

The cascade projected out from a wind girder part way down the tank spreads a little more rapidly away from the tank wall. Normally the wall flow is also somewhat longer (around the tank perimeter). On the other hand much of the momentum of the falling liquid is removed by the wind girder and the reduced fall reduces the air entrainment.

The figures below are derived from measurements made on vent flow from a 10m high tank with a wind girder at a height of 5m. The experimental liquid was hexane which should closely match the liquid dispersal of a gasoline cascade. The figures refer to a case where the free cascade over the deflector plate (A) and wall flow (B) are of equal

magnitude.

A. Hexane overflowing the deflector plate:	
Mass flow	57.5 kg
Area of cascade	4.8 m ²
Entrained mass of air	44 kg/s
B. Hexane falling close to the wall and striking the wind girder	
Mass flow	57.5 kg
Area of cascade	8 m ²
Entrained mass of air	44.3 kg/s

Table A4: Air entrainment data for a typical “Buncefield-type” tank. Total overflow rate 115 kg/s – divided equally between top and wall flows

In this case the effects of increased spreading and reduced fall for the wall flow effectively cancel. It would make little difference to the total mass entrainment rate if the balance between top flow and wall flow shifted (as it might if the deflector plate design were changed).

The VCA method assumes this kind of design (deflector plate fitted, windgirder at roughly half tank height) in calculating air entrainment.

The error if there is no deflector plate will be limited as all of the flow is directed into a top flow of similar type to that analysed.

11.1.3.2 Floating roof tanks

The nature of the liquid discharge is much more uncertain in this case. When a floating roof tank is overfilled the liquid will eventually come over the top of the tank wall. In principle it is possible that this overflow will extend all around the perimeter of the tank. In practice it is unlikely that a large tank, that has been in service for a while, will still be level enough for this to occur. It is also possible that raising the deck and associated access ladder past the design limit will deform part of the tank wall top, channelling the liquid outflow.

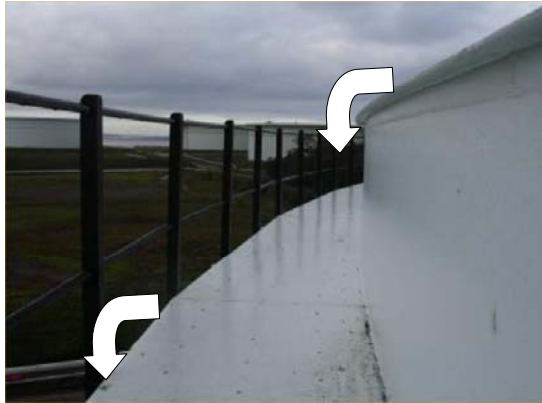


Figure A2: Windgirder/walkway at the top of a typical floating roof tank. The arrows indicate liquid path in the event of overflow.

The mass entrainment in the VCA method assumes that liquid spills over 30% of the tank perimeter. The breadth of the flow is again taken from experiment (Atkinson, G. and Coldrick, S. 2011). Whether the cascade emerges from the edge of a windgirder (Figure 2) or overtops a deflection plate (Figure 1) makes little difference to the spreading of the cascade at the tank foot.

Entrainment data fill rate similar to that in Table 4 but for a floating roof tank are shown in Table 5.

Hexane flowing from edge of wind girder in floating roof tank	
Mass flow	115 kg
Area of cascade	9.6 m ²
Entrained mass of air	88 kg/s

Table A5: Air entrainment data for a typical floating roof tank

The mass entrainment rate is co-incidentally very close to that derived for the equivalent Buncefield tank.

The VCA method consequently makes *no distinction* between Buncefield type tanks and floating roof tanks. The mass entrainment depends only on the tank diameter (strongly – as this determines the number of vents or length of overflow) on the tank height (less strongly) and the filling rate (weakly).

If the liquid discharge from an overfilled floating roof tank is concentrated in a smaller part of the tank perimeter the method will overestimate the cloud volume and underestimate the concentration. If the tank is very level and the liquid flows over a large proportion of the perimeter than 30% there will be a bigger and more dilute cloud than the method suggests.

The mass entrainment equations used in all of this work are shown in Appendix 2. These are easily solved by an appropriate spreadsheet and this would allow the user to improve the quality of parts of the analysis if specific information about the liquid flow from a particular tank is known.

11.1.3.3 Fixed roof tanks with PV valves

The liquid flow during an overflow is again uncertain. Normally attempting to vent liquid through PV valves during an overflow will rupture the tank somewhere around the roof/wall weld. This is because the internal driving pressure required increases by a factor of order 1000 when liquid reaches the valve. The size of the resulting rupture is difficult to predict as a general case.

Some tanks (especially in the tropics) are fitted with extremely large PV valves. In this case the discharge may be exclusively through the PV valve. Liquid will then run down to the edge of the tank in a manner that depends on the valve location(s).

Tanks with PV valves are relatively rare for bulk gasoline storage and it has been assumed the in this case too the final discharge occurs over 30% of the tank perimeter.

Again the mass entrainment equations can easily be solved to allow the user to improve the quality of parts of the analysis if specific information about the liquid flow from a particular tank is known.

11.1.4 EFFECTS OF HEIGHT OF FREE FALL

This has been referred to above. If the outflow conditions are kept similar and the tank height increased the mass entrainment varies as:

Mass entrainment \propto (Tank height)^{0.45}

It is worth noting that the amount of air driven by the cascade is not sensitive to the height below the release point at which the (rapid) primary dispersal of liquid occurs. Figure A3 shows the results of calculations of mass entrainment on the assumption of immediate dispersal or dispersal somewhat below the release point. These calculations are for an experimental cascade but the mass flux density is similar to that expected in overflow incidents. In the cases where

dispersal is delayed the liquid falls freely, accumulating momentum and this is rapidly shared with air when dispersal occurs. The general point is that the mass entrainment at a particular level in the cascade is largely determined by the conditions (i.e. total drop, cascade width and mass density) that apply at that point. How the flow got to this state is of secondary importance.

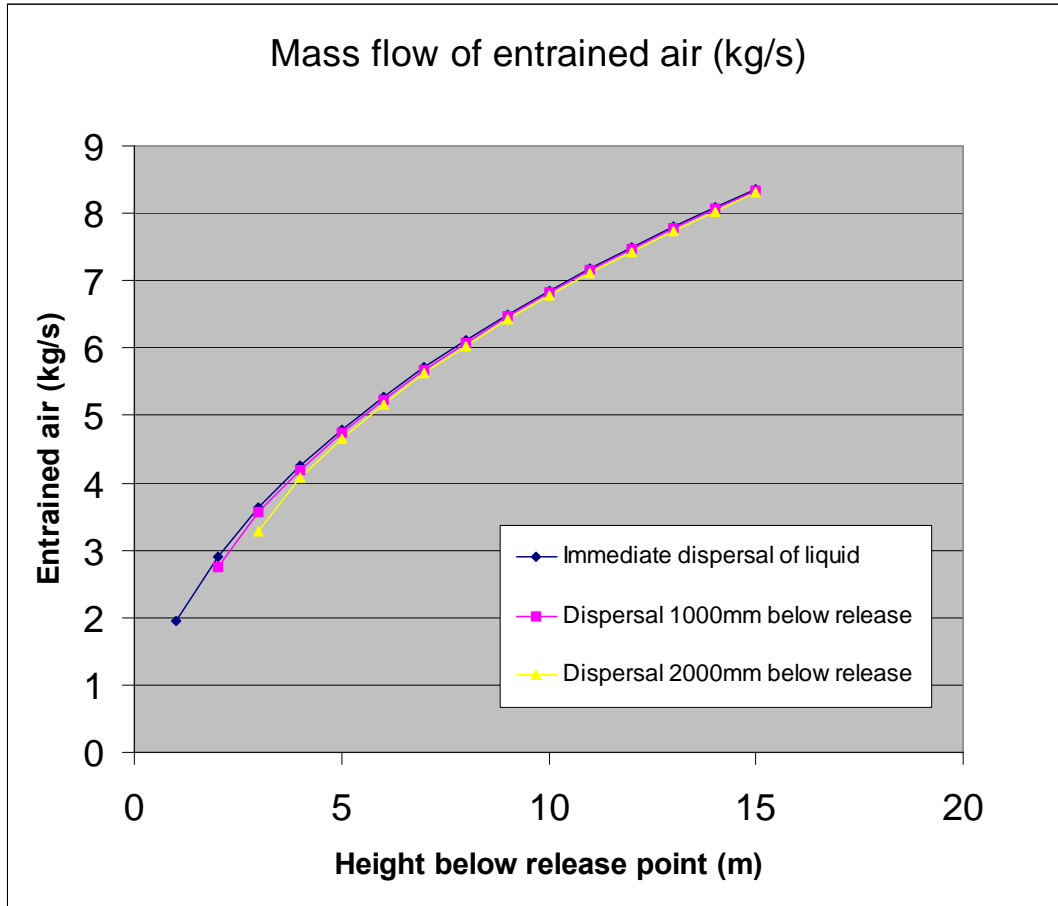


Figure A3: Effects of liquid dispersal characteristics on total mass entrainment (Mass release rate 15 kg/s , Area 0.6 m² , Mass flux density 29.3 kg/m²/s)

11.1.5 FORMULATION ADOPTED IN THE VCA METHOD

Mass entrainment has been calculated for a base case which corresponds both to the Buncefield incident apart from the tank height which matches the (full-scale) source term tests on a single vent flow (Atkinson, G. and Coldrick, S. 2011). The effects of changes in tank diameter, height and fuel flow have been studied and the results described in a parametric manner. This describes variation in entrainment well for reasonable ranges of flow and tank variables and avoids the need to solve the equations in Appendix 2 for every assessment.

The final expression for mass entrainment into a cascade M_{air} is very simple:

$$M_{air} = 90kg/s \left(\frac{D}{25m} \right)^{0.75} \left(\frac{H}{10m} \right)^{0.45} \left(\frac{F}{115kg/s} \right)^{0.25}$$

Here D is the tank diameter (m), H is the tank height (m) and F is the filling rate (kg/s).

11.2 CONCENTRATION OF FUEL AT THE TANK FOOT

The method assumes that heat and mass transfer in the cascade are sufficiently rapid to bring the entrained air and falling fuel close to full thermodynamic equilibrium. A substantial number of full-scale tests with hexane have been undertaken (some under the Buncefield JIP) and in all cases this assumption provided remarkably accurate predictions of the observed state of both phases exiting the impact zone.

This work is described in Atkinson, G. and Coldrick, S. (2011) but it is worth pointing out here that in a typical case mass vaporisation as the cascade flow approaches the ground is roughly 70% of the level to be expected when full equilibrium is reached. On the other hand vapour and liquid flows out of the impact zone (the liquid is almost all running on the floor) are extremely close to the equilibrium state. It seems that the violent disruption of droplets on impact and the high slip velocities of fragments drives a final rapid phase of heat and mass transfer and forces the flow close to full thermodynamic equilibrium.

A simplified gasoline composition has been selected for inclusion in the VCA method. This corresponds to the gasoline spilled in the Buncefield incident and is typical of a UK winter grade.

11.2.1 GASOLINE COMPOSITION

n-butane (as a surrogate for all C4 hydrocarbons)	9.6% wt/wt
n-pentane (as a surrogate for all C5)	17.2 % wt/wt
n-hexane (as a surrogate for all C6)	16% wt/wt
n-decane (as a surrogate for all low volatility materials)	57.2% wt/wt

The user inputs the temperature of this fuel and the ambient air temperature. It has been assumed that the relative humidity is 100%. This is a worst case as water vapour condensation releases some heat and supports some additional vaporisation. For moderate ambient temperatures (<15°C) the effect of humidity is quite limited. For very hot dry conditions the VCA method will overestimate the extent of vaporisation but such conditions are not typical in the UK.

For a fixed composition the main variables controlling the fuel vapour concentration in the equilibrium state are:

- i. Fuel air ratio M_{air}/F (M_{air} is the entrained air flow; F is the fuel flow rate)
- ii. Fuel storage temperature
- iii. Ambient air temperature (at the tank height)

11.2.2 FORMULATION OF THERMODYNAMIC INPUT TO THE VCA METHOD

Fuel vapour concentration has been calculated for a base case which roughly corresponds both to the Buncefield incident and the (full-scale) source term tests on a single vent flow (Atkinson, G. and Coldrick, S., 2011). The effects of changes in tank diameter, height and fuel flow have been studied and the results described in a parametric manner.

The final expression for fuel concentration at the foot of the cascade is:

$$C_{fuel} = 17\% (w/w) \left(1.28 \frac{M_{air}}{F} \right)^{-0.42} e^{0.011(T_{fuel}-10)} e^{0.0062(T_{ambient}-10)}$$

Here M_{air} is the entrained mass of air (kg/s), F is the fuel filling rate (kg/s), T_{fuel} and $T_{ambient}$ are the fuel storage and ambient temperatures ($^{\circ}C$).

This equation clearly applies only to the gasoline mixture specified in 11.2.1. Assessment of gas concentration for other substances is straightforward but will require a calculation of thermodynamic equilibrium. The mass of air to be added to the liquid feed is given by 11.1.5.

11.2.3 VAPORISATION OF FUEL IN THE CASCADE

This follows from the mass flows of air and mass concentration of fuel vapour

$$M_{vaporised} = M_{air} \cdot C_{fuel} / (100 - C_{fuel})$$

11.3 ADDITIONAL VAPORISATION OF FINE SPLASH PRODUCTS

All experiments have shown the presence of a fine liquid spray being carried out of the impact zone by the vapour flow. The size spectrum of splash products in such circumstances is discussed in Bai et al, (2002).

The high-speed, horizontal vapour flow away from the impact zone is an area of rapid vapour entrainment. Modelling studies have shown that the air entrained here includes a proportion of fresh air even when a deep vapour layer is established in and around the bund. This is described fully in Coldrick, S. et al (2011) and Atkinson, G. and Coldrick, S., (2011). The consequence is that the finely divided splash spray rapidly evaporates as fresh air becomes available.

Experiments indicate that the evaporation process is complete within a few metres of the impact zone. The amount of additional vaporisation that occurs can be studied by monitoring the effect on temperature as the flow is diluted with relatively warm air. The mass flux in the spray is fairly small - typically of order 10% of the total vaporisation rate in the cascade. The extent of splashing is dependent on mechanical factors such as the flow rate rather than temperature.

11.3.1 SPLASH FRACTION SELECTION

Only one accurate experimental determination of the proportion of total mass in the cascade channelled into a fine spray is currently available (Atkinson, G. and Coldrick, S., 2011). In this case the measured proportion was 1.5%. There may be some sensitivity to the depth of the liquid run off and consequently to the gradient of the ground around the impact point. The VCA method assumes 2% for this parameter.

$$M_{\text{splash}} \text{ (kg/s)} = 0.02 F$$

All of the HSE experiments involved volatile substances e.g. C6 mixtures. In this case the splash spray (typical size 100 microns) vaporised completely when large amounts of fresh air were entrained. This will not be case for materials with low volatility or mixtures with a substantial fraction that is involatile (e.g. crude oil). In this case there will be some rain out within a few tens of metres from the cascade.

In the case of a mixture of hydrocarbons with a wide range of volatilities it is suggested that only the fraction corresponding to C8 (or lighter) contributes to vaporisation via fine splash products. F in the above equation becomes the mass flow of C8 and lighter components. This will make little difference to the overall analysis for gasoline (where $M_{\text{vaporised}} \gg M_{\text{splash}}$) but may be significant for some crude oil analyses.

The vaporisation analysis may be used for substances that produce low vapour concentrations that are well below the flammable limit but have some toxic significance. In this case it may be appropriate to simply assume that the cloud concentration is half the saturated vapour pressure at the liquid storage temperature. In this case $M_{\text{vaporised}}$ and M_{splash} can be ignored in the estimation of cloud mass 11.4.2.

11.4 NEAR FIELD ENTRAINMENT

If there is a bund, or vapour flow away from the tank is constrained by distant changes in ground level, buildings etc. then there will some re-entrainment of contaminated air. In these circumstances the concentration in the bund and wider vapour cloud increases with time, until the pattern of re-entrainment is established. The higher the bunds or constraints, the deeper the final vapour layer and the lower the proportion of fresh air that dilutes the vapour flow from the tank before it joins the cloud.

This type of re-entrainment and the effect on vapour dilution has been investigated by HSE using CFD (Gant, S.E., and Atkinson, G. (2007,2011) and Atkinson, G. and Coldrick, S., 2011). Some typical results are shown in Table A6.

Barrier height (m)	Cloud depth (m)	Distance to barrier (m)	Dilution factor (conc. in cascade/conc. in cloud)
4	5	30	1.5
2.5	3.6	30	2.1
2	-	5	1.8
2	-	10	2.0
2	-	15	2.0

Table A6: Dilution factors for constrained vapour flows

All of the barriers in Table 6 were vertical but the effect of different (sloping) bund profiles has been investigated and makes little difference. Similarly the data shows that the location of bunds or other constraints makes little difference.

11.4.1 DILUTION FACTORS ADOPTED

The VCA method uses the Buncefield site as a model for a typical petrol storage depot in fairly flat terrain. In this case the observed cloud depth around the tank for most of the release was around 3.5 m. Table 6 shows that a relatively wide range of constraints giving a cloud of this depth lead to a dilution factor of around 2 and this figure is adopted in the method. The method therefore assumes that the mass flow from the cascade including all vaporised fuel is doubled by entrainment of fresh air (see 11.4.2).

It would be unusual for a tank to be completely surrounded by a 4m barrier but if this were the case lower rates of cloud spread than predicted might occur and fuel concentrations in the cloud would rise.

It is worth noting that the time taken for the maximum concentration (minimum dilution) to be reached does depend strongly on the location of constraints. Within a bund with wall about 10m from the tanks stable conditions are reached in about 2 minutes. If the constraints are hundreds of metres from the tank the concentration may continue to rise throughout the release. Currently there are no available methods of carrying out approximate but realistic heavy gas dispersion assessments in calm conditions without resorting to CFD.

11.4.2 TOTAL MASS FLOW IN THE CLOUD

See above - this is simply the sum of the vapour mass driven directly by the cascade during vertical fall and the mass of entrained fresh air.

$$M_{\text{cloud}} = 2 \cdot (M_{\text{air}} + M_{\text{vaporised}} + M_{\text{splash}})$$

11.5 CLOUD VOLUME AND CONCENTRATION

The temperature in the cloud is difficult to predict as the effects of evaporative cooling are partially offset by condensation of entrained air and then gradually eroded by heat transfer from the ground. From this point onwards the density of the vapour is assumed to be that of ambient air. Resulting errors in determining cloud volume from the cloud mass are small compared with the uncertainties in various other stages of the assessment.

$$V_{\text{cloud}} = M_{\text{cloud}} / \rho_{\text{ambient}}$$

The concentration of fuel vapour is

$$C_{\text{cloud}} \text{ (kg/m}^3\text{)} = (M_{\text{vaporised}} + M_{\text{splash}}) / V_{\text{cloud}}$$

For hydrocarbons a mass density of approximately 50 g/m³ corresponds to the minimum concentration required to support flash fire or explosion. Somewhat higher mass concentrations are required to support burning in oxygenated solvents.

Substance	Mass concentration at the lower flammable limit at 0°C (g/m ³)
Butane	48
Pentane	46
Hexane	47
Heptane	47
Benzene	47
Methanol	103
Ethanol	70
Propanol	60
Acetone	70
MEK	62

Table A7: Mass concentration at the lower flammable limit for selected substances

Typically the vapour cloud caused by overfilling with petrol will be flammable and the concentration is often close to the stoichiometric ratio – the concentration that supports the most powerful explosion. Application of the method to other less volatile substances will require thermodynamic analysis to derive the concentration at the foot of the tank and hence the mass vaporised in the cascade $M_{\text{vaporised}}$. The resulting concentration in the wider cloud may be below the lower flammable limit (LFL).

If the concentration at the foot of the cascade (equivalent to 11.2.2) is above the LFL but that in the wider cloud is below the LFL some form of vapour combustion in the area immediately around the tank is possible but this vapour flash is unlikely to have any significant effects on the wider site compared with the liquid spill fire which would normally follow.

11.6 HAZARD RANGES

In general the method assumes a clean separation between the fluid mechanics of the problem (which determines the cloud size from the liquid mass flow and tank geometry) and the thermodynamics (which determines the composition of the cloud). This is appropriate for the problem where the vapour flow far from the tank is non-entraining i.e. there is no wind and the cloud has a degree of negative buoyancy because of its composition (and temperature).

Hazard ranges calculated by the HSE method provide an indication of the range to which the cloud may present hazards in fairly flat sites in calm conditions. They are based on the total cloud volume and simple assumptions about the cloud geometry. Obviously a full CFD treatment of the gravity current taking into account local topography would be much more reliable but these results can provide some inputs to risk assessments and the development of emergency plans where such detailed analysis is not available.

The approach has been developed with the Buncefield experience in mind (Buncefield Major Incident Investigation Board, 2007). Excellent records of the variation in cloud depth with time for several locations exist for this case.

As has been noted previously the cloud geometry is a function of distant constraints on vapour flow. Buncefield was a very shallow dip with vapour flow confined in almost all directions at a range of about 150-400m and the timescale for development of the cloud reflects this.

In this context the terms “fairly flat” and “shallow” should be interpreted as meaning that the change in ground level is less than 2-3 m. Rises in ground level greater than this will arrest spread of the cloud.

11.6.1 RANGE TO WHICH CLOUD MAY PREVENT ESCAPE

The Jaipur incident (MoPNG Committee, 2010) provided a tragic illustration of the risk associated with people being trapped by a vapour cloud extending above head height.

On the other hand CCTV records from Buncefield show several people walking considerable distances through a stable cloud below waist level. Escape becomes impossible when the cloud depth exceeds the breathing level. Concentrations of hydrocarbons in a flammable cloud greatly exceed IDLH levels (Immediate Danger to Life and Health).

The range to which escape may be prevented is calculated from the cloud volume by assuming that the cloud geometry is a disc of constant depth. In reality parts of the cloud near the edge will be below this level, so the VCA output is a conservative estimate of the extent of the deep part of the cloud. This conservatism is somewhat reduced by choosing a critical depth of 2m – which is somewhat above breathing level.

Calculation of this range at different times during a release will give some idea of the time available for evacuation of people in on-site occupied buildings or vulnerable off-site buildings.

$$R_{\text{escape}}(t) = [1/2\pi V_{\text{cloud}} \cdot T]^{1/2}$$

T(s) is the duration of the release.

11.6.2 RANGE TO WHICH A LOW LEVEL IGNITABLE CLOUD MAY EXTEND

As noted above there are records of a shallow cloud spreading more rapidly at Buncefield. Even such a shallow cloud might be ignited by a low level ignition source. The range quoted gives some idea of the range to which the cloud is vulnerable to ignition at various times.

The range to which the low level cloud extends is calculated from the cloud volume by assuming that the cloud geometry is a disc of constant depth. In reality parts of the cloud near the source will be above this level, so the VCA output is a conservative estimate of the extent of the cloud. This conservatism is somewhat reduced by choosing a critical depth of 1m – which is somewhat greater than the minimum depth of a stable vapour cloud observed at Buncefield.

These estimates of the maximum extent of the high concentration part of the cloud may feed into zoning analyses or emergency planning.

$$R_{\text{ignition}} = [1/\pi V_{\text{cloud}} \cdot T]^{1/2}$$

11.6.3 SOURCE TERM/DISPERSION FOR WINDY CONDITIONS

In flows where there is far-field entrainment (windy conditions) there will be a stronger link between fluid mechanics and thermodynamics. The density of the cloud relative to the overlying ambient air may strongly affect the entrainment rate.

Experiments in light winds have shown that the source term (vaporisation rate) is little changed and is suitable as input to an integral dispersion model. It may however be necessary to allow for negative buoyancy in the cloud to get reliable results.

11.7 EXAMPLE CALCULATIONS

11.7.1 EXAMPLE 1: A GASOLINE TANK SIMILAR TO THAT AT BUNCEFIELD

Inputs:

Tank diameter D	25 m
Tank height H	15 m
Fuel flow rate F (Gasoline)	115 kg/s
Fuel temperature T _{fuel}	14°C
Air temperature T _{ambient}	0 °C
Duration of release	1400 s

<p>Mass entrainment in cascade</p> $M_{air} = 90 \text{ kg/s} \left(\frac{D}{25 \text{ m}} \right)^{0.75} \left(\frac{H}{10 \text{ m}} \right)^{0.45} \left(\frac{F}{115 \text{ kg/s}} \right)^{0.25}$	108 kg/s
<p>Concentration at the tank foot</p> $C_{fuel} = 17\% (w/w) \left(1.28 \frac{M_{air}}{F} \right)^{-0.42} e^{0.011(T_{fuel}-10)} e^{0.0062(T_{ambient}-10)}$ $= 17\% (w/w) (0.92) \cdot 1.04 \cdot 0.94$	15.3 % w/w
<p>Mass vaporised</p> $M_{vaporised} = M_{air} \cdot C_{fuel} / (100 - C_{fuel})$	19.5 kg/s
<p>Mass splashed</p> $M_{splash} \text{ (kg/s)} = 0.02 F$	2.2 kg/s
<p>Total mass addition rate to cloud</p> $M_{cloud} = 2 \cdot (M_{air} + M_{vaporised} + M_{splash})$	259 kg/s
<p>Volume addition rate to cloud</p> $V_{cloud} = M_{cloud} / \rho_{ambient}$	199 m ³ /s

Concentration of fuel vapour in cloud $C_{\text{cloud}} \text{ (kg/m}^3\text{)} = (M_{\text{vaporised}} + M_{\text{splash}}) / V_{\text{cloud}}$	0.11 kg/m ³
Range (after 1400s) to which cloud may hinder escape $R_{\text{escape}} = [1/ 2\pi V_{\text{cloud}} \cdot T]^{1/2}$	210 m
Range to which low level cloud might be ignited $R_{\text{ignition}} = [1/ \pi V_{\text{cloud}} \cdot T]^{1/2}$	297 m

In this gasoline case the cloud is close to the stoichiometric ratio for combustion.

After 5 minutes (300 s) the range to which the cloud might extend over head height and impede escape would be:

$$R_{\text{escape}} = [1/ 2\pi V_{\text{cloud}} \cdot 300]^{1/2} = 97 \text{ m}$$

This kind of analysis shows the need for prompt and effective evacuation in the event of an overflow in calm conditions. Early warning to allow escape before the cloud arrives can greatly reduce risk. Staying put (even in a toxic refuge) is very dangerous if the cloud is flammable.

11.7.2 EXAMPLE 2: A SHIP FILLED METHANOL TANK

Inputs

Tank diameter D	25 m
Tank height H	15 m
Fuel flow rate F (Methanol)	115 kg/s
Fuel temperature T _{fuel}	14°C
Air temperature T _{ambient}	0 °C
Duration of release	1400 s

Flat calm conditions

Mass entrainment in cascade $M_{air} = 90kg / s \left(\frac{D}{25m} \right)^{0.75} \left(\frac{H}{10m} \right)^{0.45} \left(\frac{F}{115kg / s} \right)^{0.25}$	108 kg/s
Concentration at the tank foot Cannot use the equation 11.2.2 (which is for gasoline only). Instead calculate the equilibrium state for the adiabatic mixing of 108 kg of air (at 0 °C, RH 100%) and 115 kg of methanol (at 14 °C). For reference the lower flammable limit for methanol is approximately 7% w/w at 0°C.	3.5 % w/w (33,000 ppm)
Mass vaporised $M_{vaporised} = M_{air} \cdot C_{fuel} / (100 - C_{fuel})$	3.9 kg/s
Mass splashed $M_{splash} \text{ (kg/s)} = 0.02 F$	2.2 kg/s
Total mass addition rate to cloud $M_{cloud} = 2 \cdot (M_{air} + M_{vaporised} + M_{splash})$	228 kg/s
Volume addition rate to cloud $V_{cloud} = M_{cloud} / \rho_{ambient}$	175 m ³ /s
Concentration of fuel vapour in cloud $C_{cloud} \text{ (kg/m}^3\text{)} = (M_{vaporised} + M_{splash}) / V_{cloud}$	0.035 kg/m ³
Range (after 1400s) to which cloud may hinder escape $R_{escape} = \left[1 / 2\pi V_{cloud} \cdot T \right]^{1/2}$	197 m
Range to which low level cloud might be ignited $R_{ignition} = \left[1 / \pi V_{cloud} \cdot T \right]^{1/2}$	N/A

There is no risk of a vapour fire – even close to the tank. There will be high concentrations of methanol to a range of around 200m after 1400 s.

11.8 REFERENCES FOR THE VCA METHOD

Atkinson, G. and Coldrick, S. (2011) Vapour cloud formation – Experiments and modelling, HSL Report FP/11/04.

Bai, C.X., Rusche, H., Gosman, A.D., (2002). Modeling of gasoline spray impingement. *Atomization and Sprays* 12, 1-27.

Buncefield Major Incident Investigation Board (2007). *The Buncefield Incident – 11th December 2005- the final Report of the Major Incident Investigation Board. Volume 1.* ISBN 978 07176 6270 8 (www.buncefieldinvestigation.gov.uk).

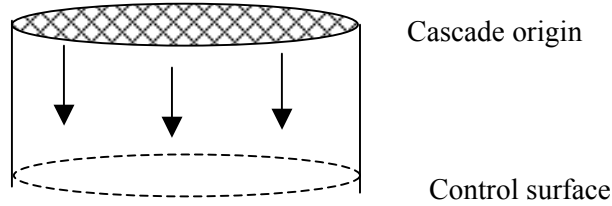
Coldrick, S., Gant S. E., Atkinson G.T. and Dakin, R. (2011) Factors affecting vapour production in large scale evaporating liquid cascades. *Process Safety and Environmental Protection* (in Press)

Gant, S.E., and Atkinson, G. (2011) Dispersion of the Vapour Cloud in the Buncefield Incident, *Process Safety and Environmental Protection* (in Press).

Gant, S.E., and Atkinson, G. (2007) Flammable Vapour Cloud Risks from Tank Overfilling Incidents, HSL report MSU/2007/03.

MoPNG Committee 2010 (constituted by Govt. of India) Independent Inquiry Committee Report on Indian Oil Terminal Fire at Jaipur on 29th October 2009; completed 29th January 2010. (<http://oisd.nic.in>).

12. APPENDIX 2 – CALCULATION OF MASS ENTRAINMENT



Assume

1. The spray has little initial non-axial velocity and the cross section remains constant.
2. The spray is uniform over a given area with a mass flux density of M ($\text{kg}/\text{m}^2/\text{s}$).
3. The induced gas phase velocity is constant across the section. The additional gas mass flow required is presumed to be entrained through the vertical boundary of the spray and rapidly mixed across the section.
4. The spray is monodisperse (i.e. all droplets are the same size).

Droplet dynamics

$$m_{\text{droplet}} \frac{du_{\text{droplet}}}{dt} = m_{\text{droplet}} \cdot g - \frac{1}{2} C_d \rho_{\text{vap}} A_{\text{drop}} (u_{\text{droplet}} - u_{\text{vapour}})^2$$

Vapour dynamics

Vapour velocity at a horizontal control surface below the origin of the spray

$$\rho_{\text{vap}} u_{\text{vapour}}^2 = \sum_{\text{droplets}} \frac{1}{2} C_d \rho_{\text{vap}} A_{\text{drop}} (u_{\text{droplet}} - u_{\text{vapour}})^2$$

The summation is carried out over droplets above the control surface

Additional relations used

$$N(x) = \frac{M}{m_{\text{droplet}} u_{\text{droplet}}(x)}$$

This relates the number density of droplets to M the mass flux density ($\text{kg}/\text{s}/\text{m}^2$) in the spray

$$\frac{A_{\text{drop}}}{m_{\text{droplet}}} = \frac{3}{4r_{\text{drop}} \rho_{\text{drop}}} \quad (\text{characteristic of spherical droplet})$$

These equations can easily be integrated (numerically) from the origin of the cascade to yield droplet and vapour velocities.

Results are shown in Figure A2.1 below.

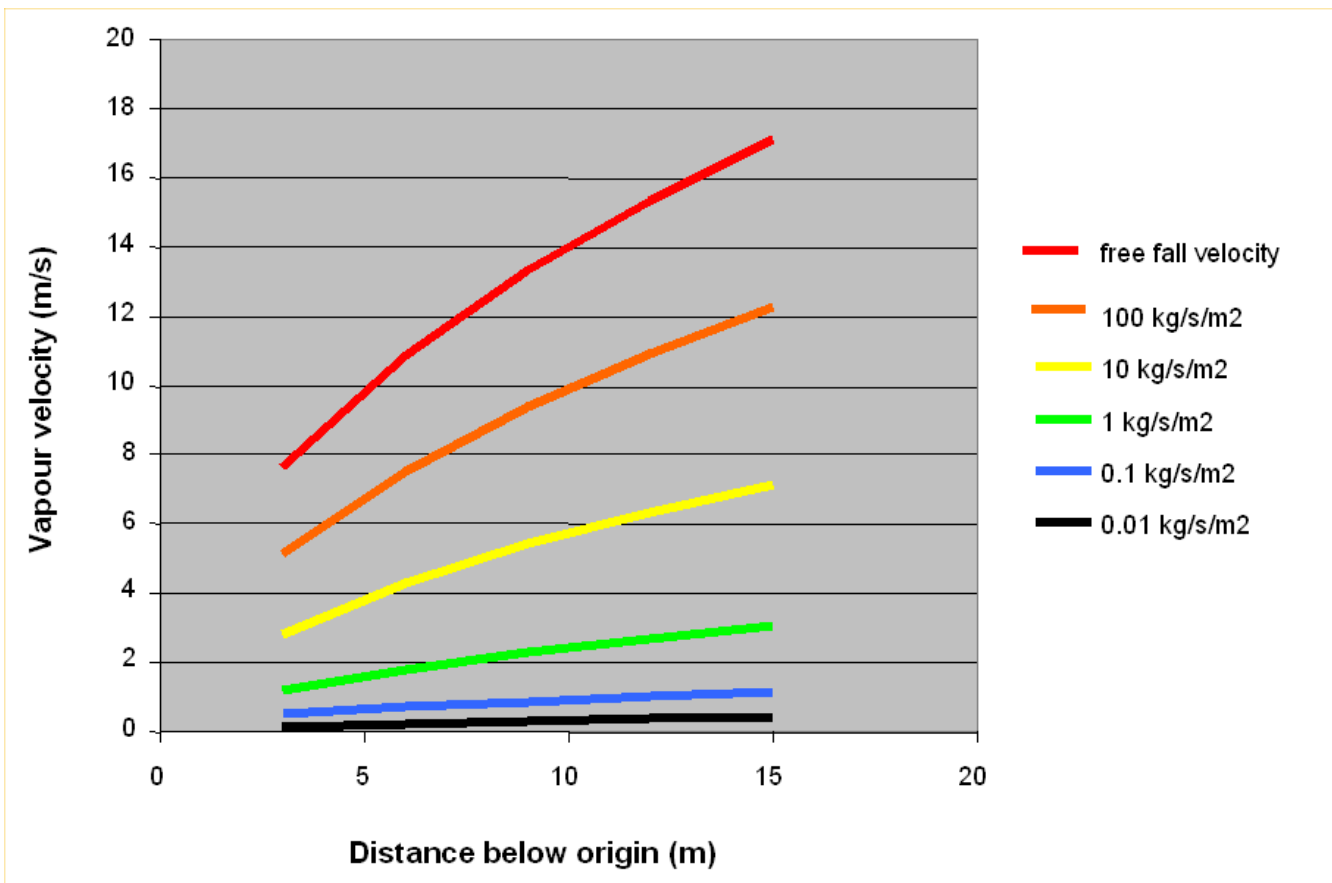
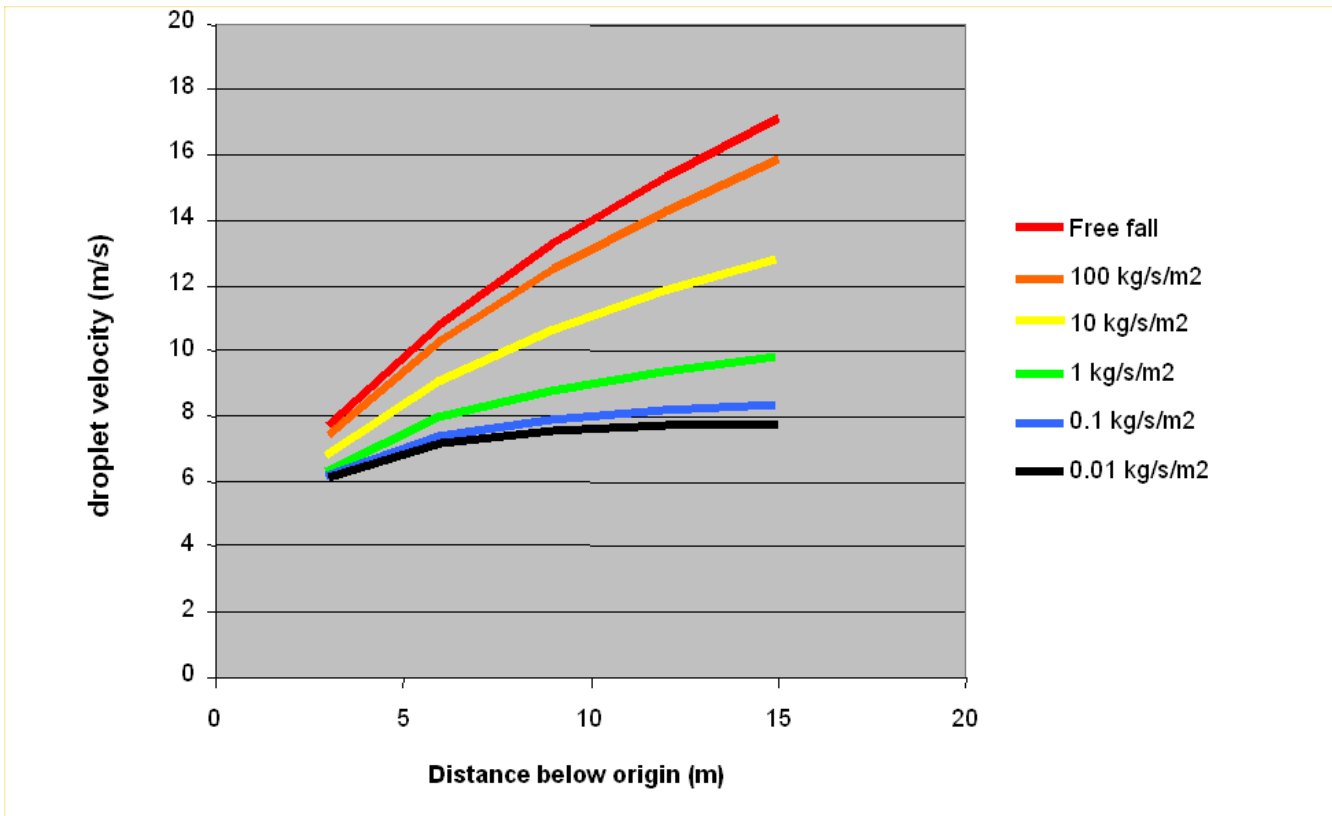


Figure A2.1: Relationship between liquid mass flow density and entrained vapour velocity

Vapour cloud formation

Experiments and modelling

Hazard analysis for overfilling of a tank with a volatile liquid is a complex and important problem but (prior to the Buncefield incident) had not been the subject of significant research effort. Since the incident [Reference 1] HSE has sponsored a programme of experimental and modelling research to investigate the technical issues involved and develop methods of analysis [References 2 and 3].

The objective is that HSE, and industries responsible for filling tanks, will be in a position agree on a reliable method to determine the character of the vapour cloud generated in the event of an overfill. This will allow appropriate consideration of the overfill scenario i.e fluid type, tank size, fill rate etc. to be taken into account in hazard assessments for land use planning and emergency planning purposes. HSE's Vapour Cloud Assessment method is detailed in Appendix 1. Some example cases are worked through in this Appendix.

This report and the work it describes were funded by the Health and Safety Executive (HSE). Its contents, including any opinions and/or conclusions expressed, are those of the authors alone and do not necessarily reflect HSE policy.